Implication of induced Reelin-KO in the deposition of Aβ plaques in Alzheimer´s Disease mouse models

Ana Rita Pires do Patrocínio

Thesis to obtain the Master of Science Degree in

Biological Engineering

Supervisors:

Dra. Yasmina Manso Sanz

Prof. Dr. Maria Margarida Fonseca Rodrigues Diogo

Examination Committee

Chairperson: Prof. Dr Marília Clemente Velez Mateus

Supervisor: Prof. Dr. Maria Margarida Fonseca Rodrigues Diogo

Member of the Committee: Prof. Dr Adelaide Maria Afonso Fernandes Borralho

November 2019

"I think, therefore I am."

—Rene Descartes, 17th-century philosopher

I declare that this document is an original work of my own authorship and that it fulfills all the requirements of the Code of Conduct and Good Practices of the Universidade de Lisboa.

Preface

The work presented in this thesis was performed at the Department of Cell Biology of the Faculty of Biology of University of Barcelona (Barcelona, Spain), during the period February - July 2019, under the supervision of Dr. Yasmina Manso and Dr. Prof. Eduardo Soriano, and within the frame of the Erasmus program. The thesis was co-supervised at Instituto Superior Técnico by Prof. Margarida Diogo.

Acknowledgments

I thank the Developmental Neurobiology and Regeneration Group of Dr. Prof. Eduardo Soriano, integrated in the University of Barcelona, for taking me in and orienting me in the development of this project. A special thank you to the other students who were doing projects in the same lab, who helped me so much, and to my friend Laura Masin who was also in the Lab doing her thesis project and who made each day there so much more joyful.

Abstract

The aim of the present experiment was to study the implication of the absence of extracellular protein reelin in the deposition of Aβ plaques in an Alzheimer´s disease (AD) mouse model. A novel strain of inducible reelin-KO mouse models, called floxed-reelin, was crossed with J20 models to obtain the JfRLn mouse strain. Floxed-reelin mice were used so that the absence of reelin in a well-developed brain could be studied, whereas J20 mice were used as an AD model, since they carry the mutated hAPP transgene, that causes Aβ plaques to accumulate in the brain (a known trait of AD). Brain sections of every J20+ animal were stained by immunohistochemistry (IHC) against Aβ plaques and analyzed so that the percentage of hippocampus area occupied by plaques was quantified in each J20+ animal. The J20+ JfRLn mice were then divided in J20-KO and J20-controls according to their reelin genotype, and a mean of hippocampal plaque percentage was calculated for the two reelin genotypes.

Reelin is viewed as a possible target for the treatment and prevention of AD, since the downregulation of its pathway in the adult brain is involved in several neurological diseases, including AD. Reelin has been observed to decrease Aβ aggregation in vitro, and reelin overexpression in J20 mouse models decreased Aβ plaque accumulation, although reelin overexpression has also been shown to cause mispositioning of adult generated neurons in the preexisting brain circuitry. It seems that precise activity levels of the reelin pathway must be maintained in the adult brain, a dysregulation either up or down causes an imbalance in brain mechanisms and a disorganization of its structures.

The hypothesis that the absence of reelin in the J20 mouse brain increases the deposition of Aβ plaques in 1-year old mice was not supported by the obtained results. The mean of the percentage of plaque area obtained for the J20 reelin-KO (no reelin) genotype was 1.98%, while for the J20 reelin-WT (reelin control) was 1,76%. The results were submitted to a statistical t-student test, being ascertained that the difference of Aβ plaque load between genotypes was non-significant.

Keywords: Alzheimer´s disease, reelin protein, Aβ plaques, mouse models, hippocampus.

Resumo

O objetivo do presente trabalho experimental foi estudar a implicação da ausência de proteína reelin na deposição de placas de βA, num modelo murino da doença de Alzheimer (DA). Uma nova estirpe de ratos KOs induzíveis de reelin, chamada floxed-reelin, foi cruzada com a linha J20 para se obter a estirpe JfRLn. Ratos floxed-reelin foram usados para que a que a ausência de reelin num cérebro adulto, bem desenvolvido, pudesse ser estudada, enquanto que os ratos J20 foram usados como modelos de DA, visto conterem o transgene hAPP mutado e por isso acumulam placas de βA no cérebro (um traço conhecido da DA). Secções de cérebro de cada animal J20+ foram tingidas por uma técnica de imunohistoquímica contra placas βA e analisadas de modo a que a percentagem de área de hipocampo ocupada por placas pudesse ser quantificada, em cada animal J20+. Os ratos foram divididos em J20-KO e J20-controlos de acordo com o seu genótipo respeitante à expressão de reelin e uma média da percentagem de placas no hipocampo foi calculada para os dois genótipos.
A proteína reelin é vista como um possível alvo para o tratamento e prevenção da DA, visto a sub-expressão da sua via metabólica, no cérebro adulto, estar envolvida em várias doenças neurológicas, como a DA. Foi observado que a reelin reduz a agregação de Aβ in vitro e a sobre-expressão de reelin em modelos murinos J20 reduziu a acumulação de placas de Aβ, embora também tenha mostrado causar o mal posicionamento, no circuito preexistente, de neurónios gerados no cérebro adulto. Assim, é necessário que sejam mantidos níveis precisos de reelin no cérebro adulto. Uma desregulação na via metabólica da reelin, para cima ou para baixo, leva ao desequilíbrio dos mecanismos cerebrais e à desorganização das suas estruturas.
A hipótese de que a ausência de reelin no cérebro de ratos J20 com 1 ano de idade, causa um aumento na deposição de placas βA não é suportada pelos resultados obtidos. O valor da percentagem de área de hipocampo ocupada por placas βA obtido para o genótipo J20 reelin-KO (sem reelin) foi de 1.98%, enquanto que para o genótipo J20 reelin-WT (controlo de reelin) foi de 1,76%. Os resultados foram submetidos a um teste estatístico t-student, tendo sido concluído que a diferença de percentagem de placas βA entre os dois genótipos não é significativa.

Palavras-chave: Doença de Alzheimer, proteína reelin, placas βA, modelos murinos, hipocampo.

Table of Contents

List of Figures

List of Tables

List of Acronyms

5HT-ergic	Serotonergic
AD	Alzheimer´s disease
Aβ	Amyloid Beta
AMPAR	α-amino-3- hydroxy-5methyl-4-isoxazolepropionic acid receptor
ACh	Acetylcholine
AChE	Enzyme acetylcholinesterase
ApoER2	Apolipoprotein E receptor 2
CNS	Central Nervous System
CSF	Cerebrospinal Fluid
CA	Cornu ammonis
ChAT	Choline acetyltransferase
CR	Cajal–Retzius
CC	Corpus callosum
DA	Dopamine
DAB	(3,3'-diaminobenzidine)
DGCs	Dentate granule cells
DG	Dentate gyrus
EFs	Executive functions
EAATs	Excitatory amino acid transporters
ER	Endoplasmic reticulum
GABA	Gamma-aminobutyric-acid
GCs	Granule cells
GCL	Granule cell layer (laminar layer of the DG)
HFS	High frequency stimulation
HC	Hippocampus
HRP	Horseradish peroxidase
iGluRs	Ionotropic glutamate receptors
IHC	Immunohistochemistry
JfRLn	J20 floxed-reelin
KO	Knockout
KA	Kainate
LC	Locus coeruleus
LTP	Long-term potentiation
LTD	Long-term depression
LV	Lateral ventricle
MA-ergic	Monoaminergic
mGluRs	Metabotropic glutamate receptors
ML	Molecular Layer

miRNAs	MicroRNAs
MSBs	Multiple synaptic boutons
nAChR	Nicotinic acetylcholine receptors
ncRNAs	Noncoding RNAs
NE	Norepinephrine
NMDA	N-methyl-D-aspartate
NHE	Na+/H+ exchange
NPS	Neuropsychiatric symptoms
NTFs	Neurofibrillary tangles
NO	Nitric oxide
OE	Overexpression
$ONOO^-$	Peroxynitrite
PB	Phosphate buffer
PBS	Saline phosphate buffer
PCR	Polymerase chain reaction
PFA	Paraformaldehyde
PHFs	Paired helical filaments
PSD	Postsynaptic density
RMS	Rostral migratory stream
ROS	Reactive oxygen species
SGZ	Subgranular zone
SVZ	Subventricular zone
WT	Wild Type
VAChT	Vesicular acetylcholine transporter
VLDLR	Very-low-density lipoprotein receptor
VGLUT1	Vesicular glutamate transporter 1
VGLUT2	Vesicular glutamate transporter 2

Chapter 1

Introduction

1.1 Motivation

Alzheimer´s Disease (AD) is a progressive neurodegenerative disorder characterized by memory loss and cognitive impairment. AD is the most common form of dementia, representing up to 75% of all dementia cases. The second most common dementia worldwide is vascular dementia (related with cardiovascular disorders). In Europe, the prevalence of dementia in people aged 65 years or older is 6.4% and 4.4% for AD. Because dementia is associated with older age, the gradual increase of the age of the population will cause the number of AD cases to increase as well. Finding a way to treat and prevent dementias like AD, is at the top of current medical priorities.

Reelin is an extracellular matrix glycoprotein that plays a vital role in brain development and lamination. It continues to be expressed in the adult brain, playing an essential part in the integration of newborn neurons in the preexisting brain circuitry. Interestingly, in the adult brain, reelin participates in the control of mechanisms that are reminiscent of developmental processes**.** In fact, reelin controls neuronal migration, in development and throughout life, by guiding newly formed neuronal cells to their proper destination, so that normal synaptic connections may be established between neurons. The downregulation of the reelin pathway in the adult brain is involved in several neurological diseases, including AD. On the other hand, the overexpression of reelin has also been shown to cause mispositioning of adult generated neurons, in mouse models. Thus, it seems that precise levels of reelin must be maintained in the adult brain, a dysregulation either up or down causes an imbalance in the brain mechanisms and a disorganization of its structures (Pujadas et al., 2010) (Teixeira et al., 2012).

The main neuropathological hallmark of AD is the extracellular deposition of Aβ plaques, formed from the aggregation of toxic Aβ oligomers. The human APP (hAPP) mutation causes the overexpression of APP (the precursor of Aβ) and the subsequent accumulation of amyloid plaques in the brain, being known as a cause for early onset, aggressive AD in humans. Reelin has previously been shown to reduce Aβ plaque formation in vitro, and its overexpression decreased Aβ plaque accumulation in the brains of AD mouse models (J20 mice) (although it also caused mispositioning of adult born neurons in preexisting brain circuits), creating a link between reelin and AD (Pujadas et al., 2014) (Pujadas et al., 2010).

The complete elimination of reelin, since the embryonic stage, has been studied with reeler mice, that display deformed brains because reelin signaling was not active in the course of brain development. The novelty of this project is the new JfRLn lineage of inducible reelin silencing mice that allows the study of the absence of reelin in a well-developed AD brain, while also allowing the control of when the reelin gene ceases to be expressed. Inducible reelin knockouts (i.e. reelin absence in a normally developed J20 adult brain), have never been thoroughly studied before. It could also be interesting to study what consequences the absence of reelin would have in a well-developed mouse brain, otherwise

healthy, i.e. without Aβ plaques, although it could be difficult to identify mental illnesses in mice, if it was the case.

The role of reelin in Aβ plaque accumulation in the AD brain has been previously studied with inducible reelin overexpression mouse models (TgRln/J20 mice) (Pujadas et al., 2014). An experiment with TgRln/J20 mice, that overexpress reelin and accumulate Aβ plaques in the brain, consisted on the measurement of plaque load in the brains of these mice and of J20 reelin-WTs, to make a comparison. It was observed that the percentage of area occupied by plaques in the HC (and in the cortex) was lower in TgRln/J20 mice than in J20s, at the 12 months-time point. It was also observed that reelin influences the kinetics of Aβ, in a concentration dependent way, by delaying the aggregation of Aβ42 into fibrils, in vitro. Figure 1.2 shows the results obtained in the TgRln/J20 mice experiment. Interestingly, the role of reelin in the reduction of Aβ plaques is only visible in mice sacrificed at 12 months of age. In the case of mice that were sacrificed at 8 months, TgRln/J20 mice present higher plaque load that J20 mice, which is a bit unexpected.

I completed an internship with the Developmental Neurobiology and Regeneration Group of Dr. Prof. Eduardo Soriano, integrated in the University of Barcelona, where I had the pleasure of developing the experiment described in the present work: the study of conditional reelin-KO J20 mice. This study was inspired by the promising results obtained with J20 reelin overexpressing mice, studied in the same laboratory (Pujadas et al., 2014). Another student, also doing an internship in the Laboratory of Dr. Prof. Eduardo Soriano, before me, had done a similar study with JFRLn mouse models in which the mice were sacrificed when 8 months old. The results that she obtained were not statistically significant (i.e. the difference between genotypes was not significative), but the trend observed was that reelin controls presented a higher plaque load mean than the reelin-KOs (figure 1.1). Although unexpected and inconclusive, these results resemble the ones obtained in the reelin-OE experiment at the 8 months-time point. Since the overexpression of reelin only seemed to influence plaque deposition when brains were observed at 12 months-time point, it was hypothesized that for the reelin-KO it could be similar. Thus, it was important to do the experiment with the brains of reelin-KO J20 mice sacrificed at the age of 12 months.

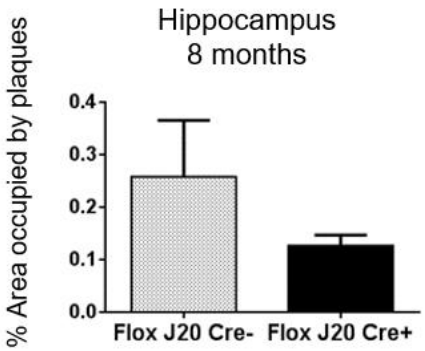

Figure 1.1: Percentage of hippocampus area occupied by Aβ plaques, in the brains of reelin-KO J20 mice sacrificed at the 8 months-time point. The Flox J20 Cre+ are the reelin-KO genotype and the Flox J20 Cre- are the reelin-controls. These results are not statistically significant (i.e. the difference between genotypes was not significative), but the trend observed was that reelin controls presented a higher plaque load mean than the reelin-KOs. Results obtained by another student in the Laboratory of Dr. Prof. Eduardo Soriano.

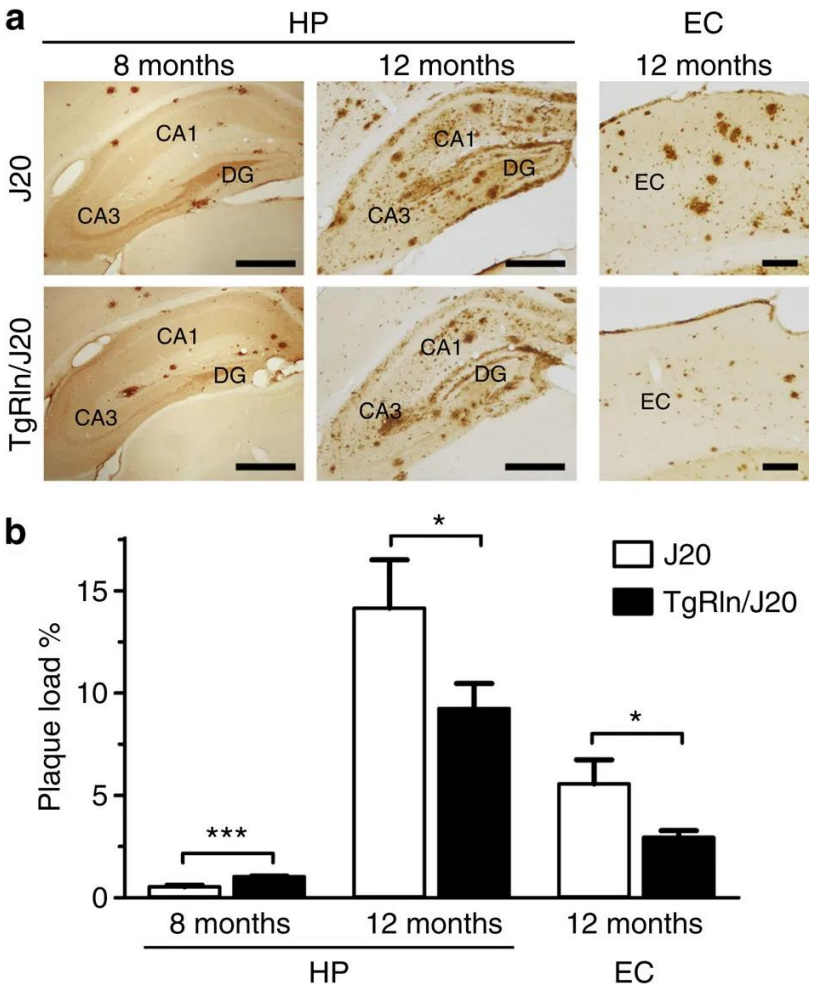

Figure 1.2: Results obtained by (Pujadas et al., 2014) in the TgRln/J20 mice experiment of reelin overexpression. The brain sections represented on top of the graphs were stained by IHC against Aβ plaques (similarly to what was done in the present experiment). the role of reelin in the reduction of Aβ plaques is only visible in mice sacrificed at 12 months of age. In the case of mice that were sacrificed at 8 months, TgRln/J20 mice present higher plaque load that J20 mice, which is a bit unexpected.

1.2 Objectives and Methodology

The aim of the experiment conducted in the present project was the attainment of further understanding on the implication of protein reelin in the deposition of Aβ plaques in an Alzheimer´s disease mouse model, in order to ascertain if reelin could be a good target for the treatment and prevention of AD. A novel strain of inducible reelin-KO mouse models, called floxed-reelin, was used so that the absence of reelin in a well-developed brain could be studied. Floxed-reelin mice were used in association with J20 mice, which carry the mutated hAPP gene that causes amyloid plaques to accumulate in the brain, to obtain the JfRLn lineage. Brain sections of each J20+ animal were cut and stained by IHC against Aβ plaques, and then analyzed (with imageJ program) so that the % of hippocampus area occupied by plaques was quantified in each animal. The J20+ JfRLn mice were divided in J20-KO and J20-controls in relation to their reelin genotype. A mean of plaque % in the HC was calculated for each J20+ animal and for the two reelin genotypes, which were then compared. The initial hypothesis of the experiment was that the absence of reelin in J20 reelin-KO mice brains would lead to a more dramatic accumulation of Aβ plaques, compared to J20-WTs.

Chapter 2

Literature Revision

The aim of this chapter is to summarize what is known about Alzheimer´s disease, its causes, symptoms and available treatments, and to explain the mechanisms of its neuropathological hallmarks. It serves also to introduce reelin protein and to describe its involvement in Alzheimer´s Disease.

2.1 Alzheimer´s disease

Alzheimer´s Disease (AD) is a progressive neurodegenerative disorder characterized by memory loss and cognitive impairment. AD is the most common form of dementia, representing up to 75 % of all dementia cases (Qiu et al., 2009). The second most common dementia worldwide is vascular dementia (related with cardiovascular disorders). The age of the worldwide population is gradually increasing, so much that the number of people aged 60 or older is predicted to reach around 1 billion by 2030. Because dementia is associated with older age, the increase in older people numbers will inevitably cause AD cases to increase as well. In developed nations, roughly 1 in 10 older people (65+ years) is affected by some degree of dementia, whereas over one third of very old people (85+ years) may have symptoms of dementia. In Europe, the prevalence of dementia in people aged 65 years or older is 6.4 % and 4.4 % for AD. After the age of 65, the prevalence of AD almost doubles every 5 years.

Data shows that the global prevalence of dementia is estimated to be 3.9 % in people aged 60 or more years, with the regional prevalence being 1.6 % in Africa, 4.0 % in China and Western Pacific regions, 4.6 % in Latin America, 5.4 % in Western Europe, and 6.4 % in North America. In developing countries, the prevalence rates of dementia were generally smaller than in developed countries, and more importantly, the prevalence rates in rural areas were much smaller than in urban ones. In fact, the prevalence rates of dementia in India and rural Latin America are approximately a quarter of the rates measured in European countries, but when the prevalence in urban populations of developing countries is measured separately, it is much higher. For example, in São Paulo (Brazil) the prevalence of dementia is 5.1 % and in Havana (Cuba) 6.4 %, for 65+ ages. This might be related with vascular dementia, which is affected by lifestyle. It seems that the sedentary lifestyle coupled with unhealthy diets and stressful routines, adopted in urban areas, leads to cardiovascular diseases and thereafter, to dementia.

AD is the most devastating disease among elderly humans, leading to inevitable death in about 7 years following disease onset. Moreover, it is a huge financial burden for health care systems and for the families of patients, that must also provide emotional support and become caregivers. Finding a way to treat and prevent dementias like AD, is at the top of current medical priorities. (H. Ferreira-Vieira et al., 2016) (Heeren et al., 1991).

AD is named after Alois Alzheimer, a psychiatrist who was the first to describe it in 1906, using criteria of progressive memory loss, disorientation, and pathological markers observable in brain autopsies. The pathological markers identified by Alzheimer were senile plaques and neurofibrillary tangles and they are still used today (Schachter and Davis, 2000). It was later understood that the cases of “senility” that

at that time were considered a normal outcome of old age are in fact cases of dementia, such as AD. The five neuropathological hallmarks of AD are the extracellular deposition of amyloid β (Aβ plaques), formation of intraneuronal neurofibrillary tangles (NTFs), neuroinflammation, acetylcholine deficiency and glutamate excitotoxicity. Moreover, extensive neuronal loss and synaptic impairment and weakening are detected in the cerebral cortex, hippocampus and other areas that are fundamental for cognition and memory, which are heavily affected in AD. Amyloid plaques are a good indicator of AD and are used to diagnose the disease because they are easily observed in postmortem brain autopsies. However, there is no correlation between plaque load and AD related cognitive impairment. Synaptic loss is the main indicator of disease progression and neurofibrillary tangles are also a good correlate. The loss of dendritic spines correlates with cognitive decline in AD, even better than loss of neurons. Interestingly, the brain changes of AD might begin 20 years or more before the symptoms are noticeable.

A healthy adult brain has about 86 billion neurons (Herculano-Houzel, 2009) and about 100 trillion synapses. They enable signals to travel fast through the brain's neuronal circuits, making up the cellular basis of memories, thoughts, sensations, emotions, and movements (Alzheimer's Association, 2019). The first noticeable symptom of AD patients is memory loss and inability to form new memories which impairs the ability to learn new information or to recall previously learned information. Sometimes the early stages are accompanied by irritability and personality changes. In the following years, other cognitive deficits manifest, namely aphasia (language disturbance), apraxia (impaired ability to carry out motor activities despite intact motor function), and agnosia (failure to recognize or identify objects despite intact sensory function). These cognitive deficits are characterized by gradual onset and continued worsening, significantly impairing social and occupational functioning in the course of disease (Bell, 1994). In the final stages, the motor capacities are also compromised, and the patient ends up mute and bedridden. Other manifestations of AD include decreased judgment ability, wandering (caused by a decreased visuospatial orientation), mood disturbance, agitation, sleep abnormalities, and even psychosis (Schachter and Davis, 2000).

2.1.1 Genetics of AD

AD can be divided in familiar and sporadic type, and in early-onset and late-onset. Familiar type AD (FTAD) means that it runs in the family of the patient, afflicting many people of the same blood line. In this case the disease is usually more aggressive and starts earlier but it is easier to find a genetic cause.

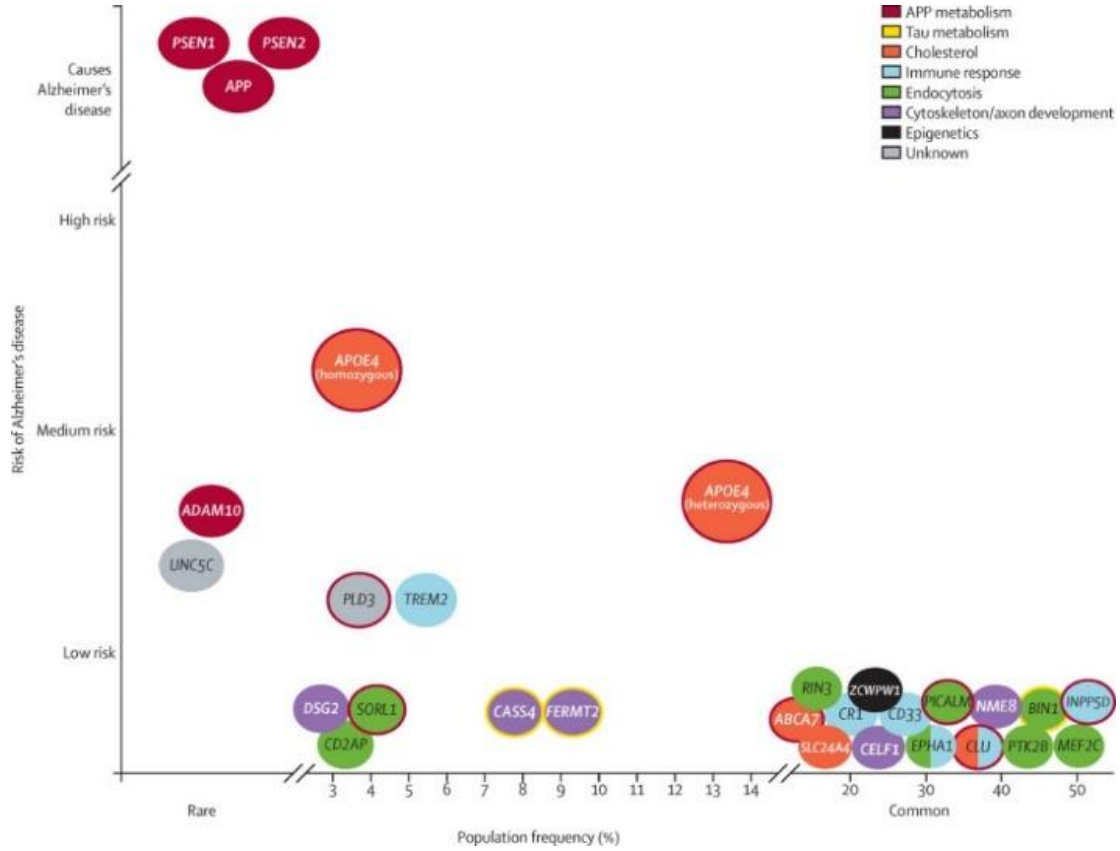

Figure 2.1: Different genetic causes for AD and respective frequency and impact on disease incidence risk.

A few rare gene mutations that are passed on in families have been identified to cause FTAD. In the sporadic type it is more difficult to discover the gene mutations behind it because there are many mutations, which are common in the population but that only increase the probability of an individual to develop AD, without necessarily causing it. On the other hand, the FTAD mutations which are few and rare, highly increase the probability of AD incidence or, in some cases, cause AD for the individual who carries it. The mutations responsible for FTAD have already been discovered, allowing such situations to be better understood, but this type of AD only represents 1% of all cases, being that the other 99% of cases are of the sporadic type (STAD), with many possible causes. AD is classified as early-onset type, when it starts before 65 years old, or as late-onset when it starts after 65 years old.

More than 32 different missense mutations in the APP gene have been identified. The APP gene was mapped to chromosome 21, it has many isoforms due to alternative splicing of exons, the 3 isoforms predominant in the brain are APP695, APP751, and APP770 (Šerý et al., 2013). These account for 10% to 15% of early-onset familial AD cases, with age of onset at mid-40s or 50s. Mutations in the genes encoding presenilin proteins PS1 and PS2 (part of the γ-secretase complex, that is one of the enzymes responsible for producing toxic Aβ oligomers from its precursor, APP) were discovered in FTAD cases. Over 1000 point mutations in PS1 and PS2 are responsible for the majority of FTAD cases (Šerý et al., 2013). The apolipoprotein E (ApoE) gene is related to both familial late-onset and sporadic late-onset AD, which accounts for most AD cases. In fact, the apoE4 has been identified as the top late-onset AD gene and as the only significant gene associated with age-related cognitive decline in humans. *APOE*

gene exists in three allelic forms (*APOE-2, -3,* and *-4*). ApoE-4 impairs Aβ clearance and promotes Aβ aggregation and deposition, and it is disproportionately represented in AD patients. Studies have revealed that *APOE-4* allele presents a dose-dependent relationship with increasing risk for AD and decreasing age of onset. The risk for sporadic late-onset AD incidence is 2.2 to 4.4 higher than normal due to the inheritance of one copy of the *APOE-4* allele on chromosome 19, whereas with the inheritance of two copies of the same allele the risk for development of AD becomes 5.1 to 17.9 higher.

High cholesterol levels have been linked to overproduction of Aβ. One of the physiological functions of Aβ has been suggested to control cholesterol transport. Cholesterol greatly increases the amount of APP that follows the amyloidogenic pathway by reducing the activity of α-secretase, which is responsible for the cleavage that generates sAPPα (which is the nontoxic product generated in the nonamyloidogenic pathway). One hypothesis for possible mechanisms triggering AD is the vascular and mitochondrial hypotheses that associates the development of AD pathologies with vascular risk factors, such as high cholesterol, high tension, and obesity. The ApoE is a cholesterol transport protein, therefore being implicated as a vascular risk factor for AD. In fact, AD patients often present cerebrovascular pathologies, such as cerebral micro-bleeding and cerebral microinfarcts. These vascular pathologies can reduce the blood flow through the brain, accelerating amyloid deposition, and synaptic and neural dysfunction. Moreover, hypoxia (i.e. low oxygen supply) and mitochondrion failure, related with AD, can cause oxidative stress. Mitochondrial disruption also leads to the lack of ATP energy in synaptic terminals, affecting synaptic function and impairing the brain metabolism.

The exact factors that promote the development of AD as well as the mechanisms in the brain that start it are not completely understood and for this reason the treatments used currently are not efficient at stopping disease progression. There are different triggers that can cause AD, and these generate diverse pathological mechanisms for disease development. It is now believed that AD is a spectrum of many different pathologies that begin through different mechanisms and are triggered differently but that have analogous outcomes, creating similar symptoms. Genetic disposition and environmental factors play an important role in the initiation of the disease. Therefore, the best treatment is not expected to be the same for all cases. The identification of the stage and driving cause of the pathology in each specific case seems to be essential for the application of the right treatment for each patient.

Age is the biggest known risk factor for AD, since all studies on the matter reveal a positive correlation between prevalence rates of AD and age (Gao et al., 1998). But though this disease was previously thought to be an inevitable consequence of aging it is now believed that age is a risk factor of AD simply because it is accompanied by biological risk factors and that if these risk factors can be identified and eliminated, AD can be separated from age. Thus, age is only a driving force that allows the development of pathological mechanisms by which this disease begins but it is not an imminent risk factor itself. This idea is supported by studies that show that the increase of incidence rates of AD and dementia slows down with increasing age, i.e., the rate of incidence increases less as age advances although it does not decrease. It would be expected that the rates of incidence would keep increasing faster and faster as age advances and that in very old ages everyone would develop dementia (i.e. that everyone would become demented eventually if they lived long enough), but there is evidence that prevalence rates level off or even decline in very-old age groups (Ritchie and Kildea, 1995), i.e., the proportion of the

population affected by the condition in very-old age groups levels of. This is mainly because many of the people who developed AD earlier died in between and they are not part of these groups, and because the analyzed older-age groups are smaller, but it also means that a group of people who did not develop AD until a certain age does not develop it in older-ages and some live until their very old (more than 100 years) without ever developing AD or any type of dementia. Therefore, if the pathological mechanisms that lead to AD never develop in the brains of some people, this disease cannot be an inescapable consequence of old age.

Men are at a higher risk for developing dementia, since they are more propense to having vascular diseases which can cause vascular dementia. On the other hand, it has been discovered that women are at a higher risk of developing AD (Gao et al., 1998). The reason for this is not yet known but there are speculations that it might be due to the hormonal changes in postmenopausal women, the lack of estrogen or other hormones could be the root of the increased risk. In a study investigating the possible advantages of estrogen replacement therapy in older women, two groups of women suffering from AD were analyzed, in which one of the groups were patients taking estrogen replacement. The group of women using estrogen performed significantly better in a cognitive test (Mini-Mental State examination). Thus, estrogen replacement therapy could decrease the risk of AD incidence in women and improve cognitive performance of female AD patients (Henderson, 1994), although it has also been linked to higher risks of developing breast cancer.

2.2 Neuropathological hallmarks of AD

2.2.1 Extracellular deposition of amyloid-β (Aβ plaques)

The amyloid hypothesis remains the leading hypothesis to interpret the neuronal dysfunctions occurring in AD. It refers to the abnormal extracellular accumulation of amyloid plaques in the brain, that consist of fibrillar aggregations of amyloid β (Aβ) peptides with 39–42 amino acids in length. Aβ plaques exert highly toxic effects on neuronal circuits, especially in the prefrontal and cingulate cortices, and in the hippocampus (HC), which are the regions most affected by Aβ, showing changes since early stages of the disease (Martorana and Koch, 2014). The presence of Aβ plaques in the brain of a patient (which can only be assessed post-mortem) is the main pathological hallmark of AD, constituting a requirement for the diagnosis of the disease, although the number of plaques measured in the brain does not seem to correlate with the severity of dementia.

Three different types of Aβ deposits are observed: diffuse plaques, immature plaques, and dense plaques (mature senile plaques). In diffuse plaques Aβ peptide is not aggregated into amyloid, in primitive deposits Aβ peptide is aggregated and associated with dystrophic neurites (axons or dendrites) and helical filaments, and in dense plaques Aβ is highly aggregated forming a central amyloid core surrounded by a ring of dystrophic neurites. It has been suggested that patients with FTAD have a larger average cluster size of the diffuse deposit in comparison with patients with STAD.

Aβ peptide is produced by the sequential cleavage of amyloid precursor protein (APP), an integral membrane protein concentrated in neuronal synapses. The physiological role of APP is not known though it has been implicated as a regulator of synapse formation and neural plasticity. According to the amyloid hypothesis, APP undergoes an impairment of its physiological cleavage system, producing oligomeric toxic species. Moreover, an imbalance between production and clearance of oligomers leads to their accumulation and assemble in plaques (Revett, et al., 2013). APP undergoes posttranslational proteolytic processing (by α-, β-, and γ-secretases), which can happen through two different pathways, the nonamyloidogenic pathway, and the amyloidogenic pathway that leads to the generation of neurotoxic species. The pathway that APP follows depends on the proteases that cleave it, since each enzyme acts in a different cleavage site. If APP is processed by α-secretase, at the plasmic membrane, it will follow the nonamyloidogenic pathway: α-secretase generates soluble amyloid protein, therefore preventing the production of neurotoxic β amyloid. APP is transported by the cytoskeleton from the cytosol to the plasma membrane, where the cleavage by α-secretase is carried out, releasing a soluble molecule named sAPPα. sAPPα has an important role in neuronal survival and it is protective against excitotoxicity.

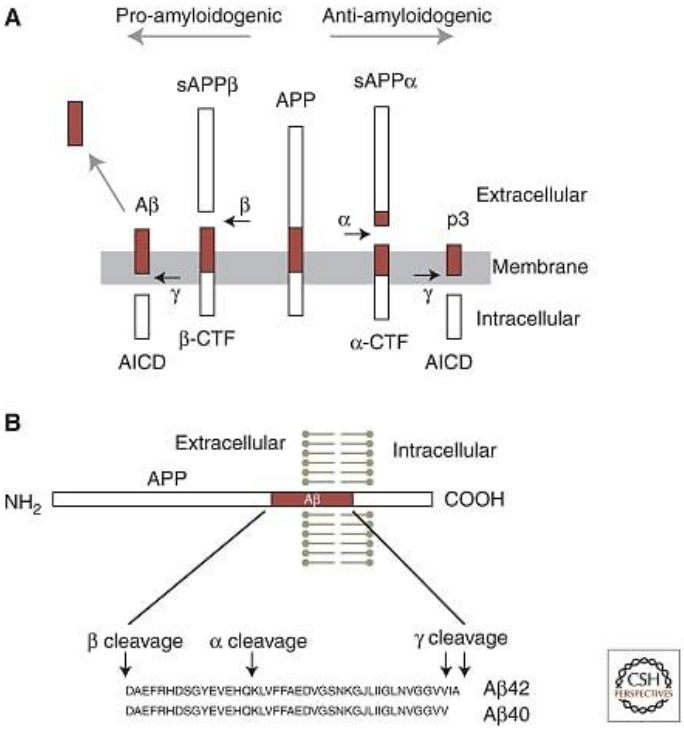

Figure 2.2: APP processing and the formation of Aβ peptide (Sheng, Sabatini and Sudhof, 2012).

If APP is not processed by α-secretase, the amyloidogenic pathway will be followed, beginning with the internalization of APP into endocytic compartments where it is cleaved by β- and γ-secretases to generate Aβ (image4). The Aβ produced intracellularly in endosome vesicles is eventually secreted to the extracellular environment where it can accumulate, forming amyloid plaques. Amyloid precursor protein β-secretase 1 (or β-site APP cleaving enzyme 1 (BACE1)) appears to be upregulated in AD patients and to become more expressed with age progression as well as with conditions such as oxidative stress, hypoxia, ischemia, and energy deprivation, according to cellular models. After APP cleavage by BACE1, the extracellular part of APP is released as a soluble peptide named sAPPβ, which mediates cell death (has the opposite effect of sAPPα). Following α- or β-cleavage, the carboxyl terminal fragments (CTFs) of APP, named αCFT or βCFT remain in the membrane where they will be cleaved by γ-secretase. αCFT is cleaved by γ-secretase originating a peptide that is readily degraded whereas βCFT is cleaved by γ-secretase producing Aβ40 and Aβ42 (Aβ40 or Aβ42 depending on the number of amino acids in the peptide). Aβ42 is the most toxic Aβ species, being part of the extracellular plaque deposits. γ-secretase is a complex containing presenilin proteins (PS, PS1 or PS2), among others. Mutations in the genes

encoding presenilin proteins PS1 and PS2 were discovered to be responsible for most of the cases of FTAD (Šerý et al., 2013).

It has been reported that neurons undergoing apoptotic cell death secrete 2- to 3-times more Aβ than healthy neurons, suggesting that overproduction of Aβ may be a consequence of neuronal damage. Aβ is neurotoxic and contributes to apoptosis so, it seems that increased Aβ production, for example due to genetic predisposition, causes increased cell death in susceptible neurons. This represents a cycle, that could explain the substantial cell death seen in brains of AD patients, in which dying neurons release more Aβ, that in turn leads to more cell death (Soriano et al., 2001) (Galli et al., 1998).

The physiological role of APP has been investigated and it appears that its extracellular domain plays a role in synapse formation. APP and BACE1 knockout mouse models, studied in an experiment (Kobayashi et al., 2008), unexpectedly displayed impaired memory and seizures, results that are quite interesting because they indicate that although excessive accumulation of Aβ is pathological, it is necessary in some amounts and at some point, in the mechanisms of normal learning and memory. Whereas high nanomolar (10^{-9} molar) concentrations of Aβ lead to neurodegeneration and reduction of potentiation in the HC, lower picomolar Aβ (10^{-12} molar) concentrations are released in normal healthy brains during synaptic activity. Another experiment showed that picomolar concentrations of Aβ42 monomers and oligomers markedly increased hippocampal long-term potentiation (LTP), suggesting a model in which Aβ has positive modulatory effects in low concentrations while having negative modulatory effects in high concentrations (Puzzo et al., 2008).

Another relevant factor is the Aβ42/Aβ40 ratio that is usually elevated in AD patients. The majority of Aβ peptides is excreted by the neurons as Aβ40 and only a small fraction of Aβ is released as Aβ42. Aβ42 self-associates in dimmers, soluble oligomers and then in insoluble aggregates of fibrils (plaques), being the main peptide in amyloid plaques. Plaques start accumulating in the synapses and then spread to connected areas in the brain, from the point where they start forming. Interestingly, the neurons most disrupted in AD are normally found in proximity to plaques, or they project to or from areas dense in plaques and tangles. Aβ is an established cause for many negative implications in cognitive function such as the disruption of LTP mechanisms. Importantly though, the cognitive deficits related with Aβ are noticeable before its deposition, suggesting that Aβ disrupts synapses well before forming plaques, i.e. the soluble forms of Aβ are neurotoxic independently of the plaques. In an experiment with mouse models, that express mutant human APP, therefore presenting Aβ accumulation in their brains, γ-secretase inhibitor was fed in order to reduce Aβ levels in the mice brains. As the Aβ accumulation was reduced, there was a noticeable restoration of LTP, reinforcing the idea that Aβ affects synaptic plasticity. Aβ has also been shown to decrease synaptic density, but it seems that only dimers and larger aggregates exert the known toxic effects, whereas monomeric Aβ peptides do not. There is experimental data from animal models supporting the idea that Aβ could possibly be removed from brains of AD patients with active Aβ immunotherapy, i.e. using antibodies directed against the Aβ present in the brain of a patient (Revett, et al., 2013).

Dendritic spines undergo notable activity-dependent structural changes. Spine head size determines the probability that a spine bears a synapse as well as its stability, and it correlates strongly with the strength of the synapse thus, large spines bear very stable and functionally strong synapses. Large spines, in the dentate gyrus, originate after synaptic potentiation, forming synapses that are part of the hippocampal storage system, and they are thought to be responsible for long-term memory. Large spines also contain ribosomes that locally regulate protein synthesis and are surrounded by astroglial cells that regulate local glutamate and Ca^{2+} levels. Dendritic spine heads appear to be targets of Aβ oligomers, implicating the decrease in large spine frequency as a link between Aβ pathology and synaptic dysfunction (Knafo et al., 2008).

A study with APP transgenic mouse models, that present Aβ deposits throughout the brain, was used to investigate the effect of Aβ in brain circuits. This study shows that Aβ plaques interfere with general dendritic spine density and shape, as well as with dendritic spine size, specifically reducing the frequency of large spines, and that dendrites in regions without plaques are affected as well. In the study the dendrites are separated in three categories according to their position in relation to plaques: dendrites that pass within plaques (plaque dendrites), dendrites that contact a plaque but don't pass within it (dendrites in contact with a plaque/in the vicinity of plaques), and dendrites in plaque free areas (plaque-free dendrites). The reported results were that plaque dendrites lose spine density significantly, while dendrites in contact with a plaque, gain spines in relation to control mice dendrites. Meanwhile, plaque-free dendrites present spine densities like those of control mice but show a decreased frequency of large spines (Knafo et al., 2008). These results differ from those of other studies that report a decrease in dendritic spine density in hippocampi containing plaques, without differentiating dendrites due to their position relative to plaques (the inclusion of plaque dendrites for the calculation of the general density of spines in the HC would decrease the value significatively, since these areas are scarce of spines).

The heightened spine density in the vicinity of the plaques could possibly be due to a compensatory mechanism, in which new spines would grow in dendrites around plaques as an attempt to compensate for the loss of spines in dendrites within the plaques. It can also be due to the release of neurotrophic factors from astrocytes that normally surround Aβ plaques. These neurotrophic factors play an important role in neural regeneration and in regulating the development of the nervous system (Razavi et al., 2015). A widespread decrease in the frequency of large spines compared to controls was observed in the APP mice, but interestingly, within plaques the frequency of large spines remained the same as in controls. Although the spine density within plaques (in plaque dendrites) was lower than in plaque-free areas it was only due to a decrease in small spines. These results seem to imply that plaques protect large spines (Knafo et al., 2008).

The prevalence of large spines within plaques explains the weak correlation between plaque load and AD progression. The widespread decrease in large spines frequency can be caused by the soluble Aβ oligomers, which would then be the most toxic forms of Aβ, whereas the plaques could be an inactivated form. Since the plaques occupy a small area percentage of the HC it is likely that the changes in the plaque-free areas are more determinant to cognitive function than those observed within plaques. The

main change observed in plaque-free areas is a substantial decrease in large spine density (the general spine density was normal). Thus, the lower density of large spines should be the cause of the cognitive impairment observed in these mice. Contrarily, the disruption in memory and synaptic plasticity observed in the mice could be impeding plasticity-related spine enlargement (i.e. lowered large spine frequency can be a consequence of the plasticity and memory loss instead of its cause) (Knafo et al., 2008).

A study developed to elucidate the pathogenic role of APP, soluble Aβ and of Aβ plaques in vivo, was conducted with different transgenic mouse models expressing different mutations in the human APP gene (hAPP) (associated with FTAD), that causes overproduction of amyloidogenic Aβ peptides and increases cerebral $A\beta_{42}$ levels. These mice were compared to transgenic mice carrying wild type hAPP (nonmutated) and to nontrangenic mice (controls). The loss of presynaptic terminals was measured and associated with Aβ levels and Aβ plaque levels. Since there is usually a good correlation between cognitive decline and the loss of presynaptic terminals, the goal was to ascertain if there is also a correlation between the loss of presynaptic terminals and Aβ levels or plaque load. First, it was observed that levels of Aβ1-x and Aβ1–42 ($A\beta_{42}$) correlated positively with overall hAPP transgene expression levels and that hAPP mutations affect the formation of amyloid plaques, since age-related Aβ plaque deposition occurs in mice expressing mutant hAPP but not in mice expressing wild-type hAPP or controls. Moreover, wild type hAPP carriers presented high levels of Aβ but did not develop plaques (Mucke et al., 2000).

Interestingly, it was observed that the reduction in presynaptic terminal density was independent of plaque load, because this reduction was observed in all the animals that presented Aβ42 peptide accumulation, both the ones with and without plaques, and the ones with plaque deposits displayed presynaptic terminal deficits before the plaques formed. In fact, mice carrying wild type hAPP, with high Aβ levels, did not develop plaques but had decreased levels of presynaptic terminals, close to those presented by mice with the mutated hAPP. Also, a significant decline in presynaptic terminal density was observed with age in all mice carrying hAPP, but not in nontransgenic controls. All the mice carrying either of the forms of the hAPP gene presented similar loads of Aβ42 or hAPP (even though the WT hAPP did not present plaques) and all of those mice also presented comparable decreases in postsynaptic terminal density, leading to the conclusion that the decrease in presynaptic terminals could be attributable to neuronal overexpression of either Aβ42 or hAPP. Across the different wild-type and mutated hAPP transgenic lines, the decrease in presynaptic terminals correlated proportionally with Aβ1-x and Aβ1–42 levels, but not with Aβ plaque levels. These results interestingly suggest that Aβ synaptic toxicity is independent of plaque formation. The toxicity provoked by Aβ could be mainly due to effects induced by the intraneuronal accumulation of soluble Aβ.

Furthermore, it was observed that plaque formation seems to depend on absolute levels of Aβ42 and on Aβ42/Aβ40 ratio. In fact, in transgenic lines carrying the mutated hAPP gene, plaque formation was closely related to Aβ42 expression levels. Critical levels of Aβ42 seem to be necessary for the development of plaques, but the absence of plaques in the WT hAPP carrier, that also overexpresses Aβ42 shows that high levels of Aβ42 are not enough for plaque formation. It has been hypothesized that different Aβ1–42/Aβ1-x ratios play a key role. It seems that higher Aβ1–42/Aβ1-x ratios lead to plaque formation whereas lower ones do not. Since most of the Aβ1-x that is not in the form of Aβ42 is the form

of Aβ40, it is possible that Aβ40 interferes with Aβ42 aggregation and that it has an antiamyloidogenic effect (Mucke et al., 2000).

2.2.2 Formation of Intraneuronal Neurofibrillary Tangles (NTFs)

Neurofibrillary tangles (NTFs) are intracellular aggregates of hyperphosphorylated tau protein, that are involved in the onset and progression of AD. Tau is a microtubule-associated protein which, in healthy neurons, stabilizes microtubules that form the cytoskeleton of the cell. Tau has other functions such as the promotion of neurite growth, the promotion of interactions between membranes, the facilitation of enzyme anchoring, and the facilitation of axonal transport of organelles to nerve terminals thus, playing a role in synaptic plasticity. Tau protein also regulates microtubule binding and assembly by a process involving its phosphorylation and dephosphorylation (Revett, et al., 2013).

NTFs are mainly found in the cortex, hippocampus and amygdala, the regions most affected by AD. The raphe nuclei and locus coeruleus are also thought to be sites of early NFT formation and aggregation; since these regions are involved in emotion circuitry this could explain the abnormal emotional symptoms (like depression and irritability) observed early in AD patients. The measured number of cortical tangles usually correlates well with the observed cognitive deficits and serves as a good marker of disease progression. Even before the formation of intraneuronal NTFs the hyperphosphorylated tau protein causes instability and disrupts axonal transport, hindering neurotransmitter synthesis, transport, release, and uptake (i.e. it precludes neuronal communication). Axonal transport is carried out by motor proteins that use energy from ATP hydrolysis, it is used to rapidly transport organelles like mitochondria from the soma to the axons and dendrites along microtubules. Its disruption implicates lack of mitochondria at the synapses of neurites which was discovered to cause oxidative stress. Mitochondrial presence at synapses is important for correct neuronal function, and synaptic activity seems to modulate mitochondrial motility and morphology and to control mitochondrial distribution in dendrites as well as their recruitment to the base of dendritic spines (Šerý et al., 2013).

The phosphorylation of tau is a posttranslational modification that has protective effects, although in excess, as is the case of hyperphosphorylation, it can cause neuronal damage. Hyperphosphorylated tau aggregates, forming paired helical filaments (PHFs), which are a major component of NFTs. When tau is hyperphosphorylated, it loses the ability to bind to microtubules, and thereafter to carry out its functions, causing microtubule collapse, axon degeneration and failure of neuronal transport, eventually leading to cell death. Interestingly, some evidence suggests that tau oligomers are the most toxic species, not the higher aggregates such as NTFs. Hyperphosphorylated tau is found in the brains of AD patients, appearing 3 to 4 times more phosphorylated than normal. This is due to an imbalance in tau phosphorylation and dephosphorylation levels caused by abnormal tau protein kinase and protein phosphatase activities, which are the enzymes responsible for the phosphorylation and dephosphorylation of tau.

Intraneuronal tau is predominantly localized in the axons, contributing to synapse physiology. Up to six tau isomers are expressed in the human brain, due to alternative splicing of the MAPT gene (tau protein

gene) at exons 2, 3, and 10, that results in some variations, like the alternative insertion of either 3 or 4 repeated amino acid sequences in the microtubule-binding domain, originating the 3R or 4R tau isomers. The ratio of 4R/3R tau isomers should be close to 1:1. In fact, an imbalance in the 4R/3R ratio can lead to neurodegeneration. More than 50 mutations have been identified in the MAPT gene. These appear to interfere with the structure of tau protein or with the splicing of exon 10, leading to abnormal 4R-tau elevation and thereafter causing excessive tau aggregation.

Tau protein phosphorylation is regulated either directly or indirectly by epigenetic modifications, creating a link between these and AD pathology. Epigenetic modifications consist on heritable alterations in factors, such as DNA or RNA methylation, histone modification, and noncoding RNA regulation, that affect gene expression without changing the DNA sequence of the gene. Changes in the surroundings of the cells, like stress inducing situations, can cause intracellular epigenetic modifications that may promote gene transcription or gene silencing. The epigenome acts as a dynamic intermediate between the external environment and the genome. Noncoding RNAs (ncRNAs), like microRNAs (miRNAs), are a type of posttranscriptional regulation, common in the central nervous system (CNS). They regulate gene expression by binding to the 3 untranslated region (3-UTR) of the mRNAs of a target gene, through complementary base pairing, precluding transcription (Yu et al., 2019).

Evidence suggests that abnormal ncRNA expression in the brain can affect AD development, since miRNAs regulate the expression of genes encoding AD-associated proteins, like APP and β-secretase. Moreover, many miRNAs can alter the 4R/3R tau isomer ratio in neurons. A downregulation of miRNA-219 and miRNA-132 in the brain of AD patients as been observed. It was then understood that miRNA-219 inhibits tau synthesis, whereas miRNA-132 represses Aβ peptide synthesis and tau hyperphosphorylation. In fact, the upregulation of miRNA-132 reduces total tau protein levels, promotes axon extension and bifurcation, enhances synapse plasticity, and prevents neuronal loss. On the contrary, its downregulation can promote tau protein overexpression, hyperphosphorylation, and aggregation. Tau acetylation was also shown to promote tau autophosphorylation and abnormal aggregation. It was observed that the genes responsible for the expression of the proteins that determine tau acetylation (acetyltransferase and deacetylase) are targets of miRNAs regulation. Thus, MiRNAs can, directly or indirectly, control the expression of several tau phosphorylation-associated proteins therefore, affecting the level of tau phosphorylation in the brain.

DNA methylation is another common epigenetic modification that is considered a form of transcriptional regulation. The methylation of promoter regions can repress the transcription of target genes. The analysis of brain sections from deceased AD patients has revealed decreased DNA methylation levels in their cortex and HC. In fact, DNA methylation appears to have an important role in the aberrant expression of genes associated to AD. Abnormal methylation levels in the promoter regions of tau phosphorylation-related genes has also been observed in brains of AD patients (Yu et al., 2019).

In chromosomes, the DNA is wound around histone proteins that maintain its configuration. Histones can be modified by acetylation, methylation, phosphorylation, among others. These modifications affect gene transcription by modulating the spatial conformation of chromatin. Acetylation and methylation of histones reduces the affinity between the DNA and histones, loosening the chromatin structure, and

making gene transcription easier (favors gene transcription). On the other hand, deacetylation of histones tightens the spatial conformation of chromatin and precludes gene transcription. Histone modifications have been shown to play a role in AD, since elevated levels of the protein responsible for histone deacetylation (HDAC) have been reported in AD patients' brains, suggesting that the downregulation of some genes implicated in brain protection (for example, genes involved in the clearance of toxic aggregates) might be due to increased tightening of the chromatin structure surrounding those genes. In conclusion, NcRNAs, DNA methylation, and histone modifications form a complex epigenetic regulatory network that modulates tau phosphorylation. Their regulation could be a possible future prevention and treatment strategy for AD. However, epigenetic-based therapy currently lacks specificity and may affect numerous collateral targets, not representing, at this moment, a viable therapy for AD (Yu et al., 2019).

Importantly, Aβ also appears to be involved in tau hyperphosphorylation, since studies have reported that Aβ40 and Aβ42 can induce tau protein phosphorylation by activating proteins that phosphorylate tau. Moreover, cells undergoing Aβ toxicity show elevated levels of tau phosphorylation and neurons cultured from tau protein knockout mice are resistant to Aβ toxicity, suggesting that the mechanism through which Aβ exerts its toxic effects in the brain involves tau. It seems possible that Aβ is the root of many pathologies that cause AD (Revett, et al., 2013).

2.2.3 Neuroinflammation

Neuroinflammation refers to inflammatory responses within the brain or spinal cord, that are mediated by microglia, the immune cells of the CNS. There are different degrees of neuroinflammatory responses, some of which have positive outcomes, defending the brain from pathogens. A low-level and chronic inflammatory response usually accompanies aging, causing reduction of neuronal plasticity and some cognitive impairment. In neurodegenerative diseases, a higher degree of chronic inflammation is observed, which is highly damaging to the nervous system (DiSabato, Quan and Godbout, 2016). In fact, evidence suggests that AD arises not only due to dysregulations at the neuronal level but also due to an imbalance of immunological mechanisms in the brain. Misfolded and aggregated proteins trigger immune responses from glial cells by binding to their pattern recognition receptors. The initiation of the immune response consists on the release of inflammatory mediators, such as cytokines or chemokines, that end up contributing to the progression of neurodegeneration. Further strengthening this idea, several genes that were discovered to increase the risk for sporadic AD, like TREM2 and CD33, are related to immunological responses in the brain, encoding for factors that regulate glial clearance of misfolded proteins.

Microglia are the resident phagocytes of the CNS, their role is to survey the brain for the presence of pathogens and cellular debris, while also providing factors that support tissue maintenance thus, protecting synapses and the plasticity of neuronal circuits. When microglia are activated by pathological triggers, like neuronal death or protein aggregates, they migrate to the site of injury and carry out an immune response. Microglial receptors can bind to soluble Aβ oligomers and to Aβ fibrils, initiating an

inflammatory reaction. Microglia then engulf Aβ fibrils by phagocytosis, and the fibrils enter the endosomal/lysosomal pathway to be destructed. Soluble Aβ can be degraded by a variety of extracellular proteases, whereas fibrillar Aβ is generally resistant to enzymatic degradation. Inefficient clearance of Aβ has been identified as a pathogenic pathway in sporadic AD cases (Heneka et al., 2015). It seems that clearance of Aβ by microglia needs to be done while it is in the form of soluble oligomers, before the formation of plaques. If the Aβ clearance is not efficient (i.e. if it is not fast enough) as it happens in AD, allowing the formation of plaques, which are more resistant, it then leads to the pointless accumulation of glial cells around plaques, creating a sterile inflammatory response.

In healthy brains, when the tissue is exposed to a damage inducing factor or to a pathogen, microglia enable the quick removal of the recognized abnormality or pathology. However, in AD, in which the accumulation of Aβ is apparently the key factor that drives neuroinflammation, the ongoing formation of Aβ compromises the cessation of the response, establishing a chronic, non-resolving inflammation. This also implies that microglial cells are engaged in the plaque sites, where their action is sterile, and are not available to deal with other damaging factors that might come up (i.e. microglial cells are impaired). Interestingly, although most neuroinflammation in AD is not beneficial, and ends up contributing to disease progression, some cases, in mouse models, have been reported in which the inflammation reduces amyloid plaque burden, suggesting that there is a good form of pro-inflammatory microglial activation (Heneka et al., 2015).

Since Aβ deposition in the brains of patients seems to precede AD symptoms by decades, it is possible that some external factors influence the immune response carried out by microglia due to Aβ exposure, accelerating or slowing down the onset of symptoms and the progression of the disease. Some factors like obesity and traumatic brain injury have been shown to increase neuroinflammation. Obesity is a neuroinflammation factor because white fat tissue contains a lot of activated macrophages, that constantly secrete proinflammatory cytokines. And traumatic brain injury may initiate an inflammatory response at the site of injury that persists for months or even years, decreasing the ability of microglia to degrade soluble Aβ (Heneka et al., 2015).

2.2.4 Acetylcholine deficiency

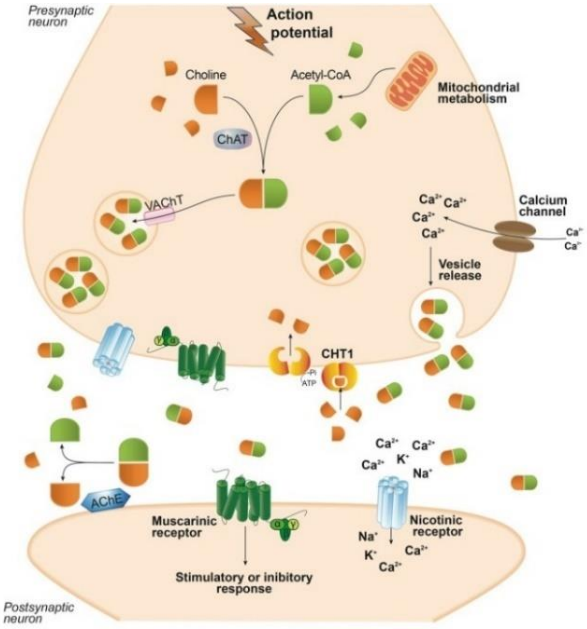

Figure 2.3: Acetylcholine neurotransmission between two cholinergic neurons (H. Ferreira-Vieira et al., 2016).

Acetylcholine (ACh) is the neurotransmitter used by cholinergic neurons, which are widely distributed in the peripheral and central nervous system (CNS). Ach is synthesized in the cytoplasm of cholinergic presynaptic neurons from choline and acetyl-coenzyme A (acetyl-CoA), which is provided by mitochondria, by the enzyme choline acetyltransferase (ChAT). The neurotransmitter is then transported to synaptic vesicles (acetylcholine transporter (VAChT)) that carry it to the plasmic membrane, where it undergoes exocytosis. Ach reaches the synaptic cleft where it can bind and activate its receptors (muscarinic and nicotinic receptors). The Ach present in the synaptic cleft is rapidly hydrolyzed by the enzyme acetylcholinesterase (AChE), which is also secreted by cholinergic neurons. The AChE binds to the plasma membrane and hydrolyses 5000 Ach molecules per second (it is one of the most kinetically efficient enzymes know), converting them to choline and acetate. The presynaptic neuron reuptakes the choline released (H. Ferreira-Vieira et al., 2016).

The cholinergic system is involved in fundamental physiological processes, such as attention, learning, memory, stress response, wakefulness and sleep, and sensory information. Cholinergic neurons located in the basal forebrain (including the ones that form the nucleus basalis of Meynert) are important in memory and are markedly lost in AD. Almost all regions of the brain are innervated by cholinergic neurons, and ACh has a crucial role in cognition. The cholinergic system seems to be a significant factor in many forms of dementia, like AD (H. Ferreira-Vieira et al., 2016). Deficits of cholinergic transmission might have a heavy influence in all aspects of cognition and behavior, including the disruption of the ability of specific brain areas like the hippocampus and the cortex to process information. The disruption of ACh inputs in the cortex can cause impairment in attention and in the ability to use instructive cues, which are necessary to make simple decisions related to ongoing behavior (Muir et al., 1992).

Choline acetyltransferase (ChAT) activity was examined in autopsy samples from 3 different groups of subjects, some with AD, others with dementia caused by cerebrovascular disease and controls (non-demented aged individuals). It was observed that ChAT activity was considerably reduced in brains of AD patients, and that this reduction correlated positively with the severity of the symptoms observed and with the numbers of neurofibrillary tangles. On the other hand, no ChAT activity reduction was observed in patients with cerebrovascular dementia or in controls. This shows that ChAT reduction is specifically related with AD type of dementia (Wilcock et al., 1982).

Attention is the first non-memory domain affected in AD patients and it seems that attention deficits are responsible for the first difficulties with their daily living. In a study aiming to detect whether a one-year treatment with cholinesterase inhibitors (to increase the activity of the cholinergic system) was more effective in preserving attention or memory it appeared that the treatment specifically attenuated the decline in attention and executive functions. A stabilization of the ability to pay attention was observed, with subsequent positive effects on executive functions, recent memory, and information acquisition which depend on attention. Therefore, attention seems to be the main mechanism through which cholinesterase inhibitors affect cognition (Bracco et al., 2014).

Executive functions (EFs) make possible to mentally play with ideas; taking time to think before acting; meeting novel, unanticipated challenges; resisting temptations; and staying focused. Many ADHD (attention-deficit/hyperactivity disorder) symptoms are related with lack of EF. If something is not right in the life of a person, EFs and the prefrontal cortex (involved in decision making) are the first to become affected. Importantly, EFs are disturbed with stress, sadness, sleep deprivation, loneliness and physical unfitness. Therefore, these conditions may cause someone to appear to have an EF disorder, like ADHD, even if they do not (Diamond, 2013).

2.2.4.1 Neuropsychiatric Symptoms in AD

Most AD patients develop neuropsychiatric symptoms (NPS), that affect mood and behavior. NPS that come with AD are a consequence of alterations in specific brain circuits and they can be used as an indication of disease progression. The most commonly observed NPS in AD are agitation, apathy, depression, and psychosis (particularly delusions). These symptoms become more apparent as the severity of brain damage increases (Rosenberg, Nowrangi and Lyketsos, 2015). Agitation is one of the most problematic NPS for AD caregivers and it is defined as emotional distress manifested by excessive motor activity and verbal or physical aggression (Cummings et al., 2014). It has been associated with volume loss in the cortex, hippocampus, amygdala and insula. Several studies using brain autopsies have associated agitation with decreased levels of cholinergic markers and with decreased levels serotonin and serotonin metabolites. It has also been linked to high levels of tau and phosphorylated tau (Rosenberg, Nowrangi and Lyketsos, 2015).

Apathy is the most common neurobehavioral symptom related with AD (Martorana and Koch, 2014). It is defined as a decrease in motivation and initiative; a decline in goal-directed behavior, goal-directed cognitive activity, and emotions; and functional impairments that persist over time (Robert et al., 2009). It is related with cortex degeneration as well as with amyloid burden in the cortex and with the presence of tau in the cerebrospinal fluid. In later stages of the disease, AD patients can also present symptoms of psychosis which include delusions, defined as a “fixed false belief”, and hallucinations. They are associated with deficits in the cortex, including reduced grey matter volume. Depression is another NPS common in AD, it seems to be associated with reduced cortical thickness and accelerated atrophy of the cortex. There are no drugs approved specifically for these NPS associated to AD, nevertheless some psychotropic medications are often prescribed for the symptoms.

There is evidence that NPS in AD are caused, not simply by the disturbance of a certain brain region, but rather, by the disruption of specific neuronal networks, which result from highly thorough and balanced interactions between regions. The variability of NPS phenotypes between patients is the consequence of the different brain networks that might become affected. An example of this is the default mode network (DMN), a circuit that is active when a person is not focused on external stimuli and the brain is in a state of wakeful rest, i.e. when a person is not thinking about anything in particular and the mind is "wandering". The DMN circuit is important for the brain to consolidate experiences, and it has been shown to be disrupted early in AD, which is thought to be the cause for some of the first cognitive impairments visible in patients, like the loss of executive functions.
Agitation in AD arises due to a misinterpretation of threats that is caused by cognitive deficits. For example, agitation can arise due to an agitation network disorder (that may cause inflated estimates of threat probability and cost, and heightened reactivity to threat uncertainty) combined with an impairment in memory circuits (such as amnesia which causes a patient to forget routine events or agnosia which causes them to not recognize familiar people). Agitation in AD is associated with elevated tau protein and decreased acetylcholine and serotonin neurotransmission, which come from deep brain structures. Since most circuits connecting deep brain structures to the cortex are inhibitory, the decreased concentration of acetylcholine and serotonin in these circuits would imply less inhibition of the cortex and agitation can be understood as a consequence of the lack of inhibition, that usually serves to control behavior (Rosenberg, Nowrangi and Lyketsos, 2015).

As for apathy, it is believed to be related with behavioral and cognitive avoidance, as a mechanism that patients use to avoid situations and thoughts that could provoke anxiety. There is evidence of a relationship between the dopaminergic system and apathy in AD. Some hypotheses even present the idea that the loss of cholinergic neurons, which creates impairment in dopaminergic transmission, could be the main cause of the observed NPS in AD (Rosenberg, Nowrangi and Lyketsos, 2015). Delusions in AD have been associated with increased dopamine receptor density. A hypothesis is that dopamine increases to compensate the decrease in acetylcholine and serotonin and that the imbalance of dopamine relative to the other neurotransmitters causes delusions (Rosenberg, Nowrangi and Lyketsos, 2015).

2.2.4.2 The involvement of Dopamine (and other monoaminergic neurotransmitters) in AD

Although the involvement of dopamine (DA) in AD is still up for debate, new factors are coming up that link this vital neurotransmitter to the disease. Distinct neuron populations use acetylcholine, serotonin, histamine, dopamine, gamma-aminobutyric-acid (GABA) or glutamate as their main neurotransmitters and are differently affected in brain disorders according to their class. The cholinergic neurons are the most sensitive to Aβ toxicity, followed by the serotoninergic. The GABA-ergic are the less sensitive and the dopaminergic present intermediate vulnerability, having an unclear relationship with Aβ pathology (Martorana and Koch, 2014). The monoamines are a subgroup of neurotransmitters that have an amino group attached to an aromatic ring by a chain of two carbons. This category comprises dopamine, norepinephrine also called noradrenaline, serotonin and histamine.

The ascending monoaminergic (MA-ergic) system contains the neuronal populations of the dopamine-ergic (DA-ergic), noradrenergic (NA-ergic), serotonergic (5HT-ergic), and histaminergic (HA-ergic) systems (Editors: Ahmad Salehi, n.d.). The MA-ergic system is constituted of sub-cortical nuclei, that are cellular structures, like the locus coeruleus, the raphe nuclei, and the tuberomamillary nucleus, where the monoaminergic neurotransmitters are produced. These mid-brain structures are notably vulnerable to neurodegeneration, because they are predisposed to neurofibrillary tangle and senile plaque accumulation and therefore, are affected significantly in AD, since the onset of the disease (Parvizi, Van Hoesen and Damasio, 2001). A link between abnormalities in the structure and function of subcortical monoaminergic systems and AD has been settled. Furthermore, recent studies in animal models of neurodegeneration have demonstrated that the MA-ergic system can be a target for the restoration of cognitive function (Trillo et al., 2013). Through huge projections to the cortex and hippocampus, the MA-ergic system exerts a strong modulatory effect on brain regions that are essential for cognition. The MA-ergic neurons are numerically sparse but one of these cells can innervate thousands of cortical and hippocampal neurons, through ascending fibers that spread the monoaminergic neurotransmitters. The cortex and hippocampus are vital for cognitive function, so their lack of enervation by the MA-ergic neurons, caused by the severe progressive degeneration of the sub-cortical nuclei in AD, can be the cause for the cognitive decline observed since early in AD patients (Editors: Ahmad Salehi, n.d.).

Mid-brain dopaminergic neurons, that originate in sub-cortical nuclei (ventral tegmental area (VTA) and substantia nigra pars compacta (SNc)), make up around 90% of all dopaminergic cells and innervate brain regions in charge of motivation, memory and motor behavior. Each nucleus has different functions, influencing diverse brain regions. The SNc gives rise to a pathway that is involved in the control of voluntary movements and the VTA leads to a pathway involved in the control of will and reward.

DA is metabolized into norepinephrine (NE). NE is produced in the neurons of the locus coeruleus (LC) nucleus and is then distributed to areas like the hippocampus, cortex and cingulate gyrus. LC neurons suffer severely in AD, even more than cholinergic neurons. It has been reported that AD patients present reductions in NE levels that correlate proportionally to disease duration and cognitive decline, although it has been observed that remaining NE-ergic neurons increase NE production as a compensatory mechanism.

Serotoninergic (5HT-ergic) neurons originate mainly in the dorsal raphe nucleus and modulate the cortex, hippocampus, hypothalamus, septum and striatum. The 5HT-ergic system is one of the most affected in AD due to neuronal loss that causes a decrease in neurotransmitter levels and metabolites combined with the absence of compensatory mechanisms. Postmortem exams of brains of AD patients have shown that levels of serotonin are decreased by 40-50%, the most accentuated neuronal loss being in the part that innervates the hippocampus. AD patients also show changes in the levels of melatonin, which is a precursor of serotonin. Postmortem exams also showed that the imbalance in serotoninergic and cholinergic systems correlates with the degree of cognitive impairment of the patient before death, indicating that these imbalances impact cognition.

Histaminergic (HA-ergic) fibers originate uniquely in the tuberomamillary nucleus of the hypothalamus and they reach nearly every part of the brain. HA fibers play an important role in cognitive function, by inducing long term potentiation (LTP). HA acts as a neuromodulator in the HC and is a central neurotransmitter, involved in attention, learning and arousal. Although loss of neurons from the tuberomamillary nucleus has been observed in postmortem assessments of brains of AD patients, the levels of HA are lower in some brains and higher in others, suggesting compensatory mechanisms of the remaining neurons (Editors: Ahmad Salehi, n.d.). Altogether, degenerations of the MA-ergic systems, which are an early event in AD, might account for the first symptoms of weakening cognition observed in patients.

The DA system changes naturally with aging, namely the levels of DA released from terminals and the expression of DA receptors in the brain decrease with age. A reduction in the release of neurotransmitter glutamate also seems to further reduce DA release. The reduction in DA leads to hypo-activity, gait disturbances and decline of executive functions. The manifestation of apathy in AD patients (and in non-demented elderly people) is suggested to be the consequence of impairment of the DA transmission and is predictive of faster cognitive decline and life shortening. Thus, implicating the impairment of the DA system as a negative prognostic of disease evolution. The earlier it appears, the faster the cognitive decline will advance (Martorana and Koch, 2014). In a study with AD mouse models, it was observed that Aβ plaques contribute to the disfunction of DA transmission. Additionally, the restoration of DA transmission seemed to be important in memory and learning in these mice, implying DA in cognitive tasks. Moreover, drugs targeting the DA-ergic system have shown good results by positively impacting cognition and neuronal plasticity mechanisms, further strengthening the hypothesis of the involvement of DA in AD.

The main hypothesis for dopamine disfunction in AD is based on the neuronal nicotinic acetylcholine (Ach) receptors (nAChR). nAChRs regulate the release of neurotransmitters and allow Ach to participate in attention, learning and memory functions, by binding to the α4β2 and α7 nAChRs. The α7nAChRs are predominantly located in the hippocampus, prefrontal cortex, thalamus, and dopaminergic and serotoninergic neurons of sub-cortical nuclei (DA neurons of the VTA and serotonin-raphe nucleus) allowing these regions to be modulated by Ach. There is evidence that Aβ oligomers can bind to α7nAChRs with high affinity and that this interaction has a positive outcome if in small concentrations. The prolonged exposure of α7nAChR to Aβ oligomers (at high Aβ concentrations), on the other hand, has a neurotoxic outcome, inducing long term depression (LTD) and damaging synaptic plasticity mechanisms.

It is possible that DA-ergic disfunction in early AD is caused by Aβ peptides binding to the α7nAChR. This interaction can cause the α7nAChR receptors to become overwhelmed and disrupted, impairing Ach modulation of the neurons affected (such as the DA-ergic and 5HT-ergic), in turn interfering with the physiological function of dopaminergic and serotoninergic systems. Moreover, the disruption of the α7nAChRs would also progressively impair the release of glutamate and GABA neurotransmitters (which are modulated by Ach as well) and in turn lead to lower DA release in the prefrontal cortex and HC, contributing to the first issues visible in AD patients namely, memory, attention and executive

function deficits. Furthermore, the progressive cut in glutamate modulation can eventually lead to a reduction of the dopaminergic neurotransmitters released in the mid-brain nuclei, being responsible for apathy.

2.2.5 Glutamate excitotoxicity

Excitatory amino acids serve as the primary excitatory neurotransmitters (which produce an excitatory response) in the cerebral cortex and hippocampus. Neurons containing excitatory amino acids play essential roles in memory formation and learning because they help mediate synaptic transmission, neuronal growth and differentiation, and synaptic plasticity. They also seem to be early targets in neurodegenerative diseases like AD and are situated in areas that are known to be affected in AD such as the cortex, the HC and amygdala. The amino acid glutamate is the most common neurotransmitter in the brain, and it is the main excitatory neurotransmitter in the mammalian central nervous system (CNS). Excitotoxicity consists of cell death provoked by toxic action of excitatory amino acids, it usually means toxicity caused by prolonged exposure to glutamate, causing excessive activation of glutamate receptors and the consequent excessive influx of ions in neurons, particularly calcium ions (Ca^{2+}), that become neurotoxic eventually leading to cell death (Dong, Wang and Qin, 2009).

The function of the glutamatergic system is to convert nerve impulses into a chemical stimulus by controlling the concentration of glutamate at the synapse (Revett et al., 2013). In the presynaptic neurons there are vesicles (VGLUT1 and 2) that maintain glutamate levels and transport it to the synaptic cleft, releasing it when the synapse is activated. Glutamate activates 2 families of receptors at the synaptic cleft, ionotropic receptors (iGluRs) and metabotropic receptors (mGluRs). Ionotropic receptors are ligand gated transmembrane ion channels permeable to some cations (Dong, Wang and Qin, 2009), the main ones that glutamate binds to are the N-methyl-D-aspartate (NMDA), the α-amino-3- hydroxy-5methyl-4-isoxazolepropionic acid (AMPA) and the kainate (KA) receptors. The NMDAR is predominantly permeable to Ca^{2+} ions, whereas AMPA and KA receptors are mainly permeable to Na^{+} and K^{+} ions. When glutamate is released into the synaptic cleft it activates AMPA receptors first, this receptor allows Na^{+} ions to enter the postsynaptic neuron, creating an action-potential in the membrane (depolarization of the membrane). When the synapse is not activated by glutamate, the channel of NMDA receptors is blocked by a Mg^{2+} ion, which is the natural antagonist of this receptor. Only when an action potential is created in the membrane by the entry of sodium ions, the magnesium liberates the channel of the NMDA, activating the receptor for the entry of Ca^{2+} ions in the postsynaptic neuron, i.e. the AMPA receptor (AMPAR) has to be activated first in order for the NMDAR to become activated. If the glutamate input in the synaptic cleft is not big enough only the AMPAR will become activated.

The entry of calcium ions in the postsynaptic membrane activates downstream pathways in the cell. Glutamate is then removed from the synaptic cleft by excitatory amino acid transporters (EAATs), that are mainly expressed in astrocytes. These transporters take the glutamate to the interior of astrocyte cells where it is converted to the amino acid glutamine. Glutamine is then transported back to presynaptic neurons and converted back to glutamate, eventually returning to the presynaptic membrane in vesicles, that maintain glutamate levels in presynaptic terminals - this is known as the glutamate-glutamine cycle. AD patients have shown disruption in this glutamate cycle (caused by Aβ

peptides) namely, increased glutamate release in the synaptic cleft and decreased glutamate removal by astrocytes, which causes excitotoxicity and perturbances in the glutamate receptors (Revett et al., 2013). Studies in AD brains have found reduced levels of VGLUT1 and VGLUT2 expression as well as of EAAT1 and EAAT2 around neurons in affected areas. Decreased AMPA receptor levels have also been observed in some areas and this decrease correlated well with how affected the specific area is. KA receptor binding has also been noticed to be reduced in the HC of individuals with AD.

The other family of glutamate receptors in the postsynaptic membrane is of the metabotropic receptors. These are linked to small intracellular chemicals called G-proteins that when activated dissociate from the receptors and activate a molecule called a second messenger which then sends a signal by activating another particle. The metabotropic receptors mediate slow synaptic responses and their roles are more varied. The second messengers might interact with an ion-channel in another part of the neuron membrane and activate it, but they can also interact with different intermediate molecules in the cell. 8 different metabotropic receptors have been identified until now and almost every step involved in their signaling pathway is modulated by calcium ions. The depletion of Ca^{2+} from the synaptic cleft, that has been observed in AD patients, leads to substantial inhibition of postsynaptic mGluRs. In fact, levels of mGluRs are reportedly reduced in a general manner in the cortex and HC of AD patients.

The excess of glutamate in the synaptic cleft causes the continuous activation of glutamate receptors (excitotoxicity), mainly NMDA receptors, which in turn will allow an excessive influx of Ca^{2+} to the cell. The excess of intracellular calcium ions promotes a cascade of events that can lead to apoptosis or necrosis. Apoptosis is the process of programmed cell death, and its excess is one of the aspects of neurodegenerative diseases. Apoptosis is a controlled and energy-dependent mechanism that can affect individual cells or cell clusters. The apoptotic process begins when caspases, which are cysteine proteases widely expressed in an inactive form in the cell, are activated, starting an apoptotic pathway that leads to rapid cell death. Necrosis, on the other hand, is an uncontrolled process that usually affects a large range of cells, it is an energy independent toxic mechanism, in which the cell is considered a passive “victim” (Elmore, 2007). The calcium ion has an essential role in apoptotic cell death and so it is thought that its excessive concentration activates apoptotic proteases such as caspases and calpains. Calpains are a family of calcium activated cysteine proteases that can regulate protein degradation in the cytosol and have been implicated in necrosis and apoptosis (Stansfield et al., 2014) (Wells and Leloup, 2010).

Acute excitotoxicity is thought to be caused by the excessive depolarization of the postsynaptic membrane, caused by NMDAR prolonged activation, that allows a disproportionate influx of Ca^{2+}, then leading to the entrance of other ions, like Cl^- and Na^+, and water, which enters by osmose (so the more ions enter the more water enters too), eventually resulting in cell lysis. (Dong, Wang and Qin, 2009). The exaggerated calcium ion concentration in neurons, due to excitotoxicity, also changes the intracellular pH leading to the activation of pH regulating systems like the Na+/H+ exchange (NHE). The NHE is an ion pump that plays an important role in maintaining the cytosolic proton concentration (which is different from the extracellular one) but, its activation decreases the activity of another ion pump that exchanges Na^+ and Ca^{2+}, leading to an even bigger accumulation of Ca^{2+} in the cytosol and, contributing

to cell death (Launikonis et al., 2017) (Dong, Wang and Qin, 2009). Therefore, blocking the excessive influx of Ca^{2+} to the postsynaptic neuron can reduce the sensitivity of the cell to apoptotic stimuli.

Several studies suggest that the increased intracellular concentration of Ca^{2+} can cause an excessive accumulation of these ions inside sensitive organelles such as mitochondria and the endoplasmic reticulum (ER). Mitochondrion produce the energy of the cell through ATP oxidative phosphorylation and allow cellular respiration. They also play an important role as buffering sinks of the cell since they have a high capacity to store ions, such as Ca^{2+}, inside themselves, balancing their concentration in the cytosol. The problem is when there is too much calcium to be taken up by mitochondrion, and the increased concentration of Ca^{2+} inside the organelle leads to the opening of mitochondrial permeability transition pores. In situations of intense stress, the opening of this pores will activate the release of pro-apoptotic factors, such as cytochrome c, and release the calcium ions back to the cytosol.

Thus, mitochondrial Ca^{2+} plays an important role in the modulation of cellular responses, such as apoptosis (Szymański et al., 2017) and autophagy, determining cell fate. Mitochondrion produce apoptotic signals by changing the permeability of its membrane and releasing protein factors into the cytosol that promote apoptosis, like cytochrome c. Those factors are believed to induce cell death by degrading cytoskeletal proteins and proteins involved in DNA repair. In cases of lower intensity stress, the mitochondrial membrane might become depolarized, as its permeability is changing, and lead to autophagy, which selectively removes damaged mitochondria as a cytoprotective mechanism. An exaggerated amount of autophagic mitochondrion in the cell can also cause apoptosis through the release of lysosomal enzymes (Dong, Wang and Qin, 2009).

Excitotoxicity is known to provoke oxidative stress, defined as an imbalance between the intracellular production of reactive oxygen species (ROS) and the ability of the cell to defend its constituents against the toxic effects of these species. Generation of high levels of ROS and the downregulation of antioxidant mechanisms results in oxidative damage and neuronal death, being a major factor in neuropathology. The main free radicals that can cause oxidative stress are superoxide radical ($O_2^{\cdot -}$), peroxynitrite ($ONOO^-$) and hydroxyl radical ($OH^{\cdot}$). Oxidative stress damages nucleic acids, proteins and lipids, and it can open the mitochondria transition pore causing energy failure and stimulating apoptosis. Besides, the production of nitric oxide (NO) is increased in neurodegenerative diseases as a result of excitotoxicity. When NO reacts with superoxide radicals ($O_2^{\cdot -}$), the oxidative agent peroxynitrite ($ONOO^-$) is formed. It is believed that the toxic effects of NO result from the action of this highly reactive metabolite. $ONOO^-$ has been shown to induce oxidative damage in the DNA and to promote the overexpression of metalloproteinases which destroy the surroundings of neurons, leading to their death by apoptosis. Thus, the presence of free radicals and of NO and $ONOO^-$ in the brain, adds up to the neuronal damage experienced by AD patients (Dong, Wang and Qin, 2009).

2.2.5.1 Aβ and glutamate excitotoxicity

The extracellular deposition of Aβ has been shown to interfere with the glutamate NMDA receptor in the synaptic cleft and stimulate excessive generation of reactive oxygen species (ROS) through a mechanism that requires the activation of the receptor. Moreover, mitochondria are an intracellular site of ROS production, and the levels of mitochondrial ROS production increase in an age-dependent

manner (Szymański et al., 2017). Excessive mitochondrial ROS production has been shown to also induce the opening of mitochondrial permeability transition pores. Furthermore, when ion levels are high, macrophages, astrocytes, and endothelial cells produce excess NO, potentially causing oxidative stress and tissue dysfunction. Thus, mitochondrial distress can cause cellular death by affecting cellular calcium homeostasis (if they release their ion storage into the cytosol), by releasing apoptogenic proteins in the cytosol, and by enhancing the production of toxic species (Dong, Wang and Qin, 2009).

There is evidence that in AD, autophagy is induced but then it is stopped in latter steps of the pathway, and more evidence shows that mutations that cause AD also interfere with the lysosomal-autophagy pathway, disrupting autophagy. The inability to carry out autophagy might explain the accumulation of intracellular Aβ peptides that eventually become part of extracellular plaques.

Long-term potentiation (LTP) and long-term depression (LTD) are the main processes of long-lasting synaptic plasticity in the vertebrate CNS. LTP and LTD make many forms of learning and memory possible and their dysregulation contributes to diverse brain disorders. LTP is a process by which synaptic connections become stronger and denser due to frequent activation. It is thought to be a way in which the brain changes in response to experience, through learning and memory formation, that are possible due to the establishment of new neuronal networks. Glutamate mediated neurotransmission is essential for LTP and thus, for memory formation (Revett, et al., 2013).

LTP is generated by high-frequency stimulation of the presynaptic plasmatic membrane, resulting in increased release of glutamate and consequent activation of its receptors at the postsynaptic membrane. One form of LTP was found to be triggered by synaptic activation of the MNDA glutamate receptors, and subsequent entry of Ca^{2+} in the postsynaptic neuron, NMDAR-LTP being the predominant form of plasticity in the brain (Park et al., 2014). However, the AMPARs and mGluRs are the ones activated by the initial glutamate release, while NMDARs only become fully active with continuous synchronized glutamate stimulation following activation of the AMPARs and mGluRs. This mechanism sets off different kinase pathways and increases transcription of specific proteins. LTD happens due to little stimulation at a synapse or because stimulation of the iGluRs is asynchronous. It can also be caused by a reduction in the levels of NMDA and AMPA receptors in the postsynaptic membrane, or by weak stimulation of AMPARs that does not lead to the depolarization of the postsynaptic membrane, and thereby does not activate NMDAR completely. LTD reduces synaptic strength and prevents memory formation, having the opposite effect of LTP (Revett, et al., 2013).

LTP and LTD are implicated in neurodegenerative diseases such as AD in which, a decrease in LTP and an increase in LTD are observed. Interestingly, the glutaminergic system is upregulated in mild AD before it appears to be disrupted (as AD progresses), which is probably an initial compensatory mechanism like the one observed in the cholinergic system. The compensatory upregulation of cholinergic presynaptic boutons happens before the compensatory upregulation of the glutaminergic system which indicates that the cholinergic system is affected first and that its disruption might drive the disruption of the glutaminergic system in AD (Revett, et al., 2013).

Pyramidal neurons are the most common neuronal class in the excitatory population of brain areas like the cortex, hippocampus and amygdala. They make up around two thirds of all cortical cells. Their function is, as many other neurons, to transform synaptic inputs into a patterned output of action

potentials, enabling the existence of high-level functions, like consciousness. They are named because of their shape, since they possess a teardrop like soma with many dendrites, some longer coming from the pointy end, arising from a long dendrite that ramifies (apical dendrites), and some shorter from the base (basal dendrites), both disposed in a conical way. These cells are “projection neurons”, because they have long axons (coming from the base of the soma) that can go long distances and modulate different regions of the brain. Because of their ubiquitous input, problems in these cells cause brain disorders, such as Epilepsy, due to excessive neuronal excitation, particularly in the HC, and degenerative disorders, due to disproportional killing of such cells (Bekkers, 2011). Cortical pyramidal neurons are known to have both cholinergic and glutaminergic receptors and to receive input from other cholinergic neurons. There is evidence that the activation of cholinergic receptors with cholinesterase inhibitors also activates glutaminergic receptors in cortical pyramidal neurons proving a close relationship between these two systems (Revett, et al., 2013).

There is also a relationship between the glutamatergic system and APP processing which is believed to be a root cause of AD development. The activation of iGluRs and mGluRs has been shown to regulate the relative activity of the amyloidogenic (β-secretase cleavage) and nonamyloidogenic (cleavage by α-secretase, which is part of the ADAM proteins family) pathways. Studies have shown that NMDA receptor and mGluR 1 activation with agonists increases nonamyloidogenic APP processing, since it has been shown to increase soluble APPα release and to reduce Aβ formation, likely by increasing trafficking and activation of α-secretases at the cell membrane.

Differently, in AD brains, NAMDRs are activated by high glutamate concentrations and for prolonged periods (i.e., more than 24 h), and in this case it is observed that they mediate increased amyloidogenic APP processing by increasing the size of the APP chain that is expressed, leading to higher Aβ levels. APP expression shifts from an APP695 isoform size to longer isoforms like APP751 and APP770, which are more amyloidogenic. Another mechanism that has been suggested is that the NMDAR mediated Ca^{2+} influx triggers the fusion of synaptic vesicles to the plasmatic membrane thus, elevating the rate of endocytosis to recycle these vesicles. The plasmatic membrane is the site of nonamyloidogenic APP cleavage so, this increase in endocytosis will cause APP to be engulfed by endosomes where it will be processed in the amyloidogenic pathway.

Studies have shown that high levels of soluble Aβ oligomers can reduce the number of spines per dendrite, impairing the formation of new neuronal networks needed for LTP, and instead driving LTD. Amyloid β can reduce the level of AMPA receptors in the postsynaptic membrane by prompting the endocytosis of these receptors, by inducing AMPAR phosphorylation in a specific site, necessary for AMPAR endocytosis during LTD. The loss of AMPARs, in turn leads to the loss of NMDAR activation and causes the loss of dendritic spines, precluding LTP. Thus, AMPARs emerge as central mediators of Aβ toxicity. In a healthy situation, brief periods of high synaptic activity open NMDA receptors and lead to a long-lasting increase of the number of AMPARs in the postsynaptic membrane, and of spine growth, resulting in LTP (i.e. permanent facilitation of synaptic transmission). On the other hand, Aβ drives the depression of glutamatergic synaptic transmission, that results in low levels of synaptic stimulation, and in turn produces NMDAR or mGluR dependent LTD, both forms being able to induce

the removal of AMPA receptors from the postsynaptic membrane and the loss of dentritic spines (Hsieh et al., 2006).

Three components are usually considered in LTP and LTD: induction, expression, and transduction. Induction corresponds to the mechanism that triggers a response; expression is what changes to result in an increase (or decrease in case of LTD) in synaptic transmission; and transduction comprises the signaling cascades that go from induction to expression and sustain the alterations in synapse efficiency. The NMDAR is an induction trigger for LTP, in most synapses that have been investigated in the CNS so far (kainate receptors are thought to trigger the induction in the rest of the synapses). NMDAR is also the trigger for the induction of some forms of LTD, since it has been observed that NMDAR antagonists prevent LTD as well as LTP.

During LTP investigation it was observed that brief periods of high frequency stimulation (HFS), or tetani, led to an enduring increase in the size of synaptic potentials observed in the dentate gyrus in response to stimulation in the cortex. Some hallmark features were soon defined for LTP, like input specificity, co-operativity, and associativity. Input specificity means that when an HFS is applied in an input (i.e. a synapse), the resulting potentiation is only observed at that specific input, meaning that LTP is not a global change at the neuronal level but rather a localized change at the synapse level (at the level of the input). The co-operativity feature means that a certain threshold number of inputs needs to be activated simultaneously for LTP to occur. Associativity refers to the fact that a weak HFS that is not enough to induce LTP in an input, if paired with a strong HFS applied in an independent input, can induce LTP. This associativity feature can relate to associative learning (Volianskis et al., 2015).

Thus, NMDA receptors have some key physiological functions, one of them being to contribute to high frequency transmission and another is to trigger the induction of most forms of synaptic plasticity. In a search for understanding the way that NMDAR triggers the induction of LTP, using exogenous application of NMDARs, it was observed that when the duration of the NMDARs application was extended a few minutes, it triggered the induction of LTD instead of LTP and interestingly, its mechanisms resembled the mechanisms of the LTD induced by low frequency stimulation (Volianskis et al., 2015). Synthetic Aβ aggregates reportedly inhibit NMDAR dependent LTP, but not NMDAR-independent LTP.

One of the main neuropathological signs observed in AD patients is cortical atrophy, namely degeneration of neurites, decreased dendritic spine density and extensive neuronal loss. Anatomical studies indicate that the induction of LTP is associated with dendritic spine formation and increased spine volume, while the induction of long-term synaptic depression (LTD) results in decreased dendritic spine volume and spine elimination. Both LTP and LTD inductions depend on a trigger by NMDAR, the different outcomes produced by the trigger of the receptor may depend on the alteration of the cytosolic Ca^{2+} concentration (Li et al., 2009). The change in intracellular Ca^{2+} concentration is probably very precise for each phenomenon, implicating the activation of different enzymes downstream and therefore distinct pathways. It seems that excitotoxicity, by leading to higher cytosolic Ca^{2+} concentrations, facilitates LTD rather than LTP. This excitotoxicity, observed in regions like the HC, appears to be mediated, in part, by inefficient glutamate clearance at the synapse, which seems to be caused by the downregulation of EAAT1 and EAAT2 glutamate transporters, (that in normal conditions remove the

glutamate from the synapse, allowing its reuptake by the presynaptic neuron). The downregulation of EAAT1 and EAAT2 transporters is one of the consequences of Aβ toxicity and it leads to the facilitation of LTD through activation of the mechanisms responsible it. Conventional hippocampal LTD also seems to require extracellular Ca^{2+} influx through NMDARs. (Harris et al., 2002).

It was shown that when an extracellular glutamate scavenger collected the glutamate from the synaptic cleft, Aβ could no longer promote LTD, and that if LTD was previously heightened it was rescued to normal levels by the glutamate scavenger, and NMDAR and mGluR inhibitors, in mouse models of AD. This knowledge strengthens the link between glutamate excitation and Aβ toxicity and suggests that soluble Aβ aggregates facilitate LTD through a mechanism dependent on glutamate accumulation at the synapse. Furthermore, it was observed that glutamate uptake at the synaptic cleft was significantly reduced in the presence of soluble Aβ oligomers, and that Aβ induced LTD was closely mimicked with the use of a pharmacological inhibitor of neuronal glutamate reuptake. Again, this implies that Aβ oligomers damage synaptic plasticity by impairing glutamate reuptake and recycling at the synapse (Li et al., 2009). Moreover, the impairment of synaptic glutamate reuptake can lead to a very high extracellular glutamate concentration and enhance glutamate spillover to other synapses.

Downregulation of EAAT1 and EAAT2 glutamatergic transporters was observed in the HC of AD patients, especially in the proximity of amyloid plaques. Down-regulation of NMDA and AMPA receptors was also observed, although kainate receptors appeared to be upregulated (KA receptors seem to be involved in excitotoxic cascades). Once again, this implies impaired glutamate clearing, that leaves neurons exposed to excess extracellular glutamate, connecting excitotoxic mechanisms to AD (Jacob et al., 2007). It is still unclear how the Aβ peptides exert their effect on NMDARs, i.e. whether these receptors are direct targets of Aβ or if the peptide interacts with other receptors that then modulate NMDAR activity, or even with targets upstream of NMDARs. Moreover, it has been hypothesized that Aβ peptides damage glutamate transporters by inducing oxidative stress.

Surprisingly, soluble Aβ reduces the amplitude of peak NMDAR currents, and several glutamate uptake inhibitors were also shown to depress NMDAR currents, which leads to the hypothesis that prolonged exposure to glutamate causes desensitization of the NMDARs. Interestingly, synaptic activity increases Aβ production whereas heightened concentrations of soluble Aβ decrease synaptic activity. Therefore, Aβ may act as regulator of synaptic activity through a negative feedback loop. This hypothesis is supported by the observation that, in APP knockout hippocampal cultured neurons, amplitudes of excitatory postsynaptic currents mediated by NMDA and AMPA receptors were significantly enhanced. Moreover, cultured slices overexpressing APP showed a reduced NMDAR dependent synaptic transmission. Thus, it seems that the dysfunctional upregulation of the negative feedback loop mediated by Aβ leads to increased silencing of neurons by the reduction of synaptic transmission, in brain regions affected by AD. One mechanism used by Aβ to reduce synaptic transmission is the induction of NMDA and AMPA receptor endocytosis from the postsynaptic membrane, since it was observed that the reduced level of these receptors in the postsynaptic membrane was due to increased removal rather than to disrupted trafficking to the membrane.

Glutamatergic neurons contain an electron dense web underneath the postsynaptic membrane called the postsynaptic density (PSD). PSD is composed of a dense network of several hundred proteins, of

different signaling pathways, such as postsynaptic receptors, cytoplasmic scaffold proteins, signaling enzymes and cytoskeletal structural elements, creating a complex that handles a wide range of functions (Boeckers, 2006). Some of its functions are the stabilization and anchoring of glutamate receptors at the synapses, and the regulation of the trafficking and insertion of receptors and ion channels along dendrites and into synapses. The PSD is also involved in maintaining synaptic homeostasis. The expression of PSD proteins has been noted to be altered in models of neurological disorders suggesting their involvement in these (Vyas and Montgomery, 2016). The PSD is regulated by cytoskeletal protein PSD-95 and the master organizing proteins Shank and Homer. PSD-95 and Shank are important in assuring that AMPA and NMDA receptors reach the membrane surface and stay there. Aβ interacts with PSD-95 and causes the breakdown of the PSD-95, Shank, and Homer clusters, leading to the reduction of NMDA and AMPA receptors levels at the plasmatic membrane.

Nanomolar concentrations of Aβ40 and Aβ42 peptides can potentiate glutamate release in the hippocampus and cortex, the areas affected in AD. It has also been noted that, in the HC, glutamatergic terminals containing VGLUT1 are found in positions close to neurons that express APP. Moreover, nanomolar concentrations of Aβ do not seem to significantly affect glutamate release in regions that are not as vulnerable to AD, such as the striatum. This suggests that Aβ, in small concentrations (picomolar), has a natural role of regulating presynaptic glutamate release in specific brain regions, which are the most vulnerable to it (and the ones most affected in AD). Thus, Aβ potentiates glutamate release from the presynaptic neurons and inhibits glutamate clearance from the synapse, which may be important in normal physiological conditions, in small controlled levels. In small doses, Aβ might have a healthy role in regulating the amount of glutamate at the synapse, therefore controlling the intensity of the signals of the glutamatergic system.

In conclusion Aβ is responsible for triggering many toxic mechanisms that lead to neurodegeneration. The main known consequences of Aβ toxicity in the glutamatergic system are reduction of glutamate reuptake at the synapse (due to downregulation of glutamate transporters EAAT1 and EAAT2); increased release of glutamate from presynaptic neurons and glia; subsequent overactivation of glutamate receptors; inhibition of LTP; facilitation of LTD; reduction of dendritic spines number; induction endocytosis of AMPA and NMDA receptors in the postsynaptic membrane; activation of enzymatic pathways that promote apoptosis and cell death.

2.3 AD Treatments

Treatments for AD are developed based on the neuropathological hallmarks of the disease. The main AD drugs being used are memantine and inhibitors of acetylcholinesterase enzyme (AChE), which hydrolyses Ach at the synaptic cleft. Treatments with acetylcholinesterase inhibitors increase ACh levels at the synaptic cleft, thereby promoting activity of the remaining cholinergic neurons (which have an important role in memory and attention) and reducing cognitive symptoms associated with AD. Even though these treatments do not change disease progression, they improve quality of life (for 1 to 3 years) and reduce caregiver burden for patients with mild to severe AD. Three cholinesterase inhibitors are approved for AD treatment: donepezil, galantamine and rivastigmine. These drugs have similar effects on patients and are identically well tolerated (H. Ferreira-Vieira et al., 2016).

Because the glutamatergic system is implicated in so many aspects of neurodegeneration, glutamate receptor antagonists are viewed as good therapeutic targets. Memantine is an antagonist of the NMDA receptor that can effectively prevent its pathological activation without affecting its physiologic functions. It can protect neurons from Aβ40/42 toxicity, thereby reducing cell death. Memantine is a noncompetitive inhibitor of the NMDAR with low to moderate affinity. Nonetheless, its affinity is higher than the one presented by its natural antagonist, the Mg^{2+} ion, that cannot block the receptor in situations of excitotoxicity. With features of an improved Mg^{2+}, memantine takes over the physiological function of the ion (Danysz and Parsons, 2003). Furthermore, studies show that memantine preferentially inhibits NMDAR activity when the channel is excessively open, not interfering with normal synaptic activity. In normal activity the channels are only open for milliseconds, in which case memantine does not have time to act.

However, memantine is unable to attenuate the synaptic accumulation of glutamate induced by Aβ and it does not alter the action of Aβ peptide. This drug has been approved by the European Union since 2002 and by the U.S. Federal Drug Administration since 2003 for the treatment of AD and it shows positive effects in the treatment of individuals with moderate-to-severe AD. On the other hand, for the cases of mild AD patients it does not seem to have any significant effect, although it has only been tested in limited doses. Because its mechanism of action is unrelated to the one used by the approved cholinesterase inhibitors it has the potential to be combined with them for a more completed treatment (Revett, et al., 2013).

Although since 2003 no new drugs have been approved for AD treatment (Hung and Fu, 2017), there is a lot of research being developed in order to ascertain witch pathological mechanisms of AD could be possible treatment targets. The amyloid hypothesis states that it is the clustering of Aβ into (toxic) oligomers, that then assemble into fibrils and finally into plaques, which are nontoxic, that initiates a cascade of toxic mechanisms that cause AD. The toxic cascade induced by Aβ production leads to local inflammation, oxidative stress, excitotoxicity, tau hyperphosphorylation, and eventually to deficits and imbalance of other neurotransmitters, such as acetylcholine, dopamine and serotonin, and to cognitive deficiencies. The focus of AD drug development is changing from treatment to prevention. The new treatments being developed aim to treat the AD triggers described, while the disease is in early stages, they are called disease-modifying drugs. Both Aβ and tau are possible targets for disease-modifying treatments in AD. The idea is to prevent and treat AD by reducing the production of Aβ and tau, precluding aggregation or misfolding of these proteins, or removing the toxic aggregates (or a combination of these methods) (Yiannopoulou and Papageorgiou, 2012).

The development of disease-modifying drugs for AD is an acknowledged worldwide necessity. These are meant to stabilize or slow down, the molecular pathological steps that lead to neurodegeneration. Since AD is now known to have presymptomatic and symptomatic phases, patient treatment should start during the presymptomatic phase or before symptoms are severe and largely irreversible. Most disease-modifying drugs developed to date target Aβ. Drugs interfering with Aβ deposition can be precluders of Aβ aggregation (anti-amyloid aggregation agents and drugs interfering with metals), selective Aβ lowering agents (inhibitors of β-secretase and inhibitors of γ-secretase), and

immunotherapy directed against Aβ (active immunization (vaccination) and passive immunization (monoclonal antibodies)) (Yiannopoulou and Papageorgiou, 2012).

Only a few of the drugs developed with these purposes have reached the third phase of clinical test trial and none of them, until now, has conclusively passed this phase and proven to prevent AD in humans, or to have any effect on cognition (Yiannopoulou and Papageorgiou, 2012). The control of cholesterol and vascular-related risk factors is also a possible disease-modifying approach, since there seems to be a link between hypercholesterolemia, cardiovascular diseases and AD. Importantly, it is necessary to test drugs indicated for the treatment of Aβ aggregation on other pathologies as well, since it has been observed that an anti-amyloid aggregation agent can promote abnormal tau aggregation, and it is also possible that a treatment for tau aggregation could have a negative impact on Aβ pathology.

For the planning of future clinical trials of disease-modifying drugs, it is important to investigate the mechanisms responsible for the pathogenesis of AD and to understand the relationship between tau, Aβ and other factors. Moreover, AD treatments seem effective only in certain phases of the disease and some disease-modifying drugs have shown benefits in mild but not moderate AD. Thus, therapeutic trials should be done as early as possible in the course of the disease, which also implies the need of accurate measurement tools for early diagnosis and for the detection of patients with mild cognitive impairment at high risk of converting to AD. These tools measure specific biomarkers related with the mechanisms of AD pathology. Another reason why the development of good measurement tools is crucial is that AD can arise from different (and mixed) causes and triggers, and for the method of treatment to be appropriate for each case of AD it is important to understand their root causes. It would also be helpful to identify subgroups of patients with homogeneous biomarkers, that could benefit from similar treatments (Yiannopoulou and Papageorgiou, 2012) (Galimberti and Scarpini, 2011).

2.4 Reelin Protein

Reelin is an extracellular matrix glycoprotein highly expressed by Cajal–Retzius (CR) cells during brain development, in which it plays a vital role in the orientation of cell migration, enabling brain layering and lamination. CR cells appear at the onset of neocorticogenesis and disappear at the end of neuronal migration, being located close to the hippocampal sulcus. Reelin signaling guides newly formed neurons to their proper destination, so that normal neuronal connections can be established. An important insight on the role of reelin in the control of neuronal migration, is the fact that the lack of its guidance during development leads to a disorganized neuronal patterning, observed in the reeler mouse. Reeler mutant mice lack the reelin gene, and display abnormalities in the neuronal layering of the cortex and cerebellum (Lombardero et al., 2007). These mice develop an inverted cortex, with early born neurons migrating to the superficial cortical plate instead of stopping at deeper layers.

Reelin is also crucial in the adult brain, being essential for the migration and lamination of adult born neurons. At postnatal stages, reelin is mainly expressed by GABAergic neurons, distributed throughout neocortical and hippocampal layers (Alcántara et al., 1998). Its pathway is involved in the integration of newborn GCs in the preexisting neuronal circuit. Adult neurogenesis is a process of generating functional neurons from adult neural precursors, it is understood as continuous postnatal neurogenic activity (Georg Kuhn and Blomgren, 2011). In mammalian brains, it persists throughout life in restricted

brain regions: the subgranular zone (SGZ) in the dentate gyrus (DG) of the hippocampus (HC), and the subventricular zone (SVZ) of the lateral ventricles where new neurons are generated and then migrate through the rostral migratory stream (RMS) to the olfactory bulb (OB). Adult neurogenesis in other regions is very limited under normal physiological conditions but could be induced after injury. In the DG, reelin signaling prevents new neurons from migrating into the region of the hilus (Ming and Song, 2011). Data suggests that reelin modulates dentate granule cell progenitor migration to maintain normal granule cell integration in the neonatal and adult mammalian dentate gyrus thus, acting as a migration guidance cue (Gong et al., 2007). Precise positioning of reelin controls the formation of the granule cell layer. Adult neurogenesis in the DG has been linked to spatial learning and pattern separation, adding flexibility to memory through the forgetting process.

It seems that reelin controls the migration directionality of the granule cells, since it has been observed that neurons in cultures from reeler mutants migrated randomly in all directions, contrarily to wild type granule cells, that migrated toward the marginal zone of the DG. Importantly, newly generated neurons migrate toward the reelin containing marginal zone, suggesting that reelin is an attractive signal for newborn migrating neurons. The protein can also act as a stop signal, since in *reeler* mice, migrating neurons invade the marginal zone, while in wild-type mice they do not (i.e. the WT neurons do not reach the reelin containing marginal zone) (Wang et al., 2017). Thus, reelin controls neuronal migration and layer formation, by modulating migration directionality of newborn granule cells, although it does not control the actual migratory process and the migration speed. Moreover, absence of Reelin in the adult HC contributes to ectopic chain migration and aberrant integration of newborn DGCs.

Reelin binds to the receptors apolipoprotein E receptor 2 (ApoER2) and very-low-density lipoprotein receptor (VLDLR), expressed in neurons and radial glia, and both receptors also bind apolipoprotein E (ApoE). It is relevant that, the variant ApoE4 is the biggest genetic risk factor known for late-onset sporadic AD (Cuchillo-Ibañez et al., 2016). ApoER2 and VLDLR mediate its functions intracellularly by triggering signaling cascades involving adaptors such as the Dab1. ApoER2 is the dominant reelin receptor, participating in the modulation of synaptic plasticity and memory formation. Inactivation of Dab1 causes a *reeler* like phenotype. In fact, Dab1, Reelin, and Reelin receptor mutant or knock-out mice have visibly abnormal dentate granule cell layers (i.e. their granule cell layers are disorganized, instead of being laminar). Interestingly, lamination defects in *reeler* hippocampal cultures can be rescued by interaction with tissue expressing reelin (Bosch et al., 2016).

In an experiment with the purpose of investigating the impact of the Reelin/Dab1 pathway in the formation of new synapses in newborn granule cells (GCs) in the mouse hippocampus, three different mouse models were used: mice that overexpress reelin, mice that are knockout for Dab1 and controls. It was discovered that the reelin pathway has an essential role in the regulation of GC adult neurogenesis and that it regulates dendritic and synaptic maturation of newborn GCs. Reelin overexpression accelerated dendritic maturation, while the disruption of the reelin pathway resulted in aberrant dendritic development and orientation. For example, Dab1-inactivated GCs extended ectopic, basal dendrites into the hilus, that were covered by a high density of spines, while WT GCs only presented apical dendrites that extend towards the molecular layer of the DG. Moreover, it was noticed that reelin/Dab1 pathway regulates adult GC spine and synapse formation and astroglial ensheathment of synapses,

since Dab1-KO models showed increased ensheathment of GC synapses, and reelin overexpression models showed decreased ensheathment of GC synapses. Astroglial ensheathment of synapses is important for the control of synaptic homeostasis and excitability (i.e. synaptic neurotransmitter levels control), neurotransmission between neurons and glial cells, and spine development and plasticity. It was also observed that reelin has a role in the regulation of the shapes and types of spines and in the complexity of their synapses (Bosch et al., 2016).

Overexpression of Reelin does not change spine density or the number of synaptic inputs in newborn GCs, whereas its downregulation leads to an acceleration in spine development (i.e. spine density increases at early stages) although the final spine frequency is also the same as in wild types. Moreover, reelin levels affect spine morphology, type, and size. GCs in Reelin overexpressing mice exhibited a bigger number of mushroom spines (i.e. spines with a head width bigger that 0,6µm), of larger spines, and of synaptic contacts. Dab1 downregulation caused a decrease in the number of mushroom spines and in the size of synaptic contacts, compared to the observations in WT mice. This suggests that mushroom spine development and stability is a primary target of the reelin pathway. Furthermore, reelin downregulation leads to hyperexcitability in immature GCs.

Hyperexcitability of the DG is observed in psychiatric pathologies such as epilepsy, a disease linked to low reelin levels and to GCs with basal dendrites like what was noticed in the Dab1-KO model. In both models, Dab1-KO model and reelin-OE, it was noticed that axons innervating newborn GCs spines established simultaneous synaptic contacts with fewer additional spines (i.e. presented fewer multiple synaptic boutons (MSBs)), which are believed to build synchronicity of the newborn GC with the preexistent circuitry. This decrease in MSB synaptic innervation, and the alteration in astroglial ensheathment show that reelin deregulation, either up or down, alters synaptic structure that is important for cognition. These alterations can probably lead, not only to changes in the newborn GCs affected, but also in the network circuitry in which they are recruited. Thus, precise control of reelin expression is necessary for the correct maturation and functional integration of adult-born GCs (Bosch et al., 2016).

In another study investigating reelin function in the adult brain, a transgenic mouse model of inducible reelin-OE was used. This mouse overexpresses reelin specifically in the postnatal and adult forebrain (i.e. the reelin gene is overexpressed only after the mouse is born), since reelin is essential in brain development and the point was to study its role in the adult brain. Neurogenesis is known to be reduced in the DG of adult reeler mice. Contrarily, reelin overexpression leads to increased neurogenesis in the adult SGZ of the DG, although in the SVZ the rate of adult neurogenesis does not appear to be altered by the variation of reelin expression. Overexpression of reelin was observed to alter the migration and lamination of newly generated neurons in the rostral migratory stream (RMS), causing the mispositioning of adult generated neurons that were generated in the SVZ. Moreover, reelin-OE was noticed to cause abnormal migration and positioning of adult generated granule cells, with newly generated neurons displaying a wide distribution along the entire granular layer (GL) in reelin-OE mice (while in wild type mice these neurons stay in the deeper zone of the GL) (Pujadas et al., 2010).

Reelin-OE mice presented an increased complexity in presynaptic and postsynaptic elements and increased density of synaptic contacts (per spine) in the HC, compared to controls. However, the number of dendritic spines is not altered by reelin-OE, only their structural properties: each spine established more synaptic contacts than normal (i.e. more than in WT). Interestingly, stopping reelin-OE decreases dendritic spine density and the percentage of double-synaptic contacts to values below those of WT animals, suggesting that overactivation of the Reelin signaling pathway can activate desensitization mechanisms. Moreover, Reelin-overexpressing mice presented a high frequency of very large, mushroom-shaped dendritic spines, often with two or more synaptic active zones, compared to wild types, where these spines were rare. These more complex spines are like those induced after learning and LTP, suggesting that reelin facilitates LTP. Thus, reelin overexpression seems to lead to the enlargement and hypertrophy of dendritic spines, traits that are related with complex and multiple synaptic junctions. It appears that precise levels of reelin must be maintained in the adult brain for certain mechanisms to be performed properly. Interestingly, in the adult brain, reelin participates in the control of processes that are reminiscent of developmental processes, such as the positioning and organization of adult generated cells (controls neural migration), the integration of these newborn cells in the preexisting circuits of the brain, and the facilitation of synaptic plasticity (induction and maintenance of LTP), especially in the hippocampus (Pujadas et al., 2010).

In an experiment to study the impact of the reelin pathway in adult neurogenesis, transgenic mice that were conditional Dab1-KOs, after the administration of tamoxifen, were used in parallel with controls (Teixeira et al., 2012). Without its receptor Dab1, reelin is unable to exert its intracellular signal, so this genotype has similar effects as the reelin-KO. It was observed that the loss of reelin signaling impairs neurogenesis in the adult DG: DGCs in controls were well organized, normally oriented and located mainly in the inner GCL, whereas in Dab1-KOs the DGCs were abnormally oriented in the GCL or located ectopically in the hilus, and sometimes in the ML. The level of GCL disorganization and mispositioning was associated with a dose-dependent reduction of Dab1. Moreover, the level of abnormality visible in the brain was dependent on the age at which the mouse received the tamoxifen treatment, the younger the silencing of the Dab1 receptor gene, the more marked the changes in the mouse brain. Most DGCs born with inactivated Dab1 signaling migrate and integrate aberrantly into the adult DG.

Moreover, the effect of Dab1 inactivation was also accessed at the single cell level. Dab1 was inactivated specifically in neuroprogenitor cells, that stayed surrounded by WT cells. It was observed that the adult-born neurons that originated from those Dab1-KO cells had severe abnormalities at all the stages studied, presented smaller dendritic trees and branched less profusely. The presence of basal dendrites in DGCs has been linked with neurological disorders, such as AD (and epilepsy). Importantly, Dab1-deficient neurons generally contained aberrant basal dendrites and smaller dendritic trees in the molecular layer (ML), while WT neurons did not display any basal dendrites. Some Dab1-deficient neurons displayed dendrites extending exclusively in the hilar region. These observations imply that the disruption of the reelin pathway in adult hippocampal neuroprogenitors causes aberrant dendritic development of DGCs.

When Dab1 was suppressed in the DG of adult mice, a reduction in the complexity of dendrites was noticed in these animals, namely a reduction of dendritic length and arborization was observed. These mice also presented an increase in the levels of glial cells, specially in the SGZ and in the ML, where glial clusters were visible. The absence of the reelin signaling pathway seems to modulate neuronal/glial fate, causing an increase in the differentiation of adult progenitor cells into glia at the expense of the generation of granule neurons, that decreases. Furthermore, it was ascertained that the abnormal basal dendrites seen in adult-born Dab1-deficient DGCs, that form towards the hilar region of the HC, are innervated by synapses, therefore establishing aberrant innervation and circuitry. Thus, the inactivation of the reelin pathway leads to the development of aberrant DGCs that become functionally integrated into adult circuits, which means that these aberrant dendrites can be disruptive to the circuitry that they integrate. These abnormal circuits might interfere with the function of the DG and be the cause for neurological diseases known to be related with altered levels of reelin, such as temporal lobe epilepsy, autism, AD, depression and schizophrenia (Teixeira et al., 2012).

2.4.1 Reelin in AD

The downregulation of the reelin pathway and reelin mutations are involved in several diseases, including Alzheimer's disease, epilepsy, and psychiatric disorders, all related with alterations of hippocampal circuits. Studies have reported that reelin signaling is influenced by Aβ, specifically amyloid impairs the biological activity of reelin. AD patients have been noticed to present elevated reelin expression but low reelin function. Different studies have demonstrated that reelin or elements in the reelin signaling pathway, like Dab1, interact with Aβ. In fact, an immunoprecipitation was preformed against reelin in human brain extracts and it was observed that Aβ co-immunoprecipitated with the protein. Also, in a size-exclusion chromatography Reelin and Aβ oligomers were present in the same fractions. Reelin influences APP trafficking and processing and antagonizes the suppression of synaptic transmission exerted by Aβ. These links indicate an involvement of reelin with Aβ and thereafter, an implication of reelin in AD, and suggest that this protein could be a target in the treatment of AD (Cuchillo-Ibañez et al., 2016).

Evidence indicates that the interaction between reelin and Aβ causes an increase in the expression of reelin, but also a decrease in the internalization of ApoER2 from the cytoplasmic membrane therefore, undermining reelin signaling. Levels of phosphorylated Dab1 were decreased in AD patients and the internalization of its receptor ApoER2 was also abnormal. A proteolytic ApoER2 fragment is generated by cleavage of the receptor after reelin binds it, the presence of this fragment was examined in the cerebrospinal fluid (CSF) since it can be used as a measure of reelin signaling. ApoER2 fragments are a better indicator of intracellular reelin signaling than reelin fragments, because these can also come from the activity of extracellular matrix metalloproteinases. In nondemented patients the levels of soluble ApoER2 fragments in the CSF correlate with the levels of reelin, while in AD subjects they do not correlate. In fact, in AD subjects the levels of the ApoER2 fragment decrease, even though ApoER2 expression does not change and reelin expression is augmented, suggesting that reelin is not binding

the ApoER2 receptor as frequently and that the reelin signaling is compromised by the disease, maybe because the protein is becoming inactivated (Cuchillo-Ibañez et al., 2016).

Through the cleavage of ApoER2 a soluble intracellular domain (ICD) is released. This ICD has been reported to down-regulate the activity of the *RELN* promoter and therefore reduce reelin expression. On the other hand, the presence of less ICD fragments causes reelin expression to increase. Importantly, by binding to the Dab1 adapter, reelin transmits an intracellular signal that triggers a signaling cascade, which prevents tau hyperphosphorylation. In AD, although there is an increase in reelin levels, there is also an abnormal glycosylation of reelin (induced by Aβ), that decreases the efficient binding to ApoER2 receptor and impairs the reelin directed downregulation of tau phosphorylation. Thus, the effect of Aβ on reelin generates a circle of chronic signaling failure in which a more glycosylated reelin is less bioactive, thereby generating fewer ApoER2-ICD fragments and increasing reelin expression. Moreover, reelin emerges as a link between Aβ and tau hyperphosphorylation, since it seems that through the alteration of reelin glycosylation, Aβ impairs the downregulation of tau phosphorylation, contributing to the progression of AD (Cuchillo-Ibañez et al., 2016).

It was observed that reelin influences the kinetics of Aβ in vitro, by delaying the aggregation of Aβ42 into fibrils. A western blot analysis of Aβ42/reelin, performed when fibril formation starts, revealed that the reelin band disappears from its expected molecular weight, appearing at the bottom of the gel instead, suggesting that it joins Aβ. In fact, reelin interacts with soluble Aβ42 species until it becomes trapped in the amyloid fibrils, thus losing its biological activity. The biological activity of protein reelin was measured, in neuronal cultures, through the level of phosphorylation of the Dab1 receptor. It was observed that in solutions containing both reelin and Aβ42, Dab1 phosphorylation remained normal until the formation of Aβ fibrils, when reelin would be trapped and lose its function, which was noticed through the decrease in Dab1 phosphorylation. However, reelin does not change the conformation of the fibrils and seems to interact with them only at the surface.

Furthermore, the plaque load was measured in the HC of mouse models overexpressing reelin postnatally (under the control of a promoter) and also carrying the hAPP mutation (i.e. accumulate Aβ in the brain) (TgRln/J20 mice), and it was compared with J20 mouse models (TgRln/J20 mice accumulate Aβ plaques and overexpress reelin, while J20s accumulate Aβ plaques in the brain but are WT for reelin) and it was observed that reelin delays Aβ42 fibril formation in a concentration dependent way, since the percentage of area occupied by plaques in the HC was lower in TgRln/J20 models than in J20 mice (Pujadas et al., 2014).

The impact of reelin in Aβ42 induced toxicity was studied in hippocampal neuronal cultures. The cultures were exposed to Aβ42 in the presence and absence of reelin (absence was the control) and it was noticed that the cultures that were in the presence of reelin presented a higher cellular survival. In order to check the influence of reelin in synaptic dysfunction induced by Aβ42, the dendritic spine densities of TgRln/J20 and J20 mice were compared. It was noted that TgRln/J20 mice presented a spine density

like that of wild type control mice, whereas J20 presented a lower number of synaptic contacts and dendritic spines. Thus, reelin protects neurons against Aβ42 toxicity and against dendritic spine loss.

The cognitive performance was also analyzed in these mouse models thought a test known as novel object recognition (NOR) task, that measures discrimination index through the time that an animal spends exploring a new object versus a familiar one (more discrimination index indicates better cognition). Control and TgRln animals spent a significantly higher proportion of time exploring the new object, in relation to the familiar one, than J20 animals, indicating a cognitive deficit in the J20 animals. Interestingly, TgRln/J20 animals presented a discrimination index like control animals, at both 4–5 and 8–10 months, implying that these animals do not have the cognitive deficit that J20 mice have.

In 12-month-old mice, the performance of control mice was equivalent to J20 animals, which can be explained by an age-dependent cognitive decline. On the other hand, the discrimination index measured in 12-month-old TgRln mice was significantly higher than that of the control group, and 12-month-old TgRln/J20 animals performed better than controls and J20 mice, maintaining a recognition capacity like TgRln mice despite the plaque load. These results show that reelin overexpression protects against recognition memory deficits caused by Aβ production and, interestingly, imply that reelin upregulation also helps slow down the age-dependent cognitive decline (although it has been previously shown to cause mispositioning of adult generated neurons in the HC) (Pujadas et al., 2014).

Chapter 3

Methodological Approach

This project was conducted between February and July of 2019 in the Neurobiology Laboratory of Dr. Prof. Eduardo Soriano of the University of Barcelona, under the supervision of Dr. Yasmina Manso, with the aim of studying the relationship between levels of reelin expression and the development of Aβ plaque deposits in AD, in the 12 months old mouse brain. More specifically, the idea was to ascertain how the absence of reelin protein in the brain of an AD mouse model would impact the accumulation of Aβ plaques in the hippocampus of these mice, in comparison to AD mouse models that express reelin at normal levels. The final purpose is to understand if reelin could be a good target in the treatment and prevention of AD.

3.1 Mouse models

The experiment made use of two transgenic mouse models that were crossed with each other: an AD mouse model and a reelin-KO mouse model. The AD mouse model carried the mutated human APP gene (hAPP), that is responsible for the overexpression of APP (the Aβ precursor), leading to the accumulation of Aβ and to its deposition as part of amyloid plaques, which are a known trait of AD. The APP mutation is known to be responsible for the occurrence of early-onset AD in humans. The reelin-KO mouse model is an inducible model that, upon tamoxifen administration at the age of interest, has the reelin gene (RELN gene) silenced, and reelin ceases to be expressed, becoming ubiquitously depleted. From the crossing of the AD model (J20) with the reelin-KO model (fRLn), the mouse line JfRLn is obtained, which is the model used in the experiment. JfRLn models overexpress the mutated human APP transgene and suffer a conditional silencing of reelin upon the administration of the hormone tamoxifen. The JfRLn line is obtained through the crossing between the lineages J20 (purchased from Jackson Lab) and fRLn (this line is a crossing of two lineages itself).

The J20 mouse strain displays the AD trait of Aβ deposition like it is observed in AD patients thus being used as a model of amyloid deposition and pathogenesis in the study of AD (is used as an AD model). J20 mice present many AD-like phenotypes, such as synaptic loss, amyloid plaque deposition and cognitive impairment. J20 mice overexpress the mutated human APP (hAPP) gene, that causes the accumulation of Aβ and deposition of plaques. The hAPP carried by the J20 line contains the Swedish (KM670/671NL) and Indiana (V717F) mutations (hAPPSwe/Ind) under the control of a platelet-derived growth factor promoter (mice overexpress $hAPP_{Swe/Ind}$) (Mucke et al., 2000).

The lineage fRLn (floxed-reelin) is the inducible reelin-KO mouse model. Floxed-relin lines are generated from the crossing between the lineages floxreelin (a kind gift of the collaborator Angus Nairn, from Yale University, to the laboratory of Dr. Prof. Eduardo Soriano) and UbiCreER (from Jackson Lab (stock number 008085)). The floxreelin lineage has the first exon of the RELN gene flanked by 2 loxP

sequences, which are identified by the Cre recombinase. The UbiCreER lineage carries the gene encoding for Cre recombinase united with a ubiquitous promoter and with the coupling domain of HBD hormone of a mutated estrogen receptor, which retains the recombinase inactivated at the level of the endoplasmic reticulum (ER). When active, the recombinase promotes the recombination between the two loxP sequences, that are flanking the first exon of the RELN gene, resulting in the ubiquitous inactivation of RELN. The tamoxifen activates Cre by setting it free from the ER to carry out the nuclear action of recognizing the loxP sections in the genome and connecting them together, cutting out the first exon of RELN.

Thus, JfRLn mice are obtained through the crossing of three different lineages (they are triple-transgenic mice), one that carries the hAPP gene (J20), one that carries the loxP sequences flanking exon 1 of RELN gene (floxed-relin), and another that carries the recombinase Cre gene (UbiCreER). Inducible reelin-KO animals were valuable for the experiment because the point was to analyze the effect of reelin deficiency in properly developed adult brains, that accumulate Aβ plaques. If the animals were KO from the embryo (i.e. reeler mice), their brains would not develop properly, since the reelin pathway is essential for cortical layering and for the neuronal migration and maturation that leads to the development of functional synaptic connections. Because reelin is not essential in adult brains, the induction of reelin-KO in developed animals does not cause them to suffer structural changes. The two mouse genotypes that carried the hAPP gene (J20s), both the KO and the WT for reelin, were the focus of the study. Some other mice obtained from the line crossings expressed reelin at normal levels and did not carry the hAPP gene (WT genotype), and others did not express reelin or hAPP (J20- reelin-KO).

Mice were injected for 3 consecutive days around p45 (i.e. 45 days post-natal) with 180 mg of tamoxifen per kg of mouse body. The animals were kept under a temperature-controlled environment in a constant 12 hours light/dark cycle and the access to food and water was ad libitum. Mice were bred in the animal research facilities at the University of Barcelona. All the experiments using animals were performed in accordance with the European Community Council directive and the National Institute of Health guidelines for the care and use of laboratory animals. Experiments were also approved by the local ethical committees and were performed by certified personnel.

3.2 DNA Extraction

In order to identify the genotype of each animal, polymerase chain reaction (PCR) genotyping was performed in all the mice. For this a small piece of tail of 1-3mm was nicked from each animal, and a bit of blood was collected. Each animal received a different mark in its ears that allowed its identification. There was a file in which the name of each animal was annotated and associated with a specific ear mark, and upon the results of the PCRs, those were also linked with a genotype.

The DNA extraction for the PCRs, from the blood and tail fragments of the mice, was done with 100uL of NaOH 50mM for the tails, whereas for the blood samples, the NaOH quantity used depended on the amount of blood obtained. The samples were centrifuged (for 90 seconds at 9000 - 10000 rpm (spin)) and incubated in a heat block. For tail samples, the incubation was done at 100°C for 30 minutes and

for blood samples it was at 95°C for 15 to 20 minutes. In case both types of samples were being used the heat-block was set at 95°C. The samples were then removed from the heat-block and kept on ice for 10 minutes. Each sample was vortexed before taking a specific amount for a PCR and putting it in a PCR tube (0,2uL).

3.3 PCR genotyping

For the elimination of reelin expression to be possible, the animal must be flox/flox (homozygous), while for J20 and for Cre it can be heterozygous. Three different PCRs were carried out on tissue samples of the mice to identify the genotype of each animal. After PCR in a thermocycler, the samples are run in an agarose gel, for electrophoresis in two dimensions (animal and relative sequence size), in an electric field of 130V. The DNA has a negative charge, which is attracted to the electrode with a positive charge placed at the bottom of the gel (the negatively charged electrode is placed at the top). The DNA sequences migrate downwards towards the bottom of the gel and since, smaller sequences migrate faster, they become separated by size (with smaller sequences lower in the gel). By running a DNA ladder (a collection of DNA fragments of known lengths) next to the samples, the sizes of the sequences observed in the gel can be determined. The goal of the PCRs was to ascertain the presence of specific known sequences, of which the length in base pairs is known.
The possible genotypes for the J20 line (presence of the hAPP gene) were J20 -/- (negative) and J20 +/- (J20 positive), from the cross of a J20+/- with a J20-/-. For the presence of loxP sequences flanking the exon1 of RELN gene, the only possible genotype was flox/flox (flox positive). All mice were homozygous for flox, since only flox/flox mice were used in the crossings. For the presence of the recombinase Cre gene, the possible genotypes were Cre -/- (Cre negative) and Cre +/- (Cre positive), from the cross of Cre+/- with Cre-/- animals.

3.3.1 Cre PCR

Cre PCR is used to detect the presence of the gene encoding the expression of recombinase Cre.

3uL of each sample are used in each tube. For Cre PCR, 12,5uL of GoTaq® Green Master Mix are used for each sample (contains the polymerase, the nucleotides, magnesium, buffer) and 8,5uL of nuclease free water, the primers used are named 1 (0,375uL), 2 (0,375uL), 3 (0,125uL) and 4 (0,125 uL). The total volume of each PCR sample is 25uL. The controls are Cre+ and Cre-.

A band corresponding to 324bp fragments always appears in this PCR, and if only this band then the PCR is negative for Cre. If an additional band corresponding to 100bp fragments also appears in the gel, then the PCR is positive for the Cre and the animal contains the Cre recombinase (Cre+).

- 2 bands (324 bp and 100 bp): positive, Cre+/-
- 1 band (324 bp): negative, Cre-/-

3.3.2 Flox PCR

Flox PCR is used to detect the presence of LoxP sequences flanking the RELN gene.

1 (or 1,5) uL of each sample are used in each PCR tube. For Flox PCR, 12,5uL of GoTaq® Green Master Mix are used for each sample and 10,5uL of nuclease free water, the primers used are A (0,25uL), B (0,5uL) and C (0,25uL). The total volume of each PCR sample is 25uL.The controls are flox+/+ (fR / fR) and flox+/- (WT / fR).

The band corresponding to 496bp represents the wild type. If the loxP sequences are properly flanking the exon 1 of the RELN gene, then the 496bp band doesn't appear. The band corresponding to 613bp represents the loxP sequences (this band always appears).

- 1 band (613 bp): flox+/+
- 2 bands (613 bp and 496 bp): flox +/-

3.3.3 J20 PCR

J20 PCR is used to detect the presence of the human hAPP transgene.

3uL of each sample are used in each PCR tube. For J20 PCR 12,5uL of GoTaq® Green Master Mix are used for each sample and 10uL of nuclease free water, the primers used are Forward (0,25uL) and Reverse (0,25uL). The total volume of each PCR sample is 25uL. The controls are J20+ and J20-.

If one band corresponding to 300 bp fragments appears it means that this animal has the hAPP gene (it is J20+). If no band appears the animal doesn't have the hAPP gene (it is J20-)

- One band (300 bp): positive, J20+
- No band: negative, J20-

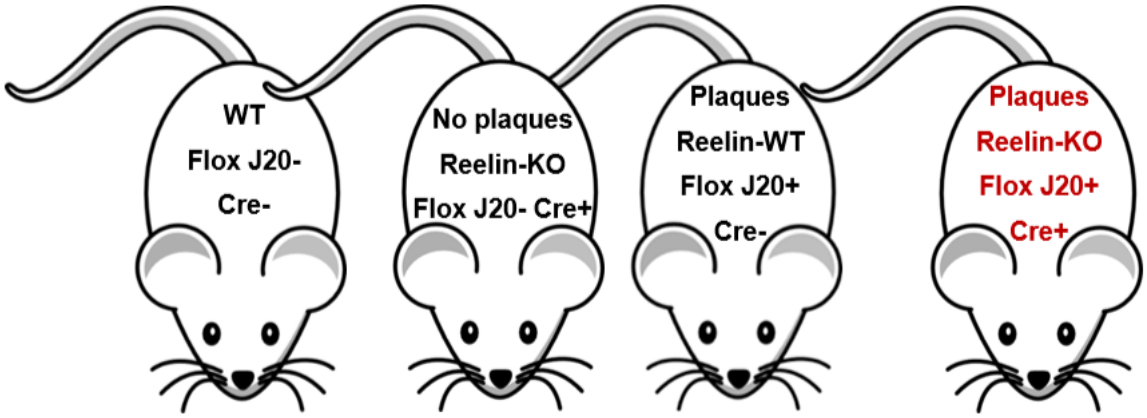

Figure 3.1: Different mouse genotypes that were obtained: WT, no plaques and reelin-KO, plaques and reelin-WT, plaques and reelin-KO. The goal genotype was the FloxJ20+Cre+ (plaques and reelin-KO).

3.4 Tissue Extraction and Cutting Sections

22 mice were sacrificed at twelve months of age (between 356 and 365 days old) through an intracardiac perfusion, for their brains to be extracted and studied. The mice were first anesthetized with a lethal dose of sedative of ketamine/xylazine. Their chests were cut, and their diaphragms were pinned up to expose the heart. Then, the left ventricle was injected, first with a vasodilator solution and then, with fixative solution (paraformaldehyde, PFA), that conserves tissue. This way, the circulatory system of the mice was used to spread the fixative to all organs. After the PFA had been running through the body for 20 minutes the brain was extracted and put in a tube with PFA. After 24h the brains were transferred to saline phosphate buffer (PBS) with 30% sucrose to allow an osmotic balance to be reached in the tissue. The brains were then frozen in 2-methilbutane at a temperature between -40°C and -50°C and kept in a freezer at -80°C. A bit of blood was collected once again from each animal; in case the genotype would need to be repeated and confirmed.

The brains were then cut coronally, one by one, with a freezing microtome, or with a cryostat in some cases, in 30µM sections which were distributed in order between ten Eppendorf tubes containing cryoprotective medium (to keep the brains from freezing). This way each tube of sections contained approximately 10% of the brain it held and was a whole representation of it (every brain region was represented by a few sections in each tube). The tubes with the sections were kept in a freezer at -20°C.

3.5 Immunohistochemistry (IHC)

Some brain sections were then differentially stained by immunohistochemistry (IHC). IHC is an application of immunostaining used to selectively identify antigens in cells of tissue sections, using the principle of antibodies binding specifically to antigens in biological tissue. In this case, the immunostaining is used to selectively bind specific proteins in brain sections. IHCs are useful to understand the distribution and localization of biomarkers and differentially expressed proteins in biological tissue (Sciences et al., 2019).

Two distinct IHCs were performed, each one with the aim of identifying a different biomarker. An IHC anti reelin is performed to selectively mark reelin protein, and two anti-Aβ IHCs are performed to selectively mark amyloid β deposits. According to the IHC that will be performed (depending on what is being observed), the tissue used can be a whole tube or just sections containing specific regions (ex: hippocampus or ventricles). Since reelin is present mostly in the hippocampus and cortex, the sections used for the IHC against reelin must contain these parts.

To begin an IHC, the tissue is washed with saline phosphate buffer (PBS) to eliminate the cryoprotective medium and is incubated in a solution that inactivates the endogenous peroxidases (to reduce non-specific background staining). The tissue is then washed again and blocked (for 2h) with a solution containing serum of the same animal where the secondary antibody was raised (the serums used are normal horse serum or normal goat serum), to minimize unspecific binding (minimize background/noise). For IHCs in which the primary antibody is raised in mouse, the block solution contains anti-mouse IgG

Fab (raised in donkey) to block mouse immunoglobulins and reduce non-specific signal. The tissue is then incubated with primary antibody, which will be specific for the antigen that is being observed (the control stays in block solution, since it will be used to see how a tissue without the stained antigen looks like). The primary antibody might be raised in mouse or rabbit, and the incubation is carried out during the whole night at 4°C (in a cold room).
In the second day the tissue sections were washed and incubated for 2h with the secondary antibody and then washed again and incubated for 2h with the tertiary antibody, which is streptavidin-HRP for both the reelin and Aβ IHCs. In the third day, the tissue is washed again and developed with DAB (3,3'-diaminobenzidine). H_2O_2 is used to activate the DAB reaction and phosphate buffer (PB) is used to stop it when the signal of differential staining is believed to be optimal. The intensity of the signal is controlled under the microscope in a few sections, it is important to leave the sections in DAB long enough for the signal to be visible, but not too long so that the tissue does not become burnt.

The sections are then mounted in treated glass slides and left to dry in an oven. The glass slides are specially treated with a solution that allows the sections to adhere to the glass, and not move once it has been placed. The sections in the slides are then dehydrated, for the tissue to be preserved longer, in a sequence of solutions of increasing alcohol concentration and then, in xylene. For the dehydration, the slides are placed for 5 minutes in distilled water, then 5 minutes in ethanol 70%, 5 minutes in ethanol 90%, 5 minutes in each of 2 absolute ethanol solutions, followed by 10 minutes or more in each of two xylene solutions. A coverslip is then glued on top of the mounted dehydrated tissue, with Eukitt® mounting medium, to protect it. This way, the sections can be preserved and easily observed in the microscope.

The secondary antibody is biotinylated, and it will bind to the primary antibody because it is against the animal where the primary was raised (the secondary will be anti-mouse (raised in goat)). The tertiary antibody is streptavidin-HRP (raised in radish) (Thermo Fisher scientific, 2019). Streptavidin has a very strong affinity for biotin (bond to the secondary antibody), this way the tertiary antibody binds the secondary, that was bond to the primary (which is bond to the antigen) forming a complex that can be detected, when in contact with DAB, because HRP (bond to streptavidin) catalyzes the conversion of chromogenic substrate DAB into brown colored products that precipitate. The horseradish peroxidase (HRP) enzyme, found in the roots of horseradish, produces a colored derivative of the labeled molecule when incubated with DAB substrate, generating a visible signal that allows the molecule of interest to be detected and quantified (Thermo Fisher scientific, 2019).

3.5.1 Reelin IHC (G10 ab)

The first IHC to be performed was against reelin protein, using the primary antibody G10 that binds to reelin, raised in mouse (ab78540), 2019). The reelin IHC was performed in all the animals. 2 sections from each animal were selected, one containing the ventricles (more anterior region of the brain) and another containing the hippocampus (more posterior region of the brain). One more section containing

ventricles, from an animal that is expected to express reelin, is selected and used as negative control (in which the primary antibody is not applied).

The reelin IHC was performed to confirm the reelin genotype of each mouse, and to verify if the silencing of the RELN gene in FloxCre+ animals was successful. The FloxCre- animals are expected to show high levels of reelin signal since they do not possess the Cre recombinase. On the other hand, FloxCre+ animals are not expected to present any reelin signal, since they do carry the Cre recombinase. After this IHC the animals were divided in reelin wild types (WT) and reelin knockouts (KO). Some reelin PCRs were repeated in order to confirm the genotypes of mice from which the reelin phenotypes did not match what was expected. It was concluded that a few inactivations were failed, since some animals were FloxCre+ but their brain sections were differentially stained for reelin.

3.5.2 Anti-Aβ (α-3D6) IHC

3.5.2.1 First Anti-Aβ (α-3D6) IHC

A first round of anti-Aβ IHC was performed to visualize amyloid β plaques in sections containing the regions of the hippocampus, cortex, and corpus callosum (white matter), since these are the zones of the brain where the accumulation of plaques is more evident. The primary antibody used to stain Aβ was α-3D6 (raised in mouse), which recognizes amino acids 1-5 of the Aβ peptide (without recognizing the APP molecule) (Alzforum.org, 2019). This HIC was first performed to all animals, in 2 sections of each animal, one containing the ventricles (anterior) and another containing the hippocampus (posterior), to confirm the J20 genotypes. The animals were then divided in genotypes, according to the results of the Aβ IHC differential staining, in J20+ (with plaques) and J20- (without plaques).

3.5.2.2 Second Anti-βA (α-3D6) IHC

The mice that presented signal for Aβ plaques in the first round of anti-Aβ IHC were selected for a second round of anti-Aβ IHC. Because the final tissue analysis is carried out to determine the percentage of hippocampal area, of each animal, that has a positive signal for Aβ peptide (i.e. the percentage of HC area that is occupied by plaques), only the sections of animals of the genotypes FloxJ20Cre- and FloxJ20Cre+ were selected for the second round of anti-Aβ IHC (since these are the ones that presented plaques). One tube of sections of each J20+ animal was used for this IHC.

The mice were divided in two turns (between 2 plates with wells and baskets): half the animals were stained in the first plate with wells (one well and basket per animal) and the other half in the second plate with wells. The IHC in the second plate started one day later than the IHC in the first plate, but they were developed with DAB together, in the same day. Upon this IHC, differentially stained sections against Aβ, representing the whole brain (from anterior to posterior), are obtained for every animal with plaques, and the plaque load of each one can be observed throughout brain regions.

3.6 Mounting of mouse brain sections

Once again, the sections were mounted in treated glass slides. In this case two slides were used for each animal and the sections were placed in order (from anterior to posterior regions). The sections in the slides were left to dry in an oven for a few days, dehydrated with solutions of ethanol and xylene, and then mounted with a coverslip and Eukitt® mounting medium. The images that follow are of two slides containing brain sections stained by IHC against Aβ, that were obtained and mounted. Each slide contains sections belonging to a different animal.

Figure 3.2: Brain sections, from J20+ animals, that were obtained and mounted in order in the slides. Each slide has written the name of the animal (JfRLn44237 and JfRLn4439), the name of the primary antibody used in the Aβ IHC (α-3D6 is the antibody against Aβ that was used), and the date when the tissue was mounted (22 of May of 2019). There is also the indication that this is the first slide with tissue of each animal since there was a second slide for each one, with sections of regions that were not photographed or quantified, such as the olfactory bulbs and the cerebellum.

3.7 Image Taking

Images of each brain section that resulted from the second anti-Aβ IHC were taken in a NIKON microscope, model ECLIPE-600, at a 10x magnification. The focus of these images was the HC, since that was the zone to be further analyzed. Most hippocampus analyzed were too big for the range of the microscope camera used, so two pictures had to be taken, one with the initial part starting where the HC starts (the HC was displayed as horizontally as possible for this step) and the second picture starting where the first picture finished, with no overlap between them. This way the range of the camera was used to control the size of the HC areas that were analyzed, especially in the case of HCs contained in sections belonging to more posterior regions of the brain. Since posterior HCs were bigger and did not fit entirely in the two photos, it was decided that the maximum HC area to be analyzed would be the area that could fit in the dimensions of two photos at 10x magnification. Anterior HCs were smaller and

could fit entirely in the two photos. The areas of HC and the plaque loads in the two pictures were then added so that the plaque % could be calculated for each HC section.
Each picture was named with the name of the animal of which brain it captured and a number, so that they could be organized in a file and identified. Pictures of each side of the cortex of each section were also taken and organized, but these were not quantified in the present project because there was not enough time. A system was created to keep track of what each image belonged to (which animal, which section and which side of the section, since some sections contained two HCs). All the slides with sections that were analyzed were photographed side by side. In this photo of the slides the different sections of each slide were numbered, and the two sides of the sections were also differentiated in a and b. An excel file was created, with a table for each animal. In the table of each animal it was annotated the number of each section and its two sides (a and b), each one corresponding to the name of the image that captured it. These images were then used for the quantification of the percentage of HC area containing Aβ plaques.

3.8 Quantification of Plaque Area

The images were processed and analyzed with the software *Fiji (Fiji Is Just ImageJ)*, based on the program *ImageJ*, which is an open source image processing program designed for scientific images. In each image, the area of interest was cropped around, in this case the hippocampus. The cropping was done using a tool available in the fiji (imageJ) program. It was important to crop out areas of the image that contained folded tissue or dust, and zones of tissue that were too dark, since these could be mistaken for Aβ plaques by the quantifier program and lead to errors in the quantification of plaque %. The macro used for the quantification of the percentage of area containing amyloid plaques was one of the plugins available in *Fiji (Fiji Is Just ImageJ)*.

After the HC areas were cropped, the *ImageJ* macro (quantifier) was trained, using the option *trainable weka segmentation*. The training of the quantifier was done with the same images (already cropped) that were to be quantified, to maximize accuracy. The program used for the Aβ plaques quantification presented four different categories - tissue, plaques, vessels and outside - in which the different regions of the image were classified. The training of the program consisted in choosing several small regions of many different images and indicating the program which category they belonged to, so that it would learn to classify according to these indications. The training process was repeated until the program was classifying the images well on its own. Each category had a specific color, which made it easy to see how the program was classifying the images: plaques were purple, vessels green, tissue yellow and outside pink. The quantification ability of the program would be tested on one of the images, and if the results were not good, the training would be prolonged, and then it would be tested again. This was repeated until the results of the quantification were satisfactory. The quantifier could differentiate the distinct categories in the sections based on color and texture.

Because some images were darker than others, it was determined that the best option to minimize errors was to analyze the light and dark images with slightly different macros. The images were divided in two folders: the light folder, containing lighter images (in which the plaques and tissue were lighter), and the dark folder containing darker images (in which the plaques and tissue were darker), and two distinct macros were trained: light macro (able to recognize light plaques) and dark macro (able to recognize dark plaques and dark tissue). The light macro was also able to recognize dark plaques, but it could wrongly classify some tissue that was darker as plaques, while the dark macro could recognize light tissue, but could also wrongly classify some light plaques as tissue.

The obtained results from the quantification were two excel files (light and dark), both with a table containing the name of every picture analyzed and the quantification, for each picture, of the fractions of area occupied by tissue, plaques, vessels and outside. The results also included each image with its different zones colored according to the category that they were classified as, to show how each picture was classified (making it easy to check if the quantification was accurate).

Chapter 4

Results and Discussion

4.1 Flox+Cre+ animals were reelin-KO

A reelin IHC was done in two brain sections of each mouse, to ascertain which animals expressed reelin in their brains and which did not. The mice had been previously genotyped by PCR, and the results of the reelin IHC were used to check the component of the genotype related to reelin expression and to check if the reelin inactivations after the injection of tamoxifen were successful (i.e. to check if the Cre+ mice were reelin-KOs as expected). Upon the reelin IHC, the mice were divided according to the results of the observed reelin signals in reelin-WT and reelin-KO.

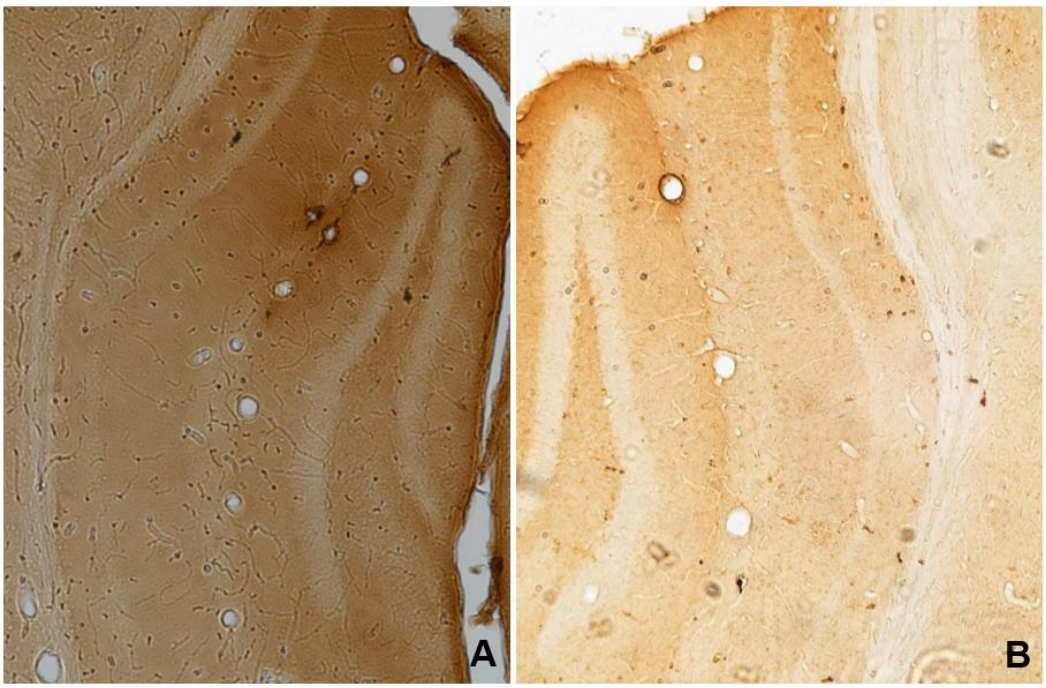

Figure 4.1: Brain sections (10x magnification), focused on the HC (and on a part of the corpus callosum, above the HC). An IHC against reelin was performed in both sections. **A)** No reelin signal was observed from the IHC. This section belongs to a mouse model of the genotype Flox+Cre+, which is not expected to express reelin. Because no reelin signal is observed in this section, the Cre+ genotype is confirmed, and the mouse is classified as a reelin-KO. **B)** Reelin signal is observed from the IHC. This section belongs to a mouse model of the genotype Flox+Cre-, that is expected to express reelin. The reelin signal consists on stained cells, which contain reelin (darker stains). The reelin signals are visible in the HC, under the corpus callosum (for example). Because reelin signal is observed in this section, the reelin genotype is confirmed, and the mouse is classified as a reelin-WT.

It was observed that the sections which did not display reelin signal (figure 4.1-A is an example of this case), belonged to mice previously genotyped by PCR as Flox+Cre+. Mice that did not express reelin were considered reelin-KOs. In fact, Cre+ animals were expected to be reelin-KOs, since they carried the Cre recombinase gene, that silences the RELN gene. If no reelin signal is observed in a brain section

of a Flox+Cre+ mouse, then the Cre+ genotype is confirmed, and it is concluded that the reelin inactivation was complete/successful in that animal. All animals were Flox+.

Moreover, it was ascertained that the brain sections from mice that had been previously genotyped by PCR as Flox+Cre-, were differentially stained by the reelin IHC, displaying reelin signals (figure 4.1-B is an example of this case). The reelin signal consists on stained cells that contain reelin (appearing darker). The animals that were Cre-, did not carry the Cre recombinase gene, and were therefore expected to be reelin-WTs (since the RELN gene was not silenced). If reelin signal was observed in a brain section of a Flox+Cre- mouse, then the Cre- genotype was confirmed in that animal. All Cre- mice expressed reelin and were therefore classified as reelin-WTs.

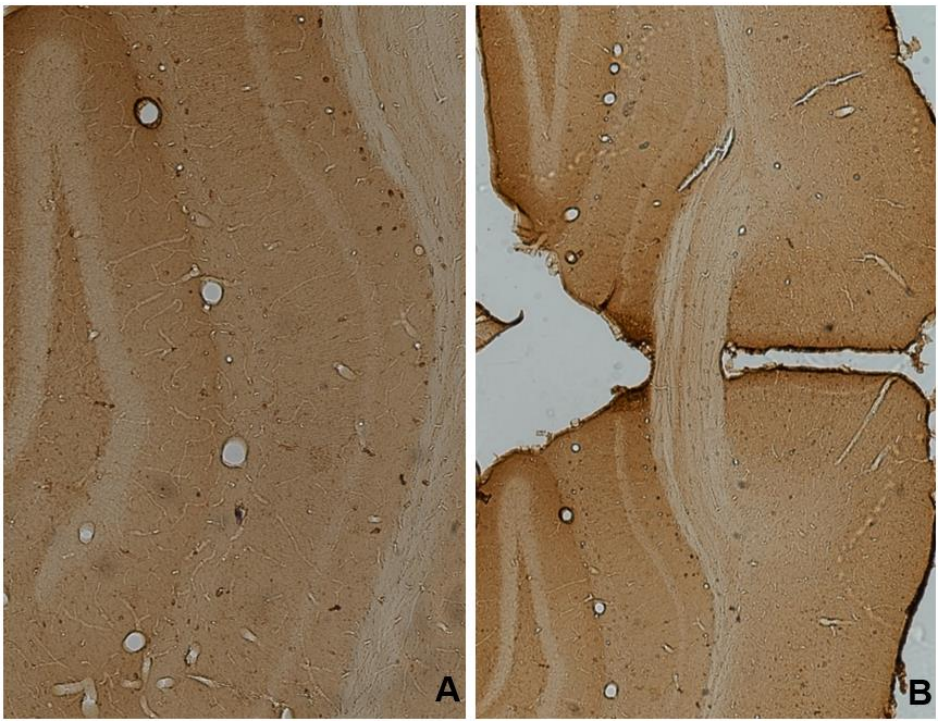

Figure 4.2: Brain sections in which an IHC against reelin was performed, and reelin signal was observed. The sections belong to the mouse model JFRLn4452, of the genotype Flox+Cre+, which is not expected to express reelin. Because the reelin signal was observed in its brain sections, this animal was classified as a failed reelin inactivation (is not included in neither one of the reelin genotype groups and becomes excluded from further calculations). **A)** Brain section (10x magnification), focused on the HC (and on a part of the corpus callosum) of mouse model considered a failed reelin inactivation. Reelin signals are visible in the HC under the corpus callosum. **B)** Brain section (4x magnification), focused on two HCs, the corpus callosum, and the superior cortex. The reelin signals are visible in the HC under the corpus callosum. Some darker stains are small vessels or dust that attached the tissue, and that also became stained, but too intensely, it is important to differentiate them from the reelin signal, which is more subtle.

Two mouse models that were expected to be reelin knockouts, because they had been previously genotyped by PCR as Flox+Cre+, displayed reelin signal (the case of JFRLn4439 and JFRLn4452, which is exemplified in figure 4.3 and figure 4.4). The first assumption upon the observation of the reelin signal was that the genotype of these animals could be wrong, so the Cre PCR was repeated for the two mice. After the Cre PCR results were Cre+ again, the genotype was confirmed, and these two mice

were classified as failed or partial inactivations. The animals considered failed inactivations were not included in neither one of the reelin genotype groups and were excluded from further calculations.
Upon observation of the differential staining resulting from the reelin IHC, in the analyzed sections, the animals were grouped: five mice presented no reelin signal and were classified as reelin-KOs (complete reelin inactivations upon tamoxifen administration), whereas fifteen displayed reelin signal (and were Cre-), being classified as reelin-WTs.

4.2 J20+ animals presented Aβ plaque deposits

After the reelin IHC, an IHC against amyloid beta (Aβ) was done, again, in two brain sections of each mouse. This Aβ IHC was carried out to analyze which animals presented Aβ plaques in their brain, and which did not. The results of the Aβ IHC were used to check the J20 genotypes previously obtained by PCR. Mice that are J20+ carry the mutated human APP (hAPP) transgene, which leads to Aβ plaque accumulation. Thus, J20+ mice are expected to present Aβ plaques, whereas J20- are not (since they do not carry the mutated hAPP gene). Upon the results of the Aβ IHC, the animals were divided according to the observed plaque phenotypes in J20+ (plaques) or J20- (no plaques).

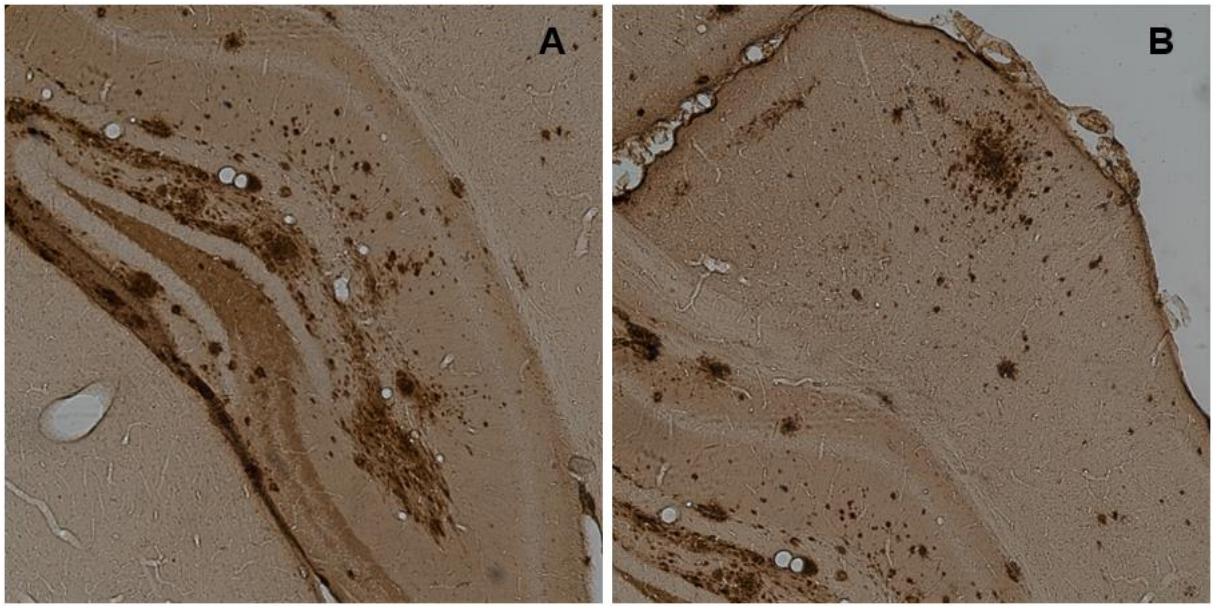

Figure 4.3: An IHC against Aβ was performed in these sections belonging to a mouse previously genotyped as J20+ by PCR. The tissue was differentially stained by the IHC: Aβ signal is observed, which consists on stained plaques (colored darker). Because plaques are observed in these sections, the J20+ genotype is confirmed. The mice of which sections presented Aβ signal from the Aβ IHC, such as this one, were classified as J20+. **A**) Brain section (10x magnification) analyzed in the first Aβ IHC, focused on the HC. **B**) Brain section (10x magnification) analyzed in the first Aβ IHC, focused on the superior part of the cortex.

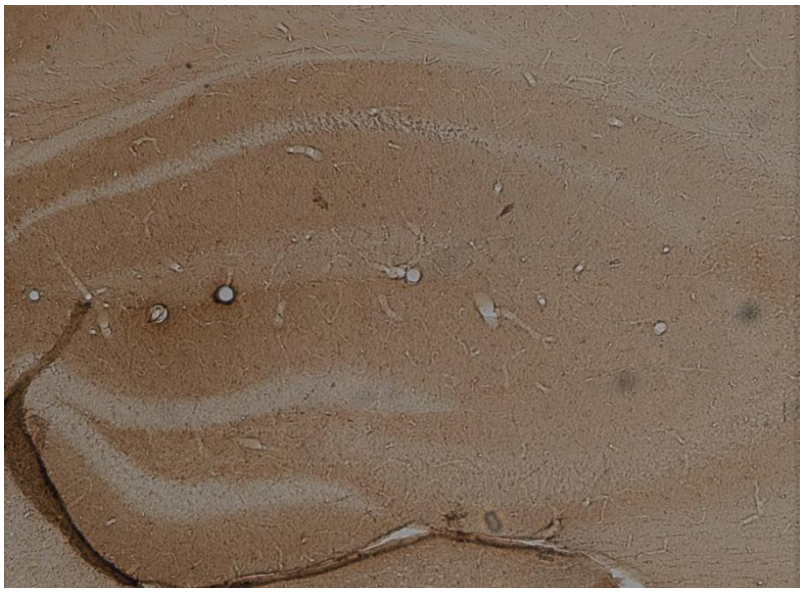

Figure 4.4: Brain section (10x magnification) analyzed in the first Aβ IHC, focused on the HC of a mouse model previously genotyped by PCR as J20-. An IHC against Aβ was performed in this section and no signal for Aβ was observed (there is no differential staining in the tissue). Because no Aβ signal is observed in the section, the J20- genotype is confirmed. The mice of which sections presented no Aβ signal from the Aβ IHC, such as this one, were classified as J20-.

It was observed that all the sections belonging to mouse models previously genotyped by PCR as J20+ displayed positive signal for Aβ plaques, obtained from the Aβ IHC, as it was expected (pictures in figure 4.6 are examples of this case). Because differentially stained Aβ plaques were observed in these tissue sections, the J20+ genotype was confirmed (the phenotype matches the genotype).

The sections belonging to mouse models previously genotyped by PCR as J20- presented no signal for Aβ plaques, as expected (figure 4.7 is an example of this case). Because no Aβ signal was observed in the brain sections of J20- mice (i.e. no differential staining for Aβ was encountered), the J20- genotypes were confirmed. The results regarding the presence of Aβ plaques of all the sections analyzed in this step matched what was expected from the genotype of the mouse they belonged to. Thus, all the J20 genotypes were confirmed in this Aβ IHC: plaque phenotypes matched the J20 genotypes. The animals were grouped according to the Aβ plaques observations: twelve mice were classified as J20+ (Aβ plaques), whereas ten were classified as J20- (no Aβ plaques). Only the J20+ animals were studied further, since the aim was to compare the plaque loads of the two reelin genotypes.

Table 4.1 shows the genotype of each animal and the respective reelin and Aβ plaques phenotypes, observed from the presence or absence of reelin and Aβ plaques signals (differential staining) resulting from the respective IHCs. The reelin IHC exposed two failed reelin inactivations, while the first round of IHC against Aβ confirmed all the J20 genotypes previously obtained by PCR.

Table 4.1: Genotypes and respective reelin and Aβ plaques phenotypes (presence or absence of reelin and Aβ plaques) of all the animals studied in the reelin IHC and in the first round of Aβ IHC. The reelin phenotypes were ascertained from the results of the reelin IHC, observed in the microscope. The Aβ plaques phenotypes were ascertained from the results of the Aβ plaques IHC, observed in the microscope (signal or no signal). Mice were divided according to their reelin phenotype: 5 mice were classified as reelin-KOs, whereas 15 were classified as reelin-WTs (the 2 failed reelin inactivations are not included in either one of the groups). Mice were also divided according to their Aβ plaques phenotype: 12 were classified as J20+ (Aβ plaques) and 10 as J20- (no Aβ plaques). JFRLn4428 and

JFRLn4437 are in red because these animals have the goal genotype in this study, being J20+ and Cre+, and complete/successful reelin inactivations.

Animal	Genotype	Reelin	Aβ plaques
JfRLn4421	Flox+J20-Cre-	+	-
JfRLn4422	Flox+J20+Cre-	+	+
JfRLn4423	Flox+J20+Cre-	+	+
JfRLn4424	Flox+J20-Cre+	-	-
JfRLn4425	Flox+J20+Cre-	+	+
JfRLn4428	Flox+J20+Cre+	-	+
JfRLn4431	Flox+J20+Cre-	+	+
JfRLn4432	Flox+J20-Cre-	+	-
JfRLn4433	Flox+J20-Cre+	-	-
JfRLn4434	Flox+J20-Cre+	-	-
JfRLn4435	Flox+J20+Cre-	+	+
JfRLn4436	Flox+J20+Cre-	+	+
JfRLn4437	Flox+J20+Cre+	-	+
JfRLn4438	Flox+J20+Cre-	+	+
JfRLn4439	Flox+J20+Cre+	failed inact. +	+
JfRLn4440	Flox+J20+Cre-	+	+
JfRLn4441	Flox+J20+Cre-	+	+
JfRLn4452	Flox+J20-Cre+	failed inact. +	-
JfRLn4455	Flox+J20-Cre-	+	-
JfRLn4456	Flox+J20-Cre-	+	-
JfRLn4483	Flox+J20-Cre-	+	-
JfRLn4484	Flox+J20-Cre-	+	-

The novelty of this experiment was the study of animals with the genotype Flox+J20+Cre+, since those mice have brains with Aβ plaques and no reelin, simultaneously (i.e. these are models of AD pathology combined with reelin absence). Only two mice were classified both as reelin-KO and J20+.

4.2.1 Second anti-Aβ IHC of J20+ sections for further plaque quantification

The J20+ animals were selected for a second round of anti-Aβ IHC. This time, one entire tube of brain sections (corresponding to approximately 10% of the brain) of each animal was used. This anti-Aβ IHC was done to differentially stain Aβ plaques in the tissue sections, making them visible under the microscope, for further plaque quantification. Photos of every brain section that was submitted to the second round of Aβ IHC and contained the hippocampus were taken in the microscope (figure 4.9 contains examples of the photos). These pictures, in which the stained plaques are easily detected, were taken so that the macro quantifier could then analyze them and quantify the plaque area.

For each side of each HC (in each section) one or two photos were taken (depending on the size of the HC). Most hippocampi analyzed were too big for the range of the microscope camera used, so two pictures had to be taken. The areas of HC and plaque loads in the two pictures were then added so that the plaque % could be calculated for each HC section.

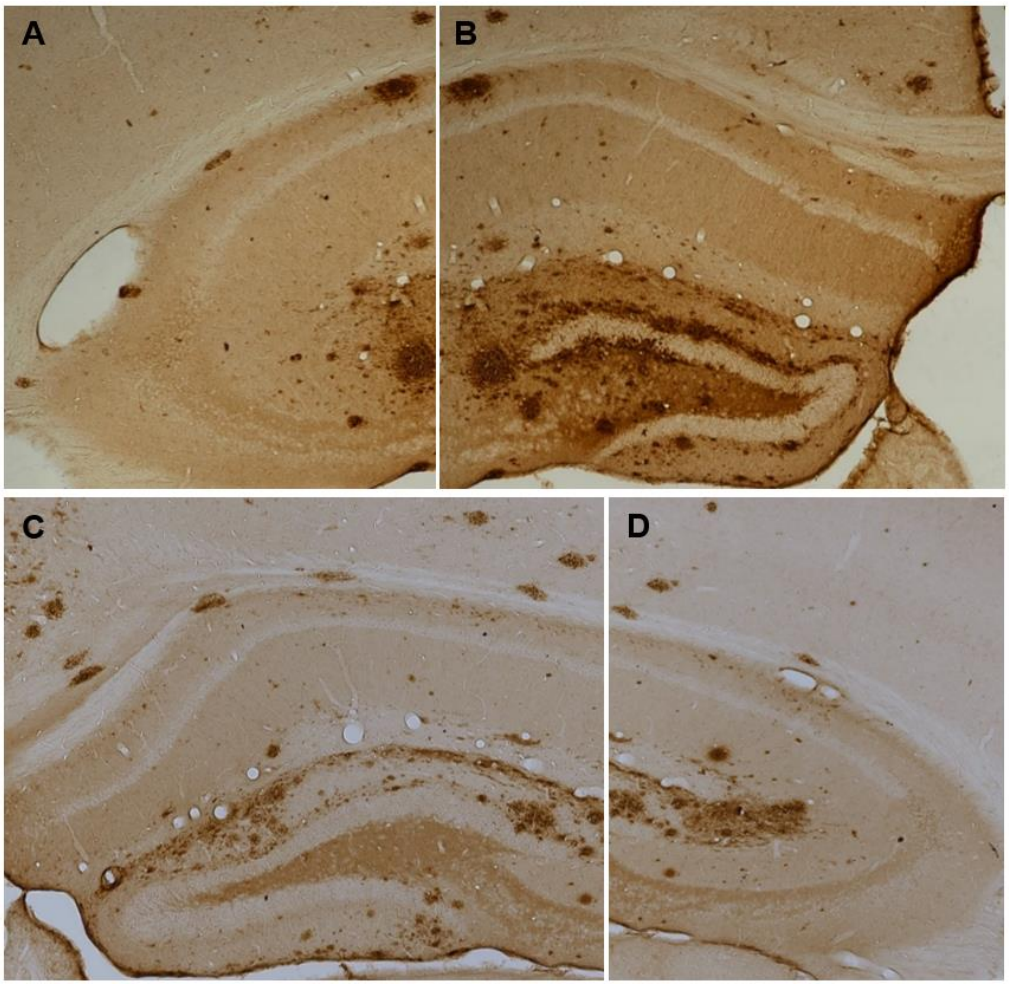

Figure 4.5: Hippocampus sections (10x magnification) of two J20+ mouse models. As in most cases the HC was bigger than the camera range of the microscope used, two pictures were taken. Pictures A and B correspond to one HC section and pictures C and D correspond to another section. An IHC against Aβ was performed in both sections, being the Aβ plaques the darker stains.

4.2.2 Pictures of sections of J20+ animals were cropped for analysis and used to train the quantifier

After pictures of every HC contained in the sections submitted to the second round of IHC against Aβ were taken, they were processed and analyzed with the software *Fiji* (*Fiji Is Just ImageJ*). The first step was to crop around the area of interest for quantification, of each picture, using tools available in the *Fiji* software. Since the brain region where the plaques were quantified was the HC, that is the zone around which the cropping was done. Figure 4.10 is an example of the cropping accomplished around the HC of a J20+ mouse model (more examples can be found in appendix 3).

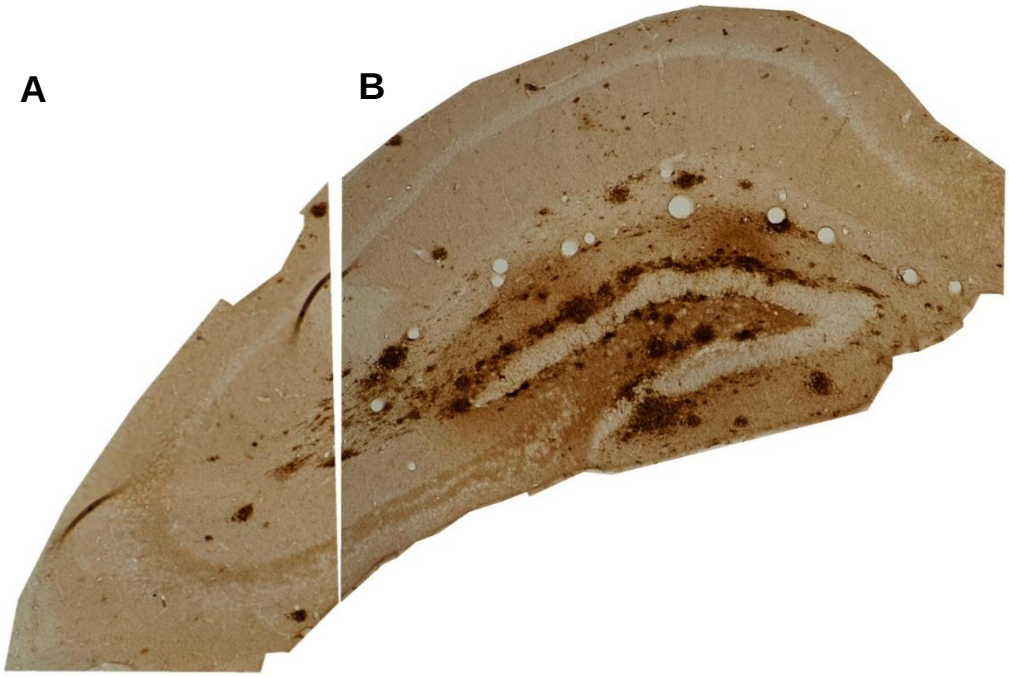

Figure 4.6: Cropping from 2 pictures of a HC from a section of a J20+ mouse model (10x magnification). Pictures A and B represent the same HC section. An IHC against Aβ was performed in this section, and differential staining for Aβ plaques was observed. The original picture was cropped around the HC, since that is the brain region in which the plaques were quantified. It was important to cut out areas with folded tissue or dust, and zones of the tissue that were too dark, that could be mistaken for Aβ plaques by the program and lead to errors in the plaque % quantification. The small area of tissue missing in the superior left side of the image in picture A was a bit of folded tissue that had to be cut out.

4.3 Aβ plaque load in J20-KOs was not statistically higher than in J20-WTs

After the HC areas were cropped, the *ImageJ* macro quantifier was trained. The training of the quantifier was done with the same images (already cropped) that were to be quantified, to increase accuracy. The macro was trained to distinguish between areas of outside, tissue, vessels, and Aβ plaques, being then able to differentiate these categories based on color and texture. After the training of the quantifier, it was run on all the images. The obtained results from the quantification were the fractions of area occupied by tissue, plaques, vessels, and outside, for every image.

With the information obtained from the analysis with *ImageJ*, of the fraction of area corresponding to tissue, plaques, vessels and outside, for each image, the fraction of total area was calculated by the sum of the fractions of tissue, plaques and vessels (only excluding the fraction of outside area) (eq. 1). The fractions of area occupied by plaques (plaque area) obtained from cropped pictures that corresponded to the same HC section were added (eq. 2) and the same was done for the fractions of total hippocampal area that corresponded to the same HC section (eq. 3). Thus, the fraction values of total plaque area and of total hippocampal area were obtained for each HC section. These values were then used to calculate the percentage of area occupied by plaques in each HC section, through the

division of the fraction of total area occupied by plaques in a HC times 100 by the fraction of total area of that same HC (eq. 4). Thus, the values of the percentage of plaque area in the HC were obtained for every HC section.

$$\text{frac. total area of HC} = \text{frac. area plaques} + \text{frac. area tissue} + \text{frac. area vessels} \quad \text{(Eq. 1)}$$

$$\text{frac. tot. plaque area of one HC} = \text{frac. plaque area (part 1)} + \text{frac. plaque area (part 2)} \quad \text{(Eq. 2)}$$

$$\text{frac. total area of one HC} = \text{frac. total area of HC (part 1)} + \text{frac. total area of HC (part 2)} \quad \text{(Eq. 3)}$$

$$\%\ \text{plaque area of one HC} = \frac{100 * \text{fraction of total plaque area of one HC}}{\text{fraction of total area of one HC}} \quad \text{(Eq. 4)}$$

Moreover, anterior and posterior means of the percentage of plaque area in the HC were calculated for each animal. The anterior mean was obtained by the calculation of the average of the values of plaque area % from HC sections considered from anterior brain regions (eq. 5), whereas the posterior mean was obtained by the calculation of the average of the values of hippocampal plaque area % from HC sections considered from posterior brain regions (eq. 6). These means were calculated to check how the plaques distributed throughout the mouse brains, to ascertain if the deposition was more intense in anterior or posterior regions. The criteria used to separate the HC in anterior and posterior was based on bregma criteria, using the Paxinos Atlas of the mouse brain (Paxinos, Charles Watson and Evan Calabrese, 2015). Bregma is the point of junction of the coronal and sagittal sutures of the skull, and it is used as a reference point in the brain. HCs that were considered from anterior regions of the brain were smaller and were disposed horizontally in the sections, while HCs that were considered from more posterior regions were bigger and appeared oblique in the sections.

$$\text{Anterior Mean of plaque area \% of an animal} = \frac{\text{Sum of \% area of plaques of all anterior HCs}}{\text{number of anterior HCs}} \quad \text{(Eq.5)}$$

$$\text{Posterior Mean of plaque area \% of an animal} = \frac{\text{Sum of \% area of plaques of all posterior HCs}}{\text{number of posterior HCs}} \quad \text{(Eq.6)}$$

Furthermore, the total mean of plaque area percentage in the HC was calculated for each animal (eq. 7). The mean of the fractions of total area of HC was also calculated for each animal (eq. 8). A standard deviation was also calculated for each mean, to control the dispersion of the sets of values used for the calculation of the animal means. The anterior plaque % mean, posterior plaque % mean, total plaque % mean, and area of hippocampus mean were calculated for each animal so that after the animals were separated, according to their genotypes, into J20 reelin-KO and J20-controls, the values of the same means could be calculated for the two genotypes.

$$\text{Total mean of plaque area \% in HC of an animal} = \frac{\text{Sum of \% area plaques of all HCs}}{\text{number of HCs}} \quad \text{(Eq.7)}$$

$$\text{Mean of fractions of total HC area of an animal} = \frac{\text{Sum of frac.total area ofall HCs}}{\text{number of HCs}} \quad \text{(Eq.8)}$$

Table 4.2: J20+ animals and their respective reelin genotypes and results of anterior plaque % mean, posterior plaque % mean, total plaque % mean, and area of hippocampus mean, calculated for each one. These results were then grouped according to the genotype of the animal that they belonged to and used to calculate the same four means for the two reelin genotypes (J20 reelin-KO and J20-controls). 9 animals were of the genotype J20 WT and 2 were of the genotype J20 KO.

Animal	Genotype	Anterior % Plaques Mean	Posterior % Plaques Mean	% Plaques Mean	HC Area Mean
JFRLn4422	Reelin	1.89698499	0.322072046	1.109528518	0.823522353
JFRLn4423	Reelin	0.83482268	0.632045193	0.733433936	0.883749333
JFRLn4425	Reelin	1.721805894	0.5873116	1.154558747	0.890085263
JFRLn4428	No Reelin	2.381670939	1.545187979	1.963429459	0.855482941
JFRLn4431	Reelin	0.729374265	1.436571594	1.08297293	0.924238889
JFRLn4435	Reelin	2.890339836	3.737329086	3.313834461	0.93930625
JFRLn4436	Reelin	1.333464171	1.096554057	1.215009114	0.937124667
JFRLn4437	No Reelin	2.149824248	1.849788886	1.999806567	0.944633846
JFRLn4438	Reelin	1.435346148	1.471559692	1.45345292	0.870728667
JFRLn4439	Reelin (failed inactivation)	4.228965099	2.024577924	3.126771512	0.76174125
JFRLn4440	Reelin	5.278066242	1.894218367	3.586142304	0.810244118
JFRLn4441	Reelin	3.418355866	1.012127677	2.215241771	0.760728421

After the mean of hippocampal plaque % was calculated for each animal, these were divided according to their reelin genotypes: J20 reelin-KO (no reelin) and J20-controls (reelin) and the same 4 means were calculated for each genotype. 9 animals were classified as J20 WT, and 2 animals were classified as J20 KO. The anterior and posterior means of plaque percentage were also calculated for both groups, to check if the different reelin genotypes influence the distribution of plaques in the brain, in terms of the deposition being more anterior or posterior.

The mean of the Aβ plaque area percentage in the HC was calculated for the two genotypes (eq. 9), to find out if the intensity of plaque deposition in the mouse brains was affected by the absence of reelin. The mean of the total HC area was also calculated for both genotypes, to verify if the two means of plaque percentage are comparable between them, i.e. to check if the areas of the HC are similar in both genotypes, because if the areas were not comparable, similar plaque loads would originate distinct plaque percentages, or vice versa.

The mouse JFRLn4439 was a failed inactivation, so it was not used in the calculations of the means of neither genotype, since although it presented reelin it cannot be considered a control mouse. The results for the two reelin genotypes of the anterior plaque % mean, posterior plaque % mean, total plaque % mean, and area of the hippocampus mean are presented in table 4.6. These results were used to do a statistical analysis in order to ascertain if there is a difference in plaque deposition between genotypes.

$$\text{Mean of plaque area \% in the HC, of a geotype} = \frac{\text{Sum of total means of plaque area \% in HC of all animals of the genotype}}{\text{size of the population of the genotype (n)}} \quad \text{(Eq.9)}$$

Table 4.3: Anterior plaque % mean, posterior plaque % mean, total plaque % mean, and area of hippocampus mean for the two reelin genotypes (both J20+) KO and WT (control).

Genotype	Anterior % Plaques Mean	Posterior % Plaques Mean	% Plaques Mean	Area of each HC Mean
J20 KO (No Reelin)	2.265747594	1.697488433	1.981618013	0.944633846
J20 Control (Reelin)	2.170951121	1.354421035	1.762686078	0.871080884

Four bar graphs representing Mean +/- SEM were created, one for each of the means, comparing the two genotypes (J20 controls and J20 reelin-KO). A t-student statistical analysis was completed to compare the results of each mean, between the two genotypes. The difference between the 2 genotypes was not significant (N.S.) for any of the means represented in the graphs, indicating no significative difference in the % of HC area occupied by plaques, between genotypes. The standard error of mean (SEM) describes the variability within the sample, it is a measure of precision for an estimated population mean (Jaykaran, 2010).

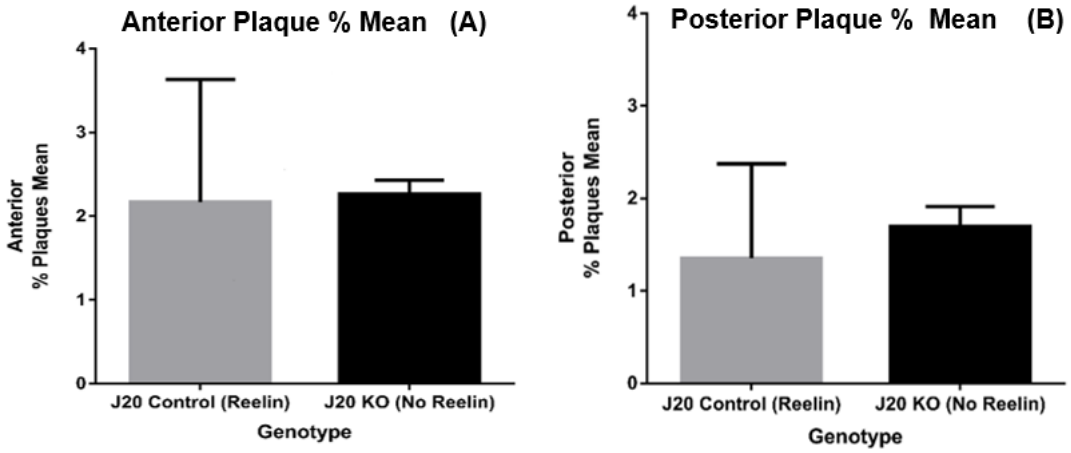

Figure 4.7: A) Anterior mean of plaque % in the HC for J20-controls and J20 reelin-KOs (Mean +/- SEM). Results of the unpaired t test: P value = 0,9319 (N.S.), t=0,08788 df=9. **B)** Posterior mean of plaque % in the HC for J20-controls and J20 reelin-KOs (Mean +/- SEM). Results of the unpaired t test: P value = 0,6603 (N.S.), t=0,4544 df=9. The results of the t-student analysis done on the results of both the anterior plaque % mean and posterior plaque % mean were that the difference between the 2 genotypes was not significant (N.S.), implying no difference in the % of area occupied by plaques in the anterior and posterior regions of the HC, between genotypes.

The outcome of the t-student analysis done on the results of both the anterior plaque % mean and posterior plaque % mean were that the difference between the 2 genotypes was not significant (N.S.). This implies that the difference between genotypes, of HC area % occupied by Aβ plaques, in the anterior brain regions, was not significant, and the same is true for posterior brain regions (i.e. the difference, between genotypes, of HC area % occupied by Aβ plaques, in the posterior brain regions, was also not significant).

Moreover, it is visible in the graphs that the value of the SEM of the J20 control genotype is considerable in both the anterior and posterior plaque % means (figure 4.7 (A, B)), indicating variability in the results of animals belonging to the control group. On the other hand, the SEM value of the J20 KO genotype is small in both cases, indicating more precision in the population of results obtained for the KO group (since this population is composed of only 2 animals, it indicates that the values of the anterior and posterior plaque % means of these 2 animals are similar).

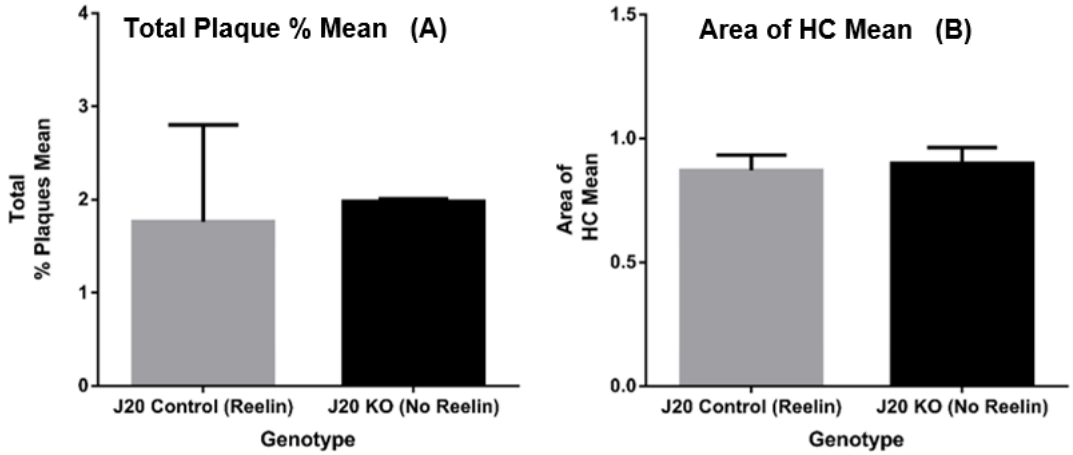

Figure 4.8: A) Total mean of plaque % for J20-controls and J20 reelin-KOs (Mean +/- SEM). Results of the unpaired t test: P value = 0,7816 (N.S.), t=0,2857 df=9. The outcome of the t-student analysis done on the results of the total plaque % means of the 2 genotypes was that the difference between genotypes was not significant (N.S.), indicating no difference in the plaque area %, in the HC, between genotypes. **B)** Mean of HC Area for J20-controls and J20 reelin-KOs (Mean +/- SEM). Results of the unpaired t test: P value = 0,5640 (N.S.), t=0,5989 df=9. The outcome of the t-student statistical test done on the results of the HC area means was that the difference between the 2 genotypes was not significant (N.S.), demonstrating that the areas of HC in the 2 genotypes are similar, which implies that the plaque means are comparable.

The outcome of the t-student analysis done on the results of the total Aβ plaque % means in the HC, of the 2 genotypes, was that the difference between the 2 genotypes was not significant (N.S.), indicating no significant difference in the % of area occupied by plaques in the HC, between genotypes. The outcome of the t-student statistical test done on the HC area means was also non-significant (N.S.), meaning that the areas of HC are similar in both genotypes, and that the values of plaque area % in the HC are comparable. It is visible in the graph of the total plaque % mean (figure 4.8 (A)) that the value of the SEM of the J20 control genotype is considerable, indicating variability in the results of animals belonging to the control group, while the SEM value of the J20 KO genotype is small in both cases, indicating more precision in the population of results obtained for the KO group.

The initial hypothesis of the experiment was that the absence of reelin would lead to the increase of amyloid beta deposition in the hippocampus and throughout the brain of J20+ mouse models, sacrificed at 12 months. The results obtained do not support the initial prediction. In fact, although the mean of HC area occupied by plaques is higher in the case of animals that were reelin-KOs than in the case of reelin-WTs, this difference is not statistically significant. The results also show that a bigger percentage of HC area is occupied by Aβ plaques in the more anterior regions of the brain versus in posterior ones, which

is explained by the fact that hippocampus considered posterior are bigger than anterior ones (the amount of plaques was not smaller).

It is important to consider that unfortunately only two reelin knockouts were J20+, which represents a very small sample (n=2). Because the sample is small it cannot be representative of the whole reelin-KO population (i.e. it cannot be easily generalized to bigger groups). Moreover, the results of the means of HC plaque area % in J20 reelin-control animals displayed a high variation between themselves (elevated SEM). In fact, most animals expressing reelin had plaque % results around 1% (i.e. 2/3 of the J20-WTs had significantly less plaque load than the 2 J20-KO animals studied), while two mice (JFRLn4435 and JFRLn4440) presented plaque means above 3% and another mouse (JFRLn4441) presented a plaque mean percentage of 2,2%. Thus, only 2/3 of the reelin-WT animals displayed the expected results of lower Aβ plaque load than reelin-KOs.

This variation in the influence of reelin on plaque deposition, seems to suggest that reelin does not cause the same effect of slowing down the deposition of plaques in every organism. It might have a more positive impact in some individuals than in others, in which case the results of its activity would be difficult to predict with certainty. The variation in plaque load between animals can also be because some animals carrying the hAPP mutation accumulate Aβ more dramatically than others, maybe because some are more susceptible to the mechanisms that lead to plaque development, induced by the mutation. The variation can also be due to the small population size, i.e. it might be rare and specific of this population of analyzed mice, in which case a bigger population of animals would cause this variance to lose significance.

Moreover, it is possible that some of the J20-WT mice presented bigger Aβ plaque percentages because the reelin activity was lower in these animals. In fact, although these mice were all WT for reelin expression, reelin activity was not measured and compared. In the brains of some animals the reelin pathway might have become less active in the course of plaque accumulation, which can be an explanation for the higher plaque loads observed in some J20-WT mice. Nonetheless, it was expected that the J20-KO mice would present significantly higher amounts of Aβ plaques than J20-WTs, and it was not the case.

Chapter 5
Conclusions and Future Work

The hypothesis that reelin deficiency increases Aβ deposition needs further investigation with more mouse models, so that larger populations can be obtained for each genotype, which could possibly lead to different results. On the other hand, if the results with more animals agreed with the ones obtained in this experiment, they would be more statistically significant. Moreover, the study of plaque load can be extended to other brain regions such as the cerebral cortex and the corpus callosum, and other tests can be performed so that more complete results can be obtained.

Plaque detection with Congo Red staining allows the observation of dense plaques (amyloid plaques can be dense or diffuse). The Congo Red is an anionic stain that recognizes the β-folded conformation of the monomers that make up the dense amyloid plaques. The stain deposits in the plaques through the formation of hydrogen bonds, specifically staining dense plaques. With the aim of understanding if the presence of reelin in the adult brain has an influence on the type of plaques that are more predominantly accumulated, some brain sections of animals being studied could be stained with Congo Red, in parallel with the analysis of IHC against Aβ.

Analyses of neuroinflammation can also be performed in the sections using Iba1 IHC and GFAP IHC. The presence of neuroinflammation, which is mediated by glial cells, is a fundamental aspect of degenerative diseases. The Iba1 IHC is used to look for the presence of activated microglia (microglia marker) and the GFAP IHC is used to look for the presence of activated astrocytes (astrocytes marker). The more signal for glial cells (such as microglia and astrocytes) is obtained, the more activated these cells are, and therefore the more inflamed the brain is. The percentage of area with positive signal for each marker can be detected and calculated in regions like the hippocampus, cortex and corpus callosum, in a similar way that was used in this experiment for plaques in the HC.

It has been observed, in previous studies, that the reelin pathway is decreased in brains of AD patients. In fact, AD patients present elevated reelin expression but low reelin function (Cuchillo-Ibañez et al., 2016). Evidence indicates that the interaction between reelin and Aβ causes an increase in reelin expression (due to a compensatory mechanism), but also a decrease in the internalization of ApoER2 (a reelin receptor) from the cytoplasmic membrane, therefore undermining intracellular reelin signaling. The results presently obtained do not indicate that reelin helps decrease Aβ accumulation and deposition in plaques, although, due to the small population tested, the results are not decisive enough to provide a conclusion that reelin does not play a role in decreasing Aβ plaque accumulation.

The problem with the present experiment might also have been that although reelin expression was kept normal in the J20-WT mice, the function of the reelin pathway might have become compromised in the brains of some mice in the course of plaque deposition, similar to what happens in the brains of AD patients. The reelin pathway might be affected differently by Aβ plaques in different individuals. In future experiments testing the impact of different levels of reelin expression, it would be interesting to also measure the activity of the reelin pathway while the animals are alive, to also compare these results,

and because the level of activity of the pathway is what actually influences brain mechanisms (rather than the level of expression of the protein responsible for initiating the pathway).

The new strategies for AD treatment focus on testing the neuroprotective activity of disease-modifying drugs in the presymptomatic stages of AD, using biomarkers to predict disease progression before the dementia becomes apparent. The aim of the new drugs being investigated for AD is disease prevention rather than treatment. Previous studies have suggested that reelin could be a good target for treatment, to help decelerate the progression of AD, by helping slow down plaque deposition (Pujadas et al., 2014). If after more complete investigation, it is learned that reelin significantly reduces the deposition of Aβ plaques (and thereafter, maybe reduces tau pathology and inflammation), then reelin treatments can be developed. The goal with reelin treatments/therapies would be to return reelin function to normal physiological levels in the brains of AD patients, since very early in disease progression (the earlier the better), or even before disease onset, if necessary, in the cases of people known to be carrying the genes for familial type AD (FTAD). The physiological activity of reelin could possibly delay AD progression or appearance, in the latter.

A practical and safe way for people to consume reelin, like a pill, could be developed, and an efficient and accurate way to measure the activity of the reelin pathway would be necessary. All the potentially disease modifying drugs developed until now, such as drugs that preclude the aggregation of Aβ oligomers, have failed to show positive effects on cognition in phase III trials (i.e. have failed to prevent AD in humans) (Yiannopoulou and Papageorgiou, 2012). Nonetheless, reelin is fundamentally different because it is a naturally present protein in the adult brain, and the aim of the treatment with reelin would simply be to keep its activity levels at a healthy, constant value. The challenge would be to measure the reelin activity levels in the course of the treatment and to adapt the dose of reelin to be taken by the patient according to the results of the measurement.

It is important that the doses of exogenous reelin intake, in the context of the suggested treatment, are not exceeded to a point that could cause reelin function to be at overexpression levels, since in experiments of reelin overexpression with mouse models it was observed that, although it seems to have a beneficial impact in the reduction of plaque load in the brain, it also leads to mispositioning of adult born neurons formed in the dentate gyrus (DG). In fact, mice overexpressing reelin presented aberrant positioning of newborn neurons (i.e. the adult generated neurons weren't introduced correctly in the preexisting brain circuitry), and showed pyramidal neurons of the granular layer of the DG with ectopic basal dendrites directed to the hillus (when these neurons should only have apical dendrites toward the molecular layer of the DG). The mispositioning of neurons and formation of useless dendrites could in turn lead to other complications and brain pathologies. Thus, the compensation of reelin levels in the brains of AD patients would need to be precise (Pujadas et al., 2010) (Teixeira et al., 2012) (Pujadas et al., 2014).

The precise control of reelin levels and reelin pathway activity levels in the brains of AD patients, and probable future AD patients, would be necessary in order to maintain healthy and constant levels of this protein in the brains of these people, therefore preserving the physiological activity of reelin. It would be important to understand when, in the course of AD progression, the reelin pathway becomes compromised. If in fact, the levels of reelin function decrease in the brains of AD patients before plaque

deposition, then this decrease could be a factor contributing to the deposition (or to the acceleration of the deposition), and a reelin reposition treatment could be a strategy for prevention of plaque formation in AD (or to slow it down). The brain levels of reelin and of the activity of the reelin pathway would need to be precisely measured, so that they could be controlled, specially and beginning earlier in cases of people known to have familial type AD in their family. The aim of a reelin compensation/reposition treatment would be to increase reelin concentration in a way that could bring the signaling activity of the protein to normal healthy levels, to compensate for the reelin that loses its function.

On the contrary, reelin pathway activity may decrease due to the formation of plaques, since it has been observed that reelin protein precludes the formation of Aβ plaques until it is captured by them and becomes stuck, losing its activity. The fact that reelin is captured by Aβ plaques might be one cause for the reduction of reelin activity in the presence of plaques, that has been observed, and the overexpression of reelin noticed in AD could be a compensatory mechanism, as it has been previously suggested. Thus, levels of active reelin may decrease because some of it becomes stuck in the plaques while trying to prevent their formation. In this case the reposition of reelin would be done only after the beginning of plaque development (since the excess of active reelin levels is to be avoided). It could be an effective way to slow down the evolution of plaque deposition, the progression of the disease, and the appearance of symptoms of cognitive decline.

It is also possible that both options are true, i.e. that the activity of the reelin pathway decreases first contributing to the accumulation of amyloid plaques, and that these plaques in turn capture the remaining reelin, which is trying to preclude plaque development thus, reducing the activity of reelin even further. Therefore, this could be a cycle in which the decreased activity of the reelin pathway contributes to an increased rate of plaque formation, which in turn leads to a bigger decrease of reelin activity, and of its pathway. In this case, reelin treatment for reposition and maintenance of its activity (at an ideal constant) could possibly be accomplished with a gradual increase of exogenous reelin consumption by the patient. In theory, this treatment would help slow down disease onset and progression as well as the arising of symptoms, but of course, it needs to be tested.

Nonetheless, it is still not clear weather Aβ plaques are in fact a toxic form of Aβ or if on the contrary plaques are an inactivated form of Aβ, while soluble oligomers are the most toxic species. If the latter is correct, the mechanism of reelin for reducing signs of cognitive impairment, which has been previously observed in reelin-overexpression experiments, will need to be investigated further and better understood.

References

[1] Schachter, A. S., & Davis, K. L. (2000). Alzheimer's disease. *Dialogues in clinical neuroscience*, *2*(2), 91–100.

[2] Bell, C. (1994). DSM-IV: Diagnostic and Statistical Manual of Mental Disorders. *JAMA: The Journal of the American Medical Association*, 272(10), p.828.

[3] Gao, S., Hendrie, H., Hall, K. and Hui, S. (1998). The Relationships Between Age, Sex, and the Incidence of Dementia and Alzheimer Disease. *Archives of General Psychiatry*, 55(9), p.809.

[4] Ritchie, K. and Kildea, D. (1995). Is senile dementia "age-related" or "ageing-related"? — evidence from meta-analysis of dementia prevalence in the oldest old. *The Lancet*, 346(8980), pp.931-934.

[5] Henderson, V. (1994). Estrogen Replacement Therapy in Older Women. *Archives of Neurology*, 51(9), p.896.

[6] Heeren, T., Lagaay, A., Hijmans, W. and Rooymans, H. (1991). Prevalence of Dementia in the 'Oldest Old' of a Dutch Community. *Journal of the American Geriatrics Society*, 39(8), pp.755-759.

[7] H. Ferreira-Vieira, T., M. Guimaraes, I., R. Silva, F. and M. Ribeiro, F. (2016). Alzheimer's disease: Targeting the Cholinergic System. *Current Neuropharmacology*, 14(1), pp.101-115.

[8] Hung, S. and Fu, W. (2017). Drug candidates in clinical trials for Alzheimer's disease. Journal of Biomedical Science, 24(1).

[9] Bracco, L., Bessi, V., Padiglioni, S., Marini, S. and Pepeu, G. (2014). Do Cholinesterase Inhibitors Act Primarily on Attention Deficit? A Naturalistic Study in Alzheimer's Disease Patients. *Journal of Alzheimer's Disease*, 40(3), pp.737-742.

[10] Diamond, A. (2013). Executive Functions. *Annual Review of Psychology*, 64(1), pp.135-168.

[11] Robert, P., Onyike, C., Leentjens, A., Dujardin, K., Aalten, P., Starkstein, S., Verhey, F., Yessavage, J., Clement, J., Drapier, D., Bayle, F., Benoit, M., Boyer, P., Lorca, P., Thibaut, F., Gauthier, S., Grossberg, G., Vellas, B. and Byrne, J. (2009). Proposed diagnostic criteria for apathy in Alzheimer's disease and other neuropsychiatric disorders. *European Psychiatry*, 24(2), pp.98-104.

[12] Wilcock, G., Esiri, M., Bowen, D. and Smith, C. (1982). Alzheimer's disease. *Journal of the Neurological Sciences*, 57(2-3), pp.407-417.

[13] Muir, J., Dunnett, S., Robbins, T. and Everitt, B. (1992). Attentional functions of the forebrain cholinergic systems: effects of intraventricular hemicholinium, physostigmine, basal forebrain lesions and intracortical grafts on a multiple-choice serial reaction time task. *Experimental Brain Research*, 89(3).

[14] Rosenberg, P., Nowrangi, M. and Lyketsos, C. (2015). Neuropsychiatric symptoms in Alzheimer's disease: What might be associated brain circuits? *Molecular Aspects of Medicine*, 43-44, pp.25-37.

[15] Cummings, J., Mintzer, J., Brodaty, H., Sano, M., Banerjee, S., Devanand, D., Gauthier, S., Howard, R., Lanctôt, K., Lyketsos, C., Peskind, E., Porsteinsson, A., Reich, E., Sampaio, C., Steffens, D., Wortmann, M. and Zhong, K. (2014). Agitation in cognitive disorders: International Psychogeriatric Association provisional consensus clinical and research definition. *International Psychogeriatrics*, 27(1), pp.7-17.

[16] Martorana, A. and Koch, G. (2014). Is dopamine involved in Alzheimer's disease? *Frontiers in Aging Neuroscience*, 6.

[17] Hampel, H., Mesulam, M.-M., Cuello, A.C., Farlow, M.R., Giacobini, E., Grossberg, G.T., Khachaturian, A.S., Vergallo, A., Cavedo, E., Snyder, P.J. and Khachaturian, Z.S. (2018). The cholinergic system in the pathophysiology and treatment of Alzheimer's disease. *Brain*, 141(7), pp.1917–1933.

[18] Chui, H. (2007). Subcortical Ischemic Vascular Dementia. *Neurologic Clinics*, 25(3), pp.717-740.

[19] de Bruijn, R.F. and Ikram, M.A. (2014). Cardiovascular risk factors and future risk of Alzheimer's disease. BMC Medicine, 12(1).

[20] Górska, A., Kamińska, K., Wawrzczak-Bargieła, A., Costa, G., Morelli, M., Przewłocki, R., Kreiner, G. and Gołembiowska, K. (2017). Neurochemical and Neurotoxic Effects of MDMA (Ecstasy) and Caffeine After Chronic Combined Administration in Mice. *Neurotoxicity Research*, 33(3), pp.532-548.

[21] Górska, A. and Gołembiowska, K. (2014). The Role of Adenosine A1 and A2A Receptors in the Caffeine Effect on MDMA-Induced DA and 5-HT Release in the Mouse Striatum. *Neurotoxicity Research*, 27(3), pp.229-245.
[22] Editors: Ahmad Salehi, M. (n.d.). *Recent advances in alzheimer research volume 1*. [Place of publication not identified]: Bentham Science Publisher, pp.273-286.
[23] Trillo, L., Das, D., Hsieh, W., Medina, B., Moghadam, S., Lin, B., Dang, V., Sanchez, M., De Miguel, Z., Ashford, J. and Salehi, A. (2013). Ascending monoaminergic systems alterations in Alzheimer's disease. Translating basic science into clinical care. *Neuroscience & Biobehavioral Reviews*, 37(8), pp.1363-1379.
[24] Parvizi, J., Van Hoesen, G. and Damasio, A. (2001). The selective vulnerability of brainstem nuclei to Alzheimer's disease. *Annals of Neurology*, 49(1), pp.53-66.
[25] Dong, X., Wang, Y. and Qin, Z. (2009). Molecular mechanisms of excitotoxicity and their relevance to pathogenesis of neurodegenerative diseases. *Acta Pharmacologica Sinica*, 30(4), pp.379-387.
[26] Revett,, T., Baker, G., Jhamandas, J. and Kar, S. (2013). Glutamate system, amyloid β peptides and tau protein: functional interrelationships and relevance to Alzheimer disease pathology. *Journal of Psychiatry & Neuroscience*, 38(1), pp.6-23.
[27] Elmore, S. (2007). Apoptosis: A Review of Programmed Cell Death. *Toxicologic Pathology*, 35(4), pp.495-516.
[28] Stansfield, W., Ranek, M., Pendse, A., Schisler, J., Wang, S., Pulinilkunnil, T. and Willis, M. (2014). The Pathophysiology of Cardiac Hypertrophy and Heart Failure. *Cellular and Molecular Pathobiology of Cardiovascular Disease*, pp.51-78.
[29] Wells, A. and Leloup, L. (2010). Calpain. *Handbook of Cell Signaling*, pp.999-1008.
[30] Launikonis, B., Cully, T., Csernoch, L. and Stephenson, D. (2017). NHE- and diffusion-dependent proton fluxes across the tubular system membranes of fast-twitch muscle fibers of the rat. *The Journal of General Physiology*, 150(1), pp.95-110.
[31] Szymański, J., Janikiewicz, J., Michalska, B., Patalas-Krawczyk, P., Perrone, M., Ziółkowski, W., Duszyński, J., Pinton, P., Dobrzyń, A. and Więckowski, M. (2017). Interaction of Mitochondria with the Endoplasmic Reticulum and Plasma Membrane in Calcium Homeostasis, Lipid Trafficking and Mitochondrial Structure. *International Journal of Molecular Sciences*, 18(7), p.1576.
[32] Park, P., Volianskis, A., Sanderson, T., Bortolotto, Z., Jane, D., Zhuo, M., Kaang, B. and Collingridge, G. (2014). NMDA receptor-dependent long-term potentiation comprises a family of temporally overlapping forms of synaptic plasticity that are induced by different patterns of stimulation. *Philosophical Transactions of the Royal Society B: Biological Sciences*, 369(1633), p.20130131.
[33] Bekkers, J. (2011). Pyramidal neurons. *Current Biology*, [online] 21(24), p.R975.
[34] Hsieh, H., Boehm, J., Sato, C., Iwatsubo, T., Tomita, T., Sisodia, S. and Malinow, R. (2006). AMPAR Removal Underlies Aβ-Induced Synaptic Depression and Dendritic Spine Loss. *Neuron*, 52(5), pp.831-843.
[35] Volianskis, A., France, G., Jensen, M., Bortolotto, Z., Jane, D. and Collingridge, G. (2015). Long-term potentiation and the role of N -methyl- d -aspartate receptors. *Brain Research*, 1621, pp.5-16.
[36] Li, S., Hong, S., Shepardson, N., Walsh, D., Shankar, G. and Selkoe, D. (2009). Soluble Oligomers of Amyloid β Protein Facilitate Hippocampal Long-Term Depression by Disrupting Neuronal Glutamate Uptake. *Neuron*, 62(6), pp.788-801.
[37] Jacob, C., Koutsilieri, E., Bartl, J., Neuen-Jacob, E., Arzberger, T., Zander, N., Ravid, R., Roggendorf, W., Riederer, P. and Grünblatt, E. (2007). Alterations in Expression of Glutamatergic Transporters and Receptors in Sporadic Alzheimer's Disease. *Journal of Alzheimer's Disease*, 11(1), pp.97-116.
[38] Boeckers, T. (2006). The postsynaptic density. *Cell and Tissue Research*, 326(2), pp.409-422.
[39] Vyas, Y. and Montgomery, J. (2016). The role of postsynaptic density proteins in neural degeneration and regeneration. *Neural Regeneration Research*, 11(6), p.0.
[40] Harris, M., Wang, Y., Pedigo, N., Hensley, K., Butterfield, D. and Carney, J. (2002). Amyloid β Peptide
[41] Galli, C., Piccini, A., Ciotti, M., Castellani, L., Calissano, P., Zaccheo, D. and Tabaton, M. (1998). Increased amyloidogenic secretion in cerebellar granule cells undergoing apoptosis. *Proceedings of the National Academy of Sciences*, 95(3), pp.1247-1252.

[42] Soriano, S., Lu, D., Chandra, S., Pietrzik, C. and Koo, E. (2001). The Amyloidogenic Pathway of Amyloid Precursor Protein (APP) Is Independent of Its Cleavage by Caspases. *Journal of Biological Chemistry*, 276(31), pp.29045-29050.
[43] LeBlanc, A. (1995). Increased production of 4 kDa amyloid beta peptide in serum deprived human primary neuron cultures: possible involvement of apoptosis. *The Journal of Neuroscience*, 15(12), pp.7837-7846.
[44] (25-35) Inhibits Na+-Dependent Glutamate Uptake in Rat Hippocampal Astrocyte Cultures. *Journal of Neurochemistry*, 67(1), pp.277-286.
[45] Sheng, M., Sabatini, B. and Sudhof, T. (2012). Synapses and Alzheimer's Disease. *Cold Spring Harbor Perspectives in Biology*, 4(5), pp.a005777-a005777.
[46] Šerý, O., Povová, J., Míšek, I., Pešák, L. and Janout, V. (2013). Molecular mechanisms of neuropathological changes in Alzheimer's disease: a review. *Folia Neuropathologica*, 1, pp.1-9.
[47] Kobayashi, D., Zeller, M., Cole, T., Buttini, M., McConlogue, L., Sinha, S., Freedman, S., Morris, R. and Chen, K. (2008). BACE1 gene deletion: Impact on behavioral function in a model of Alzheimer's disease. *Neurobiology of Aging*, 29(6), pp.861-873.
[48] Puzzo, D., Privitera, L., Leznik, E., Fa, M., Staniszewski, A., Palmeri, A. and Arancio, O. (2008). Picomolar Amyloid- Positively Modulates Synaptic Plasticity and Memory in Hippocampus. *Journal of Neuroscience*, 28(53), pp.14537-14545.
[49] Knafo, S., Alonso-Nanclares, L., Gonzalez-Soriano, J., Merino-Serrais, P., Fernaud-Espinosa, I., Ferrer, I. and DeFelipe, J. (2008). Widespread Changes in Dendritic Spines in a Model of Alzheimer's Disease. *Cerebral Cortex*, 19(3), pp.586-592.
[50] Razavi, S., Nazem, G., Mardani, M., Esfandiari, E., Esfahani, S. and Salehi, H. (2015). Neurotrophic factors and their effects in the treatment of multiple sclerosis. Advanced Biomedical Research, 4(1), p.53.
[51] Mucke, L., Masliah, E., Yu, G.-Q., Mallory, M., Rockenstein, E.M., Tatsuno, G., Hu, K., Kholodenko, D., Johnson-Wood, K. and McConlogue, L. (2000). High-Level Neuronal Expression of Aβ1–42in Wild-Type Human Amyloid Protein Precursor Transgenic Mice: Synaptotoxicity without Plaque Formation. The Journal of Neuroscience, 20(11), pp.4050–4058.
[52] Yu, C., Jiang, T., Yang, A., Du, Y., Wu, M. and Kong, L. (2019). Epigenetic Modulation on Tau Phosphorylation in Alzheimer's Disease. *Neural Plasticity*, 2019, pp.1-12.
[53] DiSabato, D., Quan, N. and Godbout, J. (2016). Neuroinflammation: the devil is in the details. *Journal of Neurochemistry*, 139, pp.136-153.
[54] Heneka, M., Carson, M., Khoury, J., Landreth, G., Brosseron, F., Feinstein, D., Jacobs, A., Wyss-Coray, T., Vitorica, J., Ransohoff, R., Herrup, K., Frautschy, S., Finsen, B., Brown, G., Verkhratsky, A., Yamanaka, K., Koistinaho, J., Latz, E., Halle, A., Petzold, G., Town, T., Morgan, D., Shinohara, M., Perry, V., Holmes, C., Bazan, N., Brooks, D., Hunot, S., Joseph, B., Deigendesch, N., Garaschuk, O., Boddeke, E., Dinarello, C., Breitner, J., Cole, G., Golenbock, D. and Kummer, M. (2015). Neuroinflammation in Alzheimer's disease. *The Lancet Neurology*, 14(4), pp.388-405.
[55] Georg Kuhn, H. and Blomgren, K. (2011). Developmental dysregulation of adult neurogenesis. *European Journal of Neuroscience*, 33(6), pp.1115-1122.
[56] Ming, G. and Song, H. (2011). Adult Neurogenesis in the Mammalian Brain: Significant Answers and Significant Questions. *Neuron*, 70(4), pp.687-702.
[57] Wang, S., Brunne, B., Zhao, S., Chai, X., Li, J., Lau, J., Failla, A., Zobiak, B., Sibbe, M., Westbrook, G., Lutz, D. and Frotscher, M. (2017). Trajectory analysis unveils Reelin's role in the directed migration of granule cells in the dentate gyrus. *The Journal of Neuroscience*, pp.0988-17.
[58] Lombardero, M., Kovacs, K., Horvath, E. and Salazar, I. (2007). Hormonal and morphological study of the pituitaries in reeler mice. *International Journal of Experimental Pathology*, 88(3), pp.165-173.
[59] Bosch, C., Masachs, N., Exposito-Alonso, D., Martínez, A., Teixeira, C.M., Fernaud, I., Pujadas, L., Ulloa, F., Comella, J.X., DeFelipe, J., Merchán-Pérez, A. and Soriano, E. (2016). Reelin Regulates the Maturation of Dendritic Spines, Synaptogenesis and Glial Ensheathment of Newborn Granule Cells. *Cerebral Cortex*, 26(11), pp.4282–4298.
[60] Pujadas, L., Rossi, D., Andrés, R., Teixeira, C., Serra-Vidal, B., Parcerisas, A., Maldonado, R., Giralt, E., Carulla, N. and Soriano, E. (2014). Reelin delays amyloid-beta fibril formation and rescues cognitive deficits in a model of Alzheimer's disease. *Nature Communications*, 5(1).
[61] Pujadas, L., Gruart, A., Bosch, C., Delgado, L., Teixeira, C., Rossi, D., de Lecea, L., Martinez, A., Delgado-Garcia, J. and Soriano, E. (2010). Reelin Regulates Postnatal Neurogenesis and

Enhances Spine Hypertrophy and Long-Term Potentiation. *Journal of Neuroscience*, 30(13), pp.4636-4649.
[62] Cuchillo-Ibañez, I., Mata-Balaguer, T., Balmaceda, V., Arranz, J., Nimpf, J. and Sáez-Valero, J. (2016). The β-amyloid peptide compromises Reelin signaling in Alzheimer's disease. *Scientific Reports*, 6(1).
[63] Pujadas, L., Gruart, A., Bosch, C., Delgado, L., Teixeira, C., Rossi, D., de Lecea, L., Martinez, A., Delgado-Garcia, J. and Soriano, E. (2010). Reelin Regulates Postnatal Neurogenesis and Enhances Spine Hypertrophy and Long-Term Potentiation. *Journal of Neuroscience*, 30(13), pp.4636-4649.
[64] Herculano-Houzel, S. (2009). The human brain in numbers: a linearly scaled-up primate brain. *Frontiers in Human Neuroscience*, 3.
[65] Alzheimer's Association (2019). 2019 Alzheimer's disease facts and figures. *Alzheimer's & Dementia*, 15(3), pp.321-387.
[66] Mucke, L., Masliah, E., Yu, G., Mallory, M., Rockenstein, E., Tatsuno, G., Hu, K., Kholodenko, D., Johnson-Wood, K. and McConlogue, L. (2000). High-Level Neuronal Expression of Aβ1–42in Wild-Type Human Amyloid Protein Precursor Transgenic Mice: Synaptotoxicity without Plaque Formation. *The Journal of Neuroscience*, 20(11), pp.4050-4058.
[67] Lane-Donovan, C., Philips, G., Wasser, C., Durakoglugil, M., Masiulis, I., Upadhaya, A., Pohlkamp, T., Coskun, C., Kotti, T., Steller, L., Hammer, R., Frotscher, M., Bock, H. and Herz, J. (2015). Reelin protects against amyloid β toxicity in vivo. *Science Signaling*, 8(384), pp.ra67-ra67.
[68] Jaykaran (2010). "Mean ± SEM" or "Mean (SD)"?. *Indian Journal of Pharmacology*, 42(5), p.329.
[69] Qiu, C., Kivipelto, M., & von Strauss, E. (2009). Epidemiology of Alzheimer's disease: occurrence, determinants, and strategies toward intervention. *Dialogues in clinical neuroscience*, *11*(2), 111–128.
[70] MartÃnez-CerdeÃ±o, V. and Noctor, S. (2014). Cajal, Retzius, and Cajalâ€“Retzius cells. *Frontiers in Neuroanatomy*, 8.
[71] Mienville, J. (1999). Feature Article: Cajal-Retzius Cell Physiology: Just in Time to Bridge the 20th Century. *Cerebral Cortex*, 9(8), pp.776-782.
[72] Tanzi, R. and Bertram, L. (2005). Twenty Years of the Alzheimer's Disease Amyloid Hypothesis: A Genetic Perspective. *Cell*, 120(4), pp.545-555.
[73] Caviness, V. and Sidman, R. (1973). Time of origin of corresponding cell classes in the cerebral cortex of normal and reeler mutant mice: An autoradiographic analysis. *The Journal of Comparative Neurology*, 148(2), pp.141-151.
[74] D'Arcangelo, G. and Curran, T. (1998). Reeler: new tales on an old mutant mouse. *BioEssays*, 20(3), pp.235-244.
[75] Sheng, M., Sabatini, B. and Sudhof, T. (2012). Synapses and Alzheimer's Disease. *Cold Spring Harbor Perspectives in Biology*, 4(5), pp.a005777-a005777.
[76] Wu, Y., Fujishima, K. and Kengaku, M. (2015). Differentiation of Apical and Basal Dendrites in Pyramidal Cells and Granule Cells in Dissociated Hippocampal Cultures. *PLOS ONE*, 10(2), p.e0118482.
[77] Alcántara, S., Ruiz, M., D'Arcangelo, G., Ezan, F., de Lecea, L., Curran, T., Sotelo, C. and Soriano, E. (1998). Regional and Cellular Patterns ofreelinmRNA Expression in the Forebrain of the Developing and Adult Mouse. *The Journal of Neuroscience*, 18(19), pp.7779-7799.
[78] D'Arcangelo, G. (2014). Reelin in the Years: Controlling Neuronal Migration and Maturation in the Mammalian Brain. *Advances in Neuroscience*, 2014, pp.1-19.
[79] Bertram, L., Lill, C. and Tanzi, R. (2010). The Genetics of Alzheimer Disease: Back to the Future. *Neuron*, 68(2), pp.270-281.
[80] Derer, P., Derer, M. and Goffinet, A. (2001). Axonal secretion of reelin by cajal-retzius cells: Evidence from comparison of normal andRelnOrl mutant mice. *The Journal of Comparative Neurology*, 440(2), pp.136-143.
[81] Tosh, J.L., Rickman, M., Rhymes, E., Norona, F.E., Clayton, E., Mucke, L., Isaacs, A.M., Fisher, E.M.C. and Wiseman, F.K. (2018b). The integration site of the APP transgene in the J20 mouse model of Alzheimer's disease. Wellcome Open Research, 2, p.84.
[82] Forny-Germano, L., Lyra e Silva, N.M., Batista, A.F., Brito-Moreira, J., Gralle, M., Boehnke, S.E., Coe, B.C., Lablans, A., Marques, S.A., Martinez, A.M.B., Klein, W.L., Houzel, J.-C., Ferreira, S.T., Munoz, D.P. and De Felice, F.G. (2014). Alzheimer's Disease-Like Pathology Induced by Amyloid-β Oligomers in Nonhuman Primates. *The Journal of Neuroscience*, 34(41), pp.13629–13643.

[83] Games, D., Adams, D., Alessandrini, R., Barbour, R., Borthelette, P., Blackwell, C., Carr, T., Clemens, J., Donaldson, T., Gillespie, F., Guido, T., Hagopian, S., Johnson-Wood, K., Khan, K., Lee, M., Leibowitz, P., Lieberburg, I., Little, S., Masliah, E., McConlogue, L., Montoya-Zavala, M., Mucke, L., Paganini, L., Penniman, E., Power, M., Schenk, D., Seubert, P., Snyder, B., Soriano, F., Tan, H., Vitale, J., Wadsworth, S., Wolozin, B. and Zhao, J. (1995). Alzheimer-type neuropathology in transgenic mice overexpressing V717F β-amyloid precursor protein. *Nature*, 373(6514), pp.523–527.

[84] Haass, C. and Selkoe, D.J. (2007). Soluble protein oligomers in neurodegeneration: lessons from the Alzheimer's amyloid β-peptide. *Nature Reviews Molecular Cell Biology*, 8(2), pp.101–112.

[85] Garre Olmo, J. (2018). Epidemiología de la enfermedad de Alzheimer y otras demencias. *Revista de Neurología*, 66(11), p.377.

[86] Hsiao, K., Chapman, P., Nilsen, S., Eckman, C., Harigaya, Y., Younkin, S., Yang, F. and Cole, G. (1996). Correlative Memory Deficits, A Elevation, and Amyloid Plaques in Transgenic Mice. *Science*, 274(5284), pp.99–103.

[87] Iqbal, K., del C. Alonso, A., Chen, S., Chohan, M.O., El-Akkad, E., Gong, C.-X., Khatoon, S., Li, B., Liu, F., Rahman, A., Tanimukai, H. and Grundke-Iqbal, I. (2005). Tau pathology in Alzheimer disease and other tauopathies. *Biochimica et Biophysica Acta (BBA) - Molecular Basis of Disease*, 1739(2–3), pp.198–210.

[88] Knuesel, I., Nyffeler, M., Mormède, C., Muhia, M., Meyer, U., Pietropaolo, S., Yee, B.K., Pryce, C.R., LaFerla, F.M., Marighetto, A. and Feldon, J. (2009). Age-related accumulation of Reelin in amyloid-like deposits. *Neurobiology of Aging*, 30(5), pp.697–716.

[89] Knuesel, I. (2010). Reelin-mediated signaling in neuropsychiatric and neurodegenerative diseases. *Progress in Neurobiology*, 91(4), pp.257–274.

[90] Tissir, F. and Goffinet, A.M. (2003). Reelin and brain development. *Nature Reviews Neuroscience*, 4(6), pp.496–505.

[91] Schmid, R.S., Jo, R., Shelton, S., Kreidberg, J.A. and Anton, E.S. (2005). Reelin, Integrin and Dab1 Interactions during Embryonic Cerebral Cortical Development. *Cerebral Cortex*, 15(10), pp.1632–1636.

[92] Bisht, K., Sharma, K. and Tremblay, M.-È. (2018). Chronic stress as a risk factor for Alzheimer's disease: Roles of microglia-mediated synaptic remodeling, inflammation, and oxidative stress. Neurobiology of Stress, 9, pp.9–21.

[93] Yiannopoulou, K. and Papageorgiou, S. (2012). Current and future treatments for Alzheimer's disease. *Therapeutic Advances in Neurological Disorders*, 6(1), pp.19-33.

[94] Galimberti, D. and Scarpini, E. (2011). Disease-modifying treatments for Alzheimer's disease. *Therapeutic Advances in Neurological Disorders*, 4(4), pp.203-216.

[95] Masumoto, K. (2019). [online] Brainstars.org. Available at: http://brainstars.org/supplement/brainCoronalImage.png [Accessed 23 Oct. 2019].

[96] Braindevelopmentmaps.org. (2019). *Postnatal Neurogenesis in the Developing Hippocampus | Brain Development*. [online] Available at: https://braindevelopmentmaps.org/home/brain-map-sets/postnatal-neurogenesis-in-the-developing-hippocampus/ [Accessed 23 Oct. 2019].

[97] WorldCare. (2019). *Study from WorldCare Consortium® member Massachusetts General Hospital identifies protein's role in mediating the brain's response to stress - WorldCare*. [online] Available at: https://www.worldcare.com/2018/06/18/study-worldcare-consortium-member-massachusetts-general-hospital-identifies-proteins-role-mediating-brains-response-stress/ [Accessed 23 Oct. 2019].

[98] Sciences, L., Biology, P., Center, P., Library, P., Methods, P. and Immunohistochemistry, O. (2019). *Overview of Immunohistochemistry | Thermo Fisher Scientific - UK*. [online] Thermofisher.com. Available at: https://www.thermofisher.com/pt/en/home/life-science/protein-biology/protein-biology-learning-center/protein-biology-resource-library/pierce-protein-methods/overview-immunohistochemistry.html [Accessed 29 Oct. 2019].

[99] Alzforum.org. (2019). *Aβ (3D6) | ALZFORUM*. [online] Available at: https://www.alzforum.org/antibodies/av-3d6 [Accessed 29 Oct. 2019].

[100] (ab78540), A. (2019). *Anti-Reelin antibody [G10] (ab78540) | Abcam*. [online] Abcam.com. Available at: https://www.abcam.com/Reelin-antibody-G10-ab78540.html [Accessed 29 Oct. 2019].

[101] Thermo Fisher scientific. (2019). *HRP-Conjugated Streptavidin*. [online] Available at: https://www.thermofisher.com/order/catalog/product/N100#/N100 [Accessed 29 Oct. 2019].

[102] Thermo Fisher scientific. (2019). *eBioscience™ DAB Advanced Chromogenic Kit*. [online] Available at: https://www.thermofisher.com/order/catalog/product/8801-4965-

72?SID=srch-srp-8801-4965-72#/8801-4965-72?SID=srch-srp-8801-4965-72 [Accessed 29 Oct. 2019].

[103] Mucke, L., Masliah, E., Yu, G., Mallory, M., Rockenstein, E., Tatsuno, G., Hu, K., Kholodenko, D., Johnson-Wood, K. and McConlogue, L. (2000). High-Level Neuronal Expression of Aβ1–42in Wild-Type Human Amyloid Protein Precursor Transgenic Mice: Synaptotoxicity without Plaque Formation. *The Journal of Neuroscience*, 20(11), pp.4050-4058.

[104] Paxinos, G., Watson, C., Calabrese, E., Badea, A. and Johnson, G. (n.d.). *MRI/DTI atlas of the rat brain*.

Appendix

Appendix 1- Tables with calculations

Table 1: Values for area fractions of outside, vessels, plaques, and tissue that were quantified by the program from the cropped pictures of the HCs of the animal JFRLn4422. This table was used to calculate the fraction of total plaque area per HC. A similar table was made for all J20+ animals. The tissue sections in blank did not contain a hippocampus and were not quantified (they were included in the table for the cortex quantification that was not completed). The table contains the information of the name of the animal, the number of each section analyzed in the second round of IHC against Aβ plaques, the side of each section and the name of each picture that was taken of each animal.

Animal	Tissue sec.	Side	Picture HC	Outside Area	Vessels Area frac.	Plaque Area frac.	Tot. Plaque Area/HC frac.	Tissue Area frac.
JFRLn4422	1	a	-	-	-	-	-	-
		b	-	-	-	-	-	-
	2	a	-	-	-	-	-	-
		b	-	-	-	-	-	-
	3	a	-	-	-	-	-	-
		b	-	-	-	-	-	-
	4	a	-	-	-	-	-	-
		b	-	-	-	-	-	-
	5	a	JFRLn4422.10x.01	0.41061	0.00077	0.01214	0.01214	0.41061
			-	-	-	-	-	-
		b	JFRLn4422.10x.03	0.58530	0.00065	0.00768	0.0077	0.40637
			JFRLn4422.10x.04	0.91971	0.00039	0.00002	-	0.07988
	6	a	JFRLn4422.10x.07	0.78353	0.00049	0.00568	0.01185	0.21030
		b	JFRLn4422.10x.09	0.73391	0.00056	0.00617	-	0.25936
	7	a	JFRLn4422.10x.60	0.68902	0.00166	0.00199	0.00314	0.30733
		b	JFRLn4422.10x.61	0.75249	0.00088	0.00115	-	0.24549
	8	a	-	-	-	-	-	-
		b	-	-	-	-	-	-
	9	a	JFRLn4422.10x.14	0.57879	0.00091	0.00766	0.00834	0.41264
			JFRLn4422.10x.15	0.68657	0.00074	0.00068	-	0.31201
		b	JFRLn4422.10x.16	0.55400	0.00098	0.00869	0.0206	0.43632
			JFRLn4422.10x.17	0.75797	0.00065	0.01191	-	0.22946
	10	a	JFRLn4422.10x.21	0.73880	0.00058	0.00032	0.00492	0.26030
			JFRLn4422.10x.62	0.55014	0.00459	0.00460	-	0.44067
		b	JFRLn4422.10x.24	0.55462	0.00093	0.00891	0.01981	0.43555
			JFRLn4422.10x.23	0.76573	0.00063	0.01090	-	0.22275
	11	-	JFRLn4422.10x.63	0.48727	0.00979	0.00241	0.00395	0.50053
		-	JFRLn4422.10x.64	0.53062	0.01100	0.00154	-	0.45685
	12	-	JFRLn4422.10x.65	0.59264	0.00450	0.00123	0.00162	0.40163
		-	JFRLn4422.10x.66	0.60268	0.00193	0.00039	-	0.39499
	13	-	JFRLn4422.10x.67	0.56103	0.00417	0.00196	0.00404	0.43284
		-	JFRLn4422.10x.68	0.54626	0.00421	0.00208	-	0.44745
	14	-	JFRLn4422.10x.69	0.51231	0.00611	0.00510	0.00921	0.47648
		-	JFRLn4422.10x.70	0.52720	0.00295	0.00411	-	0.46574
	15	-	JFRLn4422.10x.71	0.43836	0.00822	0.00129	0.00323	0.55212
		-	JFRLn4422.10x.72	0.31852	0.00905	0.00194	-	0.67049
	16	-	JFRLn4422.10x.74	0.48294	0.01164	0.00022	0.00087	0.50519
		-	JFRLn4422.10x.75	0.29648	0.01080	0.00065	-	0.69207
	17	-	JFRLn4422.10x.76	0.58496	0.00960	0.00171	0.00305	0.40374
		-	JFRLn4422.10x.77	0.66947	0.00288	0.00134	-	0.32631
	18	-	JFRLn4422.10x.78	0.24331	0.01081	0.00073	0.00073	0.74515
		-	JFRLn4422.10x.79	0.58934	0.00405	0	-	0.40661
	19	-	JFRLn4422.10x.80	0.24397	0.00716	0.00096	0.00098	0.74791
		-	JFRLn4422.10x.81	0.54570	0.00317	0.00002	-	0.45111

Table 2: Fraction of total HC area, fraction of total HC area per HC, % of plaque area per HC, anterior and posterior means of HC plaque %, and the standard deviation of these means, calculated for the animal JFRLn4422. The table also contains the information of the name of the animal, the number of each section analyzed in the second round of IHC against Aβ plaques and the side of each section. A similar table was made for all J20+ animals. (second part).

Animal	Tissue sec.	Side	Tot. Area frac.	Area/HC frac.	% Plaque Area	Plaques Mean (Ant./Post.)	Std. Dev.
JFRLn4422	1	a	-	-	-	1.89698499	1.029697
		b	-	-	-		
	2	a	-	-	-		
		b	-	-	-		
	3	a	-	-	-		
		b	-	-	-		
	4	a	-	-	-		
		b	-	-	-		
	5	a	0.42352	0.42352	2.866452588		
			-	-	-		
		b	0.4147	0.49499	1.555586982		
			0.08029	-	-		
	6	a	0.21647	0.48256	2.455653183		
		b	0.26609	-	-		
	7	a	0.31098	0.5585	0.562220233		
		b	0.24752	-	-		
	8	a	-	-	-		
		b	-	-	-		
	9	a	0.42121	0.73464	1.135249918		
			0.31343	-	-		
		b	0.44599	0.68801	2.994142527		
			0.24202	-	-		
	10	a	0.2612	0.71106	0.691924732		
			0.44986	-	-		
		b	0.44539	0.67967	2.914649756		
			0.23428	-	-		
	11	-	0.51273	0.98212	0.402191178	0.322072046	0.28359
		-	0.46939	-	-		
	12	-	0.40736	0.80467	0.201324767		
		-	0.39731	-	-		
	13	-	0.43897	0.89271	0.452554581		
		-	0.45374	-	-		
	14	-	0.48769	0.96049	0.958885569		
		-	0.4728	-	-		
	15	-	0.56163	1.24311	0.259832195		
		-	0.68148	-	-		
	16	-	0.51705	1.22057	0.071278173		
		-	0.70352	-	-		
	17	-	0.41505	0.74558	0.409077497		
		-	0.33053	-	-		
	18	-	0.75669	1.16735	0.062534801		
		-	0.41066	-	-		
	19	-	0.75603	1.21033	0.080969653		
		-	0.4543	-	-		

Table 3: Values for area fractions of outside, vessels, plaques, and tissue that were quantified by the program from the cropped pictures of the HCs of the animal JFRLn4423. *F*raction of total HC area, fraction of total HC area per HC, % of plaque area per HC, anterior and posterior means of HC plaque %, and the standard deviation of these means calculated for this animal.

Animal	Tissue section	Side	Picture HC	Outside Area	Vessels Area	Plaques Area	Total Area of Plaques per HC	Tissue Area	Total Area	Area of each HC	% Area of Plaques	Plaques Mean (Anterior/Posterior)	Standard deviation
JFRLn4423	1	a	-	-	-	-	-	-	-	-	-	0.832482268	0.509757751
		b	-	-	-	-	-	-	-	-	-		
	2	a	-	-	-	-	-	-	-	-	-		
		b	-	-	-	-	-	-	-	-	-		
	3	a	-	-	-	-	-	-	-	-	-		
		b	-	-	-	-	-	-	-	-	-		
	4	a	-	-	-	-	-	-	-	-	-		
		b	JFRLn4423.10x.01	0.57733	0.00132	0.00762	0.00762	0.41374	0.42268	0.42268	1.802782247		
	5	a	JFRLn4423.10x.02	-	-	-	-	-	-	-	-		
		b	JFRLn4423.10x.82	0.71742	0.00109	0.00109	0.00109	0.2804	0.28258	0.28258	0.385731474		
	6	a	JFRLn4423.10x.07	0.80878	0.00065	0.00051	0.00112	0.19006	0.19122	0.30904	0.362412633		
		b	JFRLn4423.10x.08	0.88218	0.00051	0.00061	-	0.1167	0.11782	-	-		
	7	a	-	-	-	-	-	-	-	-	-		
		b	-	-	-	-	-	-	-	-	-		
	8	a	-	-	-	-	-	-	-	-	-		
		b	-	-	-	-	-	-	-	-	-		
	9	a	JFRLn4423.10x.83	0.57787	0.00172	0.00297	0.00297	0.41745	0.42213	0.42213	0.703574728		
		b	-	-	-	-	-	-	-	-	-		
	10	a	JFRLn4423.10x.15	0.52805	0.00113	0.0031	0.00314	0.46772	0.47195	0.60047	0.52292371		
		b	JFRLn4423.10x.16	0.87148	0.00068	0.00004	-	0.1278	0.12852	-	-		
		a	JFRLn4423.10x.84	0.49413	0.01062	0.00680	0.00684	0.48846	0.50588	0.63415	1.078609162		
			JFRLn4423.10x.85	0.87172	0.00070	0.00004	-	0.12753	0.12827	-	-		
		b	JFRLn4423.10x.86	0.60309	0.00406	0.00434	0.00692	0.38851	0.39691	0.7006	0.987724807		
			JFRLn4423.10x.87	0.69631	0.00152	0.00258	-	0.29959	0.30369	-	-		
	11	-	JFRLn4423.10x.88	0.49756	0.00487	0.00305	0.00366	0.49453	0.50245	1.2726	0.287600189		
		-	JFRLn4423.10x.89	0.22984	0.01235	0.00061	-	0.75719	0.77015	-	-		
	12	-	JFRLn4423.10x.90	0.47231	0.00942	0.00531	0.00963	0.51295	0.52768	1.24309	0.774682445		
		-	JFRLn4423.10x.91	0.28459	0.00976	0.00432	-	0.70133	0.71541	-	-		
	13	-	JFRLn4423.10x.92	0.51735	0.00417	0.00503	0.005030658	0.47345	0.48265	0.609070658	0.825956305		
		-	JFRLn4423.10x.93	0.87359	0.00050	6.575E-7	-	0.12592	0.12642066	-	-		
	14	-	JFRLn4423.10x.94	0.58630	0.00384	0.00238	0.0051	0.40748	0.4137	0.83778	0.608751701		
		-	JFRLn4423.10x.95	0.57591	0.00163	0.00272	-	0.41973	0.42408	-	-		
	15	-	JFRLn4423.10x.96	0.52861	0.00456	0.00353	0.00631	0.46330	0.47139	1.07477	0.587102357		
		-	JFRLn4423.10x.97	0.39662	0.00934	0.00278	-	0.59126	0.60338	-	-		
	16	-	JFRLn4423.10x.98	0.38449	0.00680	0.00073	0.00247	0.60799	0.61552	1.23972	0.199238538		
		-	JFRLn4423.10x.99	0.37579	0.01164	0.00174	-	0.61082	0.6242	-	-		
	17	-	JFRLn4423.10x.100	0.07877	0.02723	0.00408	0.01288	0.88992	0.92123	1.64859	0.781273694		
		-	JFRLn4423.10x.101	0.27263	0.00915	0.00880	-	0.70941	0.72736	-	-		
	18	-	JFRLn4423.10x.102	0.55267	0.00505	0.00603	0.01268	0.43626	0.44734	1.02509	1.236964559		
		-	JFRLn4423.10x.103	0.42226	0.00298	0.00665	-	0.56812	0.57775	-	-		
	19	-	JFRLn4423.10x.104	0.24517	0.02972	0.00292	0.00292	0.72220	0.75484	0.75484	0.386836946		
		-	-	-	-	-	-	-	-	-	-		

Table 4: Values for area fractions of outside, vessels, plaques, and tissue that were quantified by the program from the cropped pictures of the HCs of the animal JFRLn4425. Fraction of total HC area, fraction of total HC area per HC, % of plaque area per HC, anterior and posterior means of HC plaque %, and the standard deviation of these means calculated for this animal.

Animal	Tissue section	Side	Picture HC	Outside Area	Vessels Area	Plaques Area	Total Area of Plaques per HC	Tissue Area	Total Area	Area of each HC	% Area of Plaques	Plaques Mean (Anterior/Posterior)	Standard deviation
JFRLn4425	1	a	-	-	-	-	-	-	-	-	-	-	-
		b	-	-	-	-	-	-	-	-	-		
	2	a	-	-	-	-	-	-	-	-	-		
		b	-	-	-	-	-	-	-	-	-		
	3	a	-	-	-	-	-	-	-	-	-		
		b	-	-	-	-	-	-	-	-	-		
	4	a	-	-	-	-	-	-	-	-	-		
		b	-	-	-	-	-	-	-	-	-		
	5	a	-	-	-	-	-	-	-	-	-		
		b	-	-	-	-	-	-	-	-	-		
	6	a	JFRLn4425.10x.108	0.81988	0.00154	0.00003	0.00015	0.17855	0.18012	0.33196	0.045186167		
		b	JFRLn4425.10x.109	0.84816	0.00095	0.00012		0.15078	0.15184				
	7	a	-	-	-	-	-	-	-	-	-		
		b	-	-	-	-	-	-	-	-	-		
	8	a	-	-	-	-	-	-	-	-	-	1.721805894	0.956904675
		b	-	-	-	-	-	-	-	-	-		
	9	a	JFRLn4425.10x.05	0.45997	0.00108	0.00685	0.00803	0.4921	0.50003	0.6189	1.297463241		
		a	JFRLn4425.10x.06	0.88113	0.00058	0.00118	-	0.1171	0.11887	-	-		
		b	JFRLn4425.10x.08	0.56976	0.00103	0.01527	0.015270438	0.41394	0.43024	0.5188	2.943415189		
		b	JFRLn4425.10x.09	0.91144	0.00052	4.38E-07	-	0.08803	0.08856	-	-		
		a	JFRLn4425.10x.11	0.51613	0.00109	0.01044	0.01061	0.47234	0.48387	0.68165	1.556517274		
		a	JFRLn4425.10x.12	0.80222	0.00071	0.00017	-	0.19691	0.19778	-	-		
	10	a	JFRLn4425.10x.15	0.44468	0.00119	0.01181	0.01189	0.54232	0.55532	0.7219	1.647042527		
		b	JFRLn4425.10x.16	0.83342	0.00072	0.00008	-	0.16578	0.16658	-	-		
		b	JFRLn4425.10x.17	0.59372	0.00093	0.01118	0.01118	0.39417	0.40628	0.40628	2.751179679		
	11	a	-	-	-	-	-	-	-	-	-		
		b	JFRLn4425.10x.20	0.56598	0.00138	0.01211	0.01211	0.42053	0.43402	0.43402	2.790194		
		b	-	-	-	-	-	-	-	-	-		
	12	a	JFRLn4425.10x.21	0.59958	0.00136	0.0045	0.00742	0.39457	0.40042	0.75723	0.979887221		
		a	JFRLn4425.10x.22	0.64319	0.00117	0.00292	-	0.35272	0.35681	-	-		
		b	JFRLn4425.10x.110	0.54842	0.00220	0.00861	0.01053	0.44077	0.45158	0.70921	1.484750638		
		b	JFRLn4425.10x.111	0.74237	0.00074	0.00192	-	0.25497	0.25763	-	-		
	13	-	JFRLn4425.10x.112	0.54322	0.00302	0.00502	0.00975	0.44874	0.45678	1.04099	0.936608421		
		-	JFRLn4425.10x.113	0.41579	0.00177	0.00473	-	0.57771	0.58421	-	-		
	14	-	JFRLn4425.10x.114	0.59304	0.00367	0.00461	0.00614	0.39869	0.40697	0.93951	0.653532216		
		-	JFRLn4425.10x.115	0.46746	0.00177	0.00153	-	0.52924	0.53254	-	-		
	15	-	JFRLn4425.10x.116	0.51430	0.00319	0.00641	0.00773	0.47610	0.4857	0.83842	0.921972281		
		-	JFRLn4425.10x.117	0.64727	0.00126	0.00132	-	0.35014	0.35272	-	-		
	16	-	JFRLn4425.10x.118	0.59995	0.00267	0.00761	0.01002	0.38977	0.40005	0.73361	1.365848339		
		-	JFRLn4425.10x.119	0.66643	0.00150	0.00241	-	0.32965	0.33356	-	-		
	17	-	JFRLn4425.10x.45	0.32868	0.00124	0.00499	0.01055	0.66509	0.67132	1.19193	0.885119093		
		-	JFRLn4425.10x.46	0.47939	0.00121	0.00556	-	0.51384	0.52061	-	-		
	18	-	JFRLn4425.10x.120	0.31004	0.00584	0.00283	0.00287	0.68129	0.68996	1.15111	0.249324565		
		-	JFRLn4425.10x.121	0.53885	0.00364	0.00004	-	0.45747	0.46115	-	-		
	19	-	JFRLn4425.10x.122	0.43374	0.00396	0.00245	0.00903	0.55985	0.56626	1.37731	0.655625821	0.5873116	
		-	JFRLn4425.10x.123	0.18896	0.00489	0.00658	-	0.79958	0.81105	-	-		
	20	-	JFRLn4425.10x.124	0.33254	0.00531	0.00055	0.00073	0.66159	0.66745	1.1463	0.063683154		
		-	JFRLn4425.10x.125	0.52116	0.00210	0.00018	-	0.47657	0.47885	-	-		
	21	-	JFRLn4425.10x.126	0.32594	0.00550	0.00379	0.0041	0.66477	0.67406	1.17067	0.350226793		
		-	JFRLn4425.10x.127	0.50339	0.00625	0.00031	-	0.49005	0.49661	-	-		
	22	-	JFRLn4425.10x.128	0.33029	0.00769	0.00219	0.00238	0.65983	0.66971	0.95978	0.247973494		
		-	JFRLn4425.10x.129	0.70993	0.00262	0.00019	-	0.28726	0.29007	-	-		
	23	-	JFRLn4425.10x.130	0.45388	0.00305	0.00239	0.00314	0.54068	0.54612	1.26702	0.247825607		
		-	JFRLn4425.10x.131	0.27910	0.00583	0.00075	-	0.71432	0.7209	-	-		
	24	-	JFRLn4425.10x.132	0.24468	0.00236	0.00355	0.00355	0.74941	0.75532	0.75532	0.469999947		
		-	JFRLn4425.10x.133	-	-	-	-	-	-	-	-		

Table 5: Values for area fractions of outside, vessels, plaques, and tissue that were quantified by the program from the cropped pictures of the HCs of the animal JFRLn4428. Fraction of total HC area, fraction of total HC area per HC, % of plaque area per HC, anterior and posterior means of HC plaque %, and the standard deviation of these means calculated for this animal.

Animal	Tissue section	Side	Picture HC	Outside Area	Vessels Area	Plaques Area	Total Area of Plaques per HC	Tissue Area	Total Area	Area of each HC	% Area of Plaques	Plaques Mean (Anterior/Posterior	Standard deviation
JFRLn4428	1	a	-	-	-	-	-	-	-	-	-	-	-
		b	-	-	-	-	-	-	-	-	-	-	-
	2	a	-	-	-	-	-	-	-	-	-	-	-
		b	-	-	-	-	-	-	-	-	-	-	-
	3	a	-	-	-	-	-	-	-	-	-	-	-
		b	-	-	-	-	-	-	-	-	-	-	-
	4	a	-	-	-	-	-	-	-	-	-	-	-
		b	-	-	-	-	-	-	-	-	-	-	-
	5	a	-	-	-	-	-	-	-	-	-	-	-
		b	-	-	-	-	-	-	-	-	-	-	-
	6	a	JFRLn4428.10x.09	0.49014	0.00244	0.01569	0.01594	0.49173	0.50986	0.68716	2.319692648	2.381670939	1.672081283
			JFRLn4428.10x.10	0.8227	0.00087	0.00025	-	0.17618	0.1773	-	-		
		b	JFRLn4428.10x.13	0.47275	0.00152	0.00668	0.00669	0.51905	0.52725	0.64754	1.03314081		
			JFRLn4428.10x.14	0.87971	0.00076	0.00001	-	0.11951	0.12029	-	-		
	7	a	JFRLn4428.10x.05	0.49787	0.00072	0.02277	0.02277	0.47865	0.50214	0.50214	4.534591946		
			-	-	-	-	-	-	-	-	-		
		b	JFRLn4428.10x.07	0.53496	0.00067	0.02145	0.02145	0.44292	0.46504	0.46504	4.612506451		
			-	-	-	-	-	-	-	-	-		
	8	a	JFRLn4428.10x.02	0.7781	0.00076	0.0001	0.00155	0.22105	0.2219	0.45286	0.342269134		
		b	JFRLn4428.10x.03	0.76904	0.00084	0.00145	-	0.22866	0.23096	-	-		
	9	a	-	-	-	-	-	-	-	-	-		
			-	-	-	-	-	-	-	-	-		
		b	-	-	-	-	-	-	-	-	-		
			-	-	-	-	-	-	-	-	-		
	10	a	JFRLn4428.10x.137	0.44855	0.00406	0.01566	0.02063	0.53172	0.55145	0.81689	2.525431821		
			JFRLn4428.10x.138	0.73456	0.00068	0.00497	-	0.25979	0.26544	-	-		
		b	JFRLn4428.10x.139	0.44107	0.00442	0.00935	0.00998	0.54516	0.55893	0.7653	1.304063766		
			JFRLn4428.10x.140	0.79363	0.00058	0.00063	-	0.20516	0.20637	-	-		
	11	a	JFRLn4428.10x.33	0.46323	0.00195	0.00814	0.00891	0.52668	0.53677	0.83877	1.062269752		
			JFRLn4428.10x.34	0.698	0.00107	0.00077	-	0.30016	0.302	-	-		
		b	JFRLn4428.10x.37	0.52918	0.00195	0.00374	0.00542	0.46514	0.47082	0.88076	0.615377628		
			JFRLn4428.10x.38	0.59006	0.00117	0.00168	-	0.40709	0.40994	-	-		
	12	a	JFRLn4428.10x.41	0.43161	0.00206	0.02205	0.02558	0.54429	0.56839	0.7594	3.368448775		
			JFRLn4428.10x.42	0.80899	0.00067	0.00353	-	0.18681	0.19101	-	-		
		b	JFRLn4428.10x.45	0.46323	0.00195	0.00814	0.00891	0.52668	0.53677	0.83877	1.062269752		
			JFRLn4428.10x.46	0.698	0.00107	0.00077	-	0.30016	0.302	-	-		
	13	a	JFRLn4428.10x.49	0.44473	0.00092	0.01798	0.02205	0.53637	0.55527	0.95353	2.312460017		
			JFRLn4428.10x.50	0.60174	0.00108	0.00407	-	0.39311	0.39826	-	-		
		b	JFRLn4428.10x.53	0.52918	0.00195	0.00374	0.00542	0.46514	0.47082	0.88076	0.615377628	1.545187979	1.174227375
			JFRLn4428.10x.54	0.59006	0.00117	0.00168	-	0.40709	0.40994	-	-		
	14	a	JFRLn4428.10x.141	0.48057	0.00105	0.01082	0.01426	0.50755	0.51942	1.30419	1.093398968		
			JFRLn4428.10x.142	0.21523	0.00143	0.00344	-	0.77990	0.78477	-	-		
		b	JFRLn4428.10x.143	0.42781	0.00097	0.01179	0.0183	0.55943	0.57219	1.29435	1.413837061		
			JFRLn4428.10x.144	0.27784	0.00116	0.00651	-	0.71449	0.72216	-	-		
	15	a	JFRLn4428.10x.145	0.40413	0.00127	0.00257	0.0033	0.59203	0.59587	1.27215	0.259403372		
			JFRLn4428.10x.146	0.32373	0.00141	0.00073	-	0.67414	0.67628	-	-		
		b	JFRLn4428.10x.147	0.34692	0.00109	0.03508	0.04319	0.61691	0.65308	1.1836	3.649036837		
			JFRLn4428.10x.148	0.46948	0.00136	0.00811	-	0.52105	0.53052	-	-		

Table 6: Values for area fractions of outside, vessels, plaques, and tissue that were quantified by the program from the cropped pictures of the HCs of the animal JFRLn4431. Fraction of total HC area, fraction of total HC area per HC, % of plaque area per HC, anterior and posterior means of HC plaque %, and the standard deviation of these means calculated for this animal.

Animal	Tissue section	Side	Picture HC	Outside Area	Vessels Area	Plaques Area	Total Area of Plaques per HC	Tissue Area	Total Area	Area of each HC	% Area of Plaques	Plaques Mean (Anterior/Posterior)	Standard deviation
JFRLn4431	1	a	-	-	-	-	-	-	-	-	-	0.729374265	0.318693636
		b	-	-	-	-	-	-	-	-	-		
	2	a	-	-	-	-	-	-	-	-	-		
		b	-	-	-	-	-	-	-	-	-		
	3	a	-	-	-	-	-	-	-	-	-		
		b	-	-	-	-	-	-	-	-	-		
	4	a	-	-	-	-	-	-	-	-	-		
		b	-	-	-	-	-	-	-	-	-		
	5	a	JFRLn4431.10x.153	0.51005	0.00277	0.00421	0.00421	0.48298	0.48995	0.48995	0.859271354	1.436571594	0.637618887
		b	-	-	-	-	-	-	-	-	-		
		b	JFRLn4431.10x.154	0.50437	0.00327	0.00177	0.00177	0.49059	0.49563	0.49563	0.35712124		
		b	-	-	-	-	-	-	-	-	-		
	6	a	-	-	-	-	-	-	-	-	-		
		b	-	-	-	-	-	-	-	-	-		
	7	a	JFRLn4431.10x.08	0.72629	0.00106	0.00456	0.00688	0.2681	0.27371	0.54541	1.261436351		
		b	JFRLn4431.10x.09	0.7283	0.00096	0.00232	-	0.26842	0.2717	-	-		
	8	a	-	-	-	-	-	-	-	-	-		
		b	-	-	-	-	-	-	-	-	-		
	9	a	JFRLn4431.10x.13	0.47583	0.00203	0.00532	0.00588	0.51682	0.52417	0.63488	0.926159274		
		a	JFRLn4431.10x.14	0.88929	0.00066	0.00056	-	0.10949	0.11071	-	-		
		b	JFRLn4431.10x.155	0.49299	0.00328	0.00408	0.00411	0.49965	0.50701	0.6401	0.642087174		
		b	JFRLn4431.10x.156	0.86691	0.0011	0.00003	-	0.13196	0.13309	-	-		
	10	a	JFRLn4431.10x.157	0.48358	0.00259	0.00447	0.00463	0.50937	0.51642	0.68139	0.679493389		
		a	JFRLn4431.10x.158	0.83503	0.00104	0.00016	-	0.16377	0.16497	-	-		
		b	JFRLn4431.10x.159	0.45456	0.00328	0.00228	0.00253	0.53988	0.54544	0.6657	0.380051074		
		b	JFRLn4431.10x.160	0.87974	0.00081	0.00025	-	0.1192	0.12026	-	-		
	11	a	JFRLn4431.10x.31	0.49409	0.00175	0.005	0.0074	0.49916	0.50591	0.87128	0.849325131		
		a	JFRLn4431.10x.32	0.63463	0.00159	0.0024	-	0.36138	0.36537	-	-		
		b	JFRLn4431.10x.35	0.51102	0.00229	0.00394	0.0099	0.48275	0.48898	0.87248	1.134696497		
		b	JFRLn4431.10x.36	0.6165	0.00132	0.00596	-	0.37622	0.3835	-	-		
	12	a	JFRLn4431.10x.39	0.52058	0.00146	0.00559	0.00736	0.47237	0.47942	0.85872	0.857089622		
		a	JFRLn4431.10x.40	0.6207	0.00136	0.00177	-	0.37617	0.3793	-	-		
		b	JFRLn4431.10x.43	0.52165	0.00172	0.00731	0.01259	0.46931	0.47835	0.88126	1.428636271		
		b	JFRLn4431.10x.44	0.59709	0.0012	0.00528	-	0.39643	0.40291	-	-		
	13	-	JFRLn4431.10x.45	0.43869	0.00113	0.01735	0.02354	0.54282	0.5613	1.32784	1.772803952		
		-	JFRLn4431.10x.46	0.23346	0.00177	0.00619	-	0.75858	0.76654	-	-		
	14	-	JFRLn4431.10x.161	0.54168	0.00254	0.00474	0.01107	0.45105	0.45832	0.89383	1.238490541		
		-	JFRLn4431.10x.163	0.56450	0.00099	0.00633	-	0.42819	0.43551	-	-		
	15	-	JFRLn4431.10x.164	0.36017	0.00115	0.01852	0.03762	0.62015	0.63982	1.31658	2.857403272		
		-	JFRLn4431.10x.165	0.32323	0.00125	0.01910	-	0.65641	0.67676	-	-		
	16	-	JFRLn4431.10x.166	0.40991	0.00103	0.01696	0.02407	0.57210	0.59009	1.28152	1.878238342		
		-	JFRLn4431.10x.167	0.30857	0.00172	0.00711	-	0.68260	0.69143	-	-		
	17	-	JFRLn4431.10x.168	0.50739	0.0047	0.00141	0.00943	0.4865	0.49261	1.01604	0.928113066		
		-	JFRLn4431.10x.169	0.47658	0.00139	0.00802	-	0.51402	0.52343	-	-		
	18	-	JFRLn4431.10x.170	0.52016	0.00158	0.00921	0.0153	0.46905	0.47984	1.0748	1.423520655		
		-	JFRLn4431.10x.171	0.40504	0.00135	0.00609	-	0.58752	0.59496	-	-		
	19	-	JFRLn4431.10x.172	0.44796	0.00121	0.00862	0.03019	0.54220	0.55203	1.39216	2.168572578		
		-	JFRLn4431.10x.173	0.15987	0.00138	0.02157	-	0.81718	0.84013	-	-		
	20	-	JFRLn4431.10x.174	0.28156	0.00119	0.00651	0.00837	0.71074	0.71844	1.19236	0.701969204		
		-	JFRLn4431.10x.176	0.52608	0.00107	0.00186	-	0.47099	0.47392	-	-		

Table 7: Values for area fractions of outside, vessels, plaques, and tissue that were quantified by the program from the cropped pictures of the HCs of the animal JFRLn4435. Fraction of total HC area, fraction of total HC area per HC, % of plaque area per HC, anterior and posterior means of HC plaque %, and the standard deviation of these means calculated for this animal.

Animal	Tissue section	Side	Picture HC	Outside Area	Vessels Area	Plaques Area	Total Area of Plaques per HC	Tissue Area	Total Area	Area of each HC	% Area of Plaques	Plaques Mean (Anterior/Posterior	Standard deviation
JFRLn4435	1	a	-	-	-	-	-	-	-	-	-		
		b	-	-	-	-	-	-	-	-	-		
	2	a	-	-	-	-	-	-	-	-	-		
		b	-	-	-	-	-	-	-	-	-		
	3	a	-	-	-	-	-	-	-	-	-		
		b	-	-	-	-	-	-	-	-	-		
	4	a	-	-	-	-	-	-	-	-	-		
		b	-	-	-	-	-	-	-	-	-		
	5	a	-	-	-	-	-	-	-	-	-		
		b	-	-	-	-	-	-	-	-	-		
	6	a	RLn4435.10x.1	0.60316	0.00185	0.00584	0.00584	0.38916	0.39684	0.39684	1.471625844		
		b	RLn4435.10x.1	0.63974	0.0015	0.00751	0.00751	0.35125	0.36026	0.36026	2.084605563		
	7	a	-	-	-	-	-	-	-	-	-	2.890339836	2.460196285
		b	-	-	-	-	-	-	-	-	-		
	8	a	-	-	-	-	-	-	-	-	-		
		b	-	-	-	-	-	-	-	-	-		
	9	a	-	-	-	-	-	-	-	-	-		
		b	-	-	-	-	-	-	-	-	-		
	10	a	RLn4435.10x.1	0.76393	0.00244	0.00163	0.0177	0.23201	0.23607	0.64676	2.736718412		
		b	RLn4435.10x.1	0.58931	0.00091	0.01607	-	0.39371	0.41069	-	-		
	11	a	RLn4435.10x.1	0.44918	0.00409	0.00841	0.00846	0.53832	0.55082	0.62689	1.349519054		
		b	RLn4435.10x.2	0.92394	0.00042	0.00005	-	0.07560	0.07607	-	-		
	12	a	RLn4435.10x.2	0.52626	0.00111	0.01120	0.01426	0.46143	0.47374	0.75462	1.889692826		
		b	RLn4435.10x.2	0.71912	0.00081	0.00306	-	0.27701	0.28088	-	-		
	13	a	RLn4435.10x.2	0.41301	0.00090	0.05606	0.05723	0.53003	0.58699	0.73279	7.809877318		
		b	RLn4435.10x.2	0.85420	0.00055	0.00117	-	0.14408	0.1458	-	-		
	14	a	RLn4435.10x.2	0.48875	0.00098	0.01524	0.01955	0.49493	0.51125	0.82395	2.372716791		
		b	RLn4435.10x.2	0.68729	0.00080	0.00421	-	0.30769	0.3127	-	-		
	15	a	RLn4435.10x.2	0.46824	0.00093	0.03974	0.05326	0.49109	0.53176	0.79931	6.663247051		
		b	RLn4435.10x.2	0.73244	0.00063	0.01352	-	0.25340	0.26755	-	-		
	16	a	RLn4435.10x.C	0.32917	0.00100	0.03659	0.04397	0.63324	0.67083	1.43034	3.074094271		
		b	RLn4435.10x.C	0.24049	0.00135	0.00738	-	0.75078	0.75951	-	-		
	17	a	RLn4435.10x.C	0.33241	0.00127	0.00469	0.00618	0.66163	0.66759	1.18041	0.523546903		
		b	RLn4435.10x.2	0.48718	0.00151	0.00149	-	0.50982	0.51282	-	-		
	18	a	RLn4435.10x.2	0.49209	0.00081	0.04082	0.07147	0.46628	0.50791	1.01913	7.012844289		
		b	RLn4435.10x.2	0.48877	0.00087	0.03065	-	0.47970	0.51122	-	-		
	19	a	RLn4435.10x.2	0.51705	0.00096	0.01851	0.02361	0.46348	0.48295	0.91395	2.583292303		
		b	RLn4435.10x.2	0.56901	0.00092	0.00510	-	0.42498	0.431	-	-		
		a	RLn4435.10x.C	0.41491	0.00070	0.05467	0.05652	0.52972	0.58509	0.74998	7.536200965	3.737329086	2.250044763
		a	RLn4435.10x.C	0.83510	0.00058	0.00185	-	0.16246	0.16489	-	-		
		b	RLn4435.10x.C	0.57523	0.00074	0.01472	0.02282	0.40931	0.42477	0.76382	2.987614883		
		b	RLn4435.10x.C	0.66095	0.00075	0.00810	-	0.33020	0.33905	-	-		
		-	RLn4435.10x.C	0.32006	0.00105	0.04287	0.04732	0.63602	0.67994	1.23365	3.835771896		
		-	RLn4435.10x.C	0.44630	0.00118	0.00445	-	0.54808	0.55371	-	-		
		-	RLn4435.10x.C	0.58791	0.00091	0.01892	0.03146	0.39226	0.41209	1.06233	2.961415003		
		-	RLn4435.10x.C	0.34976	0.00112	0.01254	-	0.63658	0.65024	-	-		
		-	RLn4435.10x.2	0.40580	0.00162	0.00552	0.01555	0.58706	0.5942	1.3463	1.155017455		
		-	RLn4435.10x.2	0.24790	0.00135	0.01003	-	0.74072	0.7521	-	-		
		-	RLn4435.10x.2	0.49882	0.00093	0.02330	0.03913	0.47696	0.50119	0.94467	4.142187219		
		-	RLn4435.10x.2	0.55652	0.00075	0.01583	-	0.42690	0.44348	-	-		

Table 8: Values for area fractions of outside, vessels, plaques, and tissue that were quantified by the program from the cropped pictures of the HCs of the animal JFRLn4436. Fraction of total HC area, fraction of total HC area per HC, % of plaque area per HC, anterior and posterior means of HC plaque %, and the standard deviation of these means calculated for this animal.

Animal	Tissue section	Side	Picture HC	Outside Area	Vessels Area	Plaques Area	Total Area of Plaques per HC	Tissue Area	Total Area	Area of each HC	% Area of Plaques	Plaques Mean (Anterior/Posterior)	Standard deviation
JFRLn4436	1	a	-	-	-	-	-	-	-	-	-	1.333464171	0.47931924
		b	-	-	-	-	-	-	-	-	-		
	2	a	-	-	-	-	-	-	-	-	-		
		b	-	-	-	-	-	-	-	-	-		
	3	a	-	-	-	-	-	-	-	-	-		
		b	-	-	-	-	-	-	-	-	-		
	4	a	-	-	-	-	-	-	-	-	-		
		b	-	-	-	-	-	-	-	-	-		
	5	a	-	-	-	-	-	-	-	-	-		
		b	-	-	-	-	-	-	-	-	-		
	6	a	JFRLn4436.10x.I	0.74745	0.00074	0.00238	0.00238	0.24943	0.25255	0.25255	0.942387646		
		b	JFRLn4436.10x.I	0.84948	0.00058	0.00046	-	0.14948	0.15052	-	-		
	7	a	-	-	-	-	-	-	-	-	-		
		b	-	-	-	-	-	-	-	-	-		
	8	a	-	-	-	-	-	-	-	-	-		
		b	-	-	-	-	-	-	-	-	-		
	9	a	-	-	-	-	-	-	-	-	-		
		b	-	-	-	-	-	-	-	-	-		
	10	a	JFRLn4436.10x.I	0.56017	0.00138	0.00676	0.00682	0.43169	0.43983	0.48624	1.402599539		
		b	JFRLn4436.10x.I	0.95359	0.00047	0.00006	-	0.04587	0.04641	-	-		
		b	JFRLn4436.10x.I	0.62477	0.00086	0.00795	0.00795	0.36642	0.37523	0.37523	2.118700053		
	11	b	JFRLn4436.10x.I	-	-	-	-	-	-	-	-		
		a	JFRLn4436.10x.I	0.51311	0.00124	0.00603	0.00603	0.47962	0.48689	0.48689	1.238472756		
		a	JFRLn4436.10x.I	0.82600	0.00058	0.00232	-	0.17110	0.174	-	-		
		b	JFRLn4436.10x.I	0.54812	0.00183	0.00501	0.00501285	0.44504	0.45188	0.51938	0.965160384		
		b	JFRLn4436.10x.I	0.9325	0.00055	2.85E-06	-	0.06695	0.0675	-	-		
	12	a	JFRLn4436.10x.I	0.55793	0.00115	0.00746	0.01296	0.43345	0.44207	0.80859	1.602790042		
		a	JFRLn4436.10x.I	0.63348	0.00169	0.0055	-	0.35933	0.36652	-	-		
		b	JFRLn4436.10x.I	0.59676	0.00215	0.00402	0.00973	0.39707	0.40324	0.63175	1.540166205		
		b	JFRLn4436.10x.I	0.77149	0.00057	0.00571	-	0.22223	0.22851	-	-		
	13	a	JFRLn4436.10x.I	0.56228	0.00118	0.00569	0.00919	0.43085	0.43772	0.81817	1.123238447		
		a	JFRLn4436.10x.I	0.61955	0.00102	0.0035	-	0.37594	0.38045	-	-		
	14	a	JFRLn4436.10x.I	0.51624	0.00119	0.00228	0.00337	0.48029	0.48376	0.95018	0.354669642		
		a	JFRLn4436.10x.I	0.53358	0.00114	0.00109	-	0.4642	0.46642	-	-		
	15	a	JFRLn4436.10x.I	0.49300	0.00113	0.00654	0.00654153	0.49932	0.50699	0.6852	0.954689142		
		a	JFRLn4436.10x.I	0.82179	0.00071	1.53E-06	-	0.1775	0.17821	-	-		
	16	a	JFRLn4436.10x.I	0.48377	0.00090	0.01106	0.01118	0.50427	0.51623	0.65894	1.696666434		
		a	JFRLn4436.10x.I	0.85729	0.00049	0.00012	-	0.14210	0.14271	-	-		
	17	a	JFRLn4436.10x.I	0.24049	0.00135	0.00738	0.01527	0.75078	0.75951	1.45553	1.049102389		
		a	JFRLn4436.10x.I	0.30398	0.00117	0.00789	-	0.68696	0.69602	-	-	1.096554057	0.564083694
	18	a	JFRLn4436.10x.I	0.48062	0.00107	0.00994	0.01224	0.50837	0.51938	1.32681	0.922513397		
		a	JFRLn4436.10x.I	0.19257	0.00134	0.00230	-	0.80379	0.80743	-	-		
	19	a	JFRLn4436.10x.I	0.42818	0.00104	0.00699	0.01713	0.56378	0.57181	1.33595	1.282233617		
		a	JFRLn4436.10x.I	0.23585	0.00134	0.01014	-	0.75266	0.76414	-	-		
	20	a	JFRLn4436.10x.I	0.39375	0.00129	0.01179	0.01215	0.59316	0.60624	1.1386	1.067099947		
		a	JFRLn4436.10x.I	0.46764	0.00129	0.00036	-	0.53071	0.53236	-	-		
	21	a	JFRLn4436.10x.I	0.32705	0.00124	0.00333	0.00374	0.66837	0.67294	1.22258	0.305910452		
		a	JFRLn4436.10x.I	0.45037	0.00136	0.00041	-	0.54787	0.54964	-	-		
	22	a	JFRLn4436.10x.I	0.52530	0.00090	0.01637	0.02331	0.45743	0.4747	1.10607	2.107461553		
		a	JFRLn4436.10x.I	0.36863	0.00114	0.00694	-	0.62329	0.63137	-	-		
	23	a	JFRLn4436.10x.I	0.30982	0.00120	0.00221	0.00227	0.68677	0.69018	0.91288	0.24866357		
		a	JFRLn4436.10x.I	0.77730	0.00102	0.00006	-	0.22162	0.2227	-	-		

Table 9: Values for area fractions of outside, vessels, plaques, and tissue that were quantified by the program from the cropped pictures of the HCs of the animal JFRLn4437. Fraction of total HC area, fraction of total HC area per HC, % of plaque area per HC, anterior and posterior means of HC plaque %, and the standard deviation of these means calculated for this animal.

Animal	Tissue section	Side	Picture HC	Outside Area	Vessels Area	Plaques Area	Total Area of Plaques per HC	Tissue Area	Total Area	Area of each HC	% Area of Plaques	Plaques Mean (Anterior/Posterior)	Standard deviation
JFRLn4437	1	a	-	-	-	-	-	-	-	-	-	2.149824248	1.757015111
		b	-	-	-	-	-	-	-	-	-		
	2	a	-	-	-	-	-	-	-	-	-		
		b	-	-	-	-	-	-	-	-	-		
	3	a	-	-	-	-	-	-	-	-	-		
		b	-	-	-	-	-	-	-	-	-		
	4	a	-	-	-	-	-	-	-	-	-		
		b	-	-	-	-	-	-	-	-	-		
	5	a	-	-	-	-	-	-	-	-	-		
		b	JFRLn4437.10x.225	0.42917	0.00087	0.02683	0.02683	0.54313	0.57083	0.57083	4.700173432		
	6	a	JFRLn4437.10x.227	0.82097	0.00061	0.00178	0.00526	0.17664	0.17903	-	-		
		b	JFRLn4437.10x.228	0.43642	0.00249	0.00526		0.55584	0.56358	0.56358	0.933319138		
		b	JFRLn4437.10x.229	0.83300	0.00068	0.00068	-	0.16563	0.16699	-	-		
	7	a	-	-	-	-	-	-	-	-	-		
		b	-	-	-	-	-	-	-	-	-		
	8	a	-	-	-	-	-	-	-	-	-		
		b	-	-	-	-	-	-	-	-	-		
	9	a	-	-	-	-	-	-	-	-	-		
		b	-	-	-	-	-	-	-	-	-		
	10	a	JFRLn4437.10x.230	0.53201	0.00079	0.01960	0.02624	0.44761	0.468	0.73846	3.553340736		
			JFRLn4437.10x.231	0.72954	0.00063	0.00664	-	0.26319	0.27046	-	-		
			JFRLn4437.10x.232	0.50911	0.00084	0.01474	0.02176	0.47531	0.49089	0.76495	2.844630368		
		b	JFRLn4437.10x.233	0.72594	0.00080	0.00702	-	0.26624	0.27406	-	-		
			JFRLn4437.10x.234	0.49571	0.00123	0.00598	0.01589	0.49708	0.50429	0.8093	1.963425182		
	11	a	JFRLn4437.10x.236	0.69499	0.00071	0.00991	-	0.29439	0.30501	-	-		
		b	JFRLn4437.10x.237	0.47009	0.00094	0.01475	0.02253	0.51422	0.52991	0.80887	2.785367241		
		b	JFRLn4437.10x.238	0.72104	0.00070	0.00778	-	0.27048	0.27896	-	-		
			JFRLn4437.10x.240	0.46337	0.00249	0.01032	0.01032	0.52381	0.53663	0.53663	1.923112759		
	12	a	-	-	-	-	-	-	-	-	-		
		b	JFRLn4437.10x.241	0.42073	0.00295	0.00604	0.00604	0.57028	0.57927	0.57927	1.042691664		
			-	-	-	-	-	-	-	-	-		
	13	-	JFRLn4437.10x.242	0.40726	0.00115	0.01017	0.02146	0.58142	0.59274	1.27471	1.683520173		
		-	JFRLn4437.10x.243	0.31804	0.00142	0.01129	-	0.66926	0.68197	-	-		
	14	-	JFRLn4437.10x.244	0.39310	0.00113	0.01658	0.01905	0.58918	0.60689	1.27188	1.49778281		
		-	JFRLn4437.10x.245	0.33501	0.00122	0.00247	-	0.66130	0.66499	-	-		
	15	-	JFRLn4437.10x.246	0.56374	0.00096	0.02663	0.02764	0.40867	0.43626	0.86139	3.208767225		
		-	JFRLn4437.10x.247	0.57487	0.00193	0.00101	-	0.4222	0.42513	-	-		
	16	-	JFRLn4437.10x.248	0.48304	0.00292	0.00174	0.00225	0.5123	0.51696	0.93264	0.241250643		
		-	JFRLn4437.10x.249	0.58432	0.00218	0.00051	-	0.413	0.41568	-	-		
	17	-	JFRLn4437.10x.250	0.52985	0.00274	0.00326	0.00438	0.46415	0.47015	0.8364	0.523672884		
		-	JFRLn4437.10x.251	0.63375	0.00171	0.00112	-	0.36342	0.36625	-	-		
	18	-	JFRLn4437.10x.252	0.42543	0.00112	0.00794	0.01427	0.56551	0.57457	1.14214	1.249409004		
		-	JFRLn4437.10x.253	0.43243	0.00124	0.00633	-	0.56000	0.56757	-	-		
	19	-	JFRLn4437.10x.254	0.45082	0.00096	0.01023	0.01164	0.53799	0.54918	1.09937	1.491763465		
		-	JFRLn4437.10x.255	0.44981	0.00114	0.00617	-	0.54288	0.55019	-	-		
	20	-	JFRLn4437.10x.256	0.44385	0.00109	0.01109	0.0135	0.54398	0.55616	1.1693	1.154536902		
		-	JFRLn4437.10x.257	0.38686	0.00219	0.00241	-	0.60854	0.61314	-	-		

Table 10: Values for area fractions of outside, vessels, plaques, and tissue that were quantified by the program from the cropped pictures of the HCs of the animal JFRLn4438. Fraction of total HC area, fraction of total HC area per HC, % of plaque area per HC, anterior and posterior means of HC plaque %, and the standard deviation of these means calculated for this animal.

Animal	Tissue section	Side	Picture HC	Outside Area	Vessels Area	Plaques Area	Total Area of Plaques per HC	Tissue Area	Total Area	Area of each HC	% Area of Plaques	Plaques Mean (Anterior/Posterior)	Standard deviation
JFRLn4438	1	a	-	-	-	-	-	-	-	-	-	-	-
		b	-	-	-	-	-	-	-	-	-	-	-
	2	a	-	-	-	-	-	-	-	-	-	-	-
		b	-	-	-	-	-	-	-	-	-	-	-
	3	a	-	-	-	-	-	-	-	-	-	-	-
		b	-	-	-	-	-	-	-	-	-	-	-
	4	a	-	-	-	-	-	-	-	-	-	-	-
		b	-	-	-	-	-	-	-	-	-	-	-
		a	JFRLn4438.10x.01	0.68006	0.00089	0.0012	0.0012	0.31786	0.31994	0.31994	0.375070326	1.435346148	1.123700055
	5	a	-	-	-	-	-	-	-	-	-	-	-
		b	JFRLn4438.10x.274	0.56400	0.00080	0.00686	0.00686	0.42834	0.436	0.436	1.573394495	-	-
		b	-	-	-	-	-	-	-	-	-	-	-
	6	a	JFRLn4438.10x.275	0.82794	0.00065	0.0005	0.00132	0.17091	0.17206	0.28288	0.466628959	-	-
		b	JFRLn4438.10x.276	0.88918	0.00044	0.00082	-	0.10956	0.11082	-	-	-	-
	7	a	-	-	-	-	-	-	-	-	-	-	-
		b	-	-	-	-	-	-	-	-	-	-	-
	8	a	-	-	-	-	-	-	-	-	-	-	-
		b	-	-	-	-	-	-	-	-	-	-	-
		a	JFRLn4438.10x.18	0.52984	0.00119	0.00541	0.00548	0.46356	0.47016	0.66714	0.821416794	-	-
	9	a	JFRLn4438.10x.19	0.80302	0.00082	0.00007	-	0.19609	0.19698	-	-	-	-
		b	JFRLn4438.10x.22	0.52383	0.00167	0.001113	0.001124	0.46337	0.47617	0.56792	1.979151993	-	-
		b	JFRLn4438.10x.23	0.90825	0.00058	0.00011	-	0.09106	0.09175	-	-	-	-
		a	JFRLn4438.10x.14	0.50793	0.00104	0.00686	0.00851	0.48417	0.49207	0.70219	1.211922699	-	-
		a	JFRLn4438.10x.15	0.78988	0.00079	0.00165	-	0.20768	0.21012	-	-	-	-
	10	a	JFRLn4438.10x.277	0.47571	0.00080	0.02409	0.0274	0.49941	0.5243	0.75694	3.619837768	-	-
		b	JFRLn4438.10x.278	0.76736	0.00066	0.00331	-	0.22867	0.23264	-	-	-	-
		a	JFRLn4438.10x.279	0.47340	0.00083	0.02390	0.02727	0.50187	0.5266	0.7002	3.894601542	-	-
		a	JFRLn4438.10x.280	0.82640	0.00049	0.00337	-	0.16974	0.1736	-	-	-	-
	11	a	-	-	-	-	-	-	-	-	-	-	-
		b	-	-	-	-	-	-	-	-	-	-	-
		a	JFRLn4438.10x.281	0.54035	0.00098	0.01530	0.02574	0.44338	0.45966	1.11381	2.310986614	-	-
	12	a	JFRLn4438.10x.282	0.34586	0.00119	0.01044	-	0.64252	0.65415	-	-	-	-
		b	-	-	-	-	-	-	-	-	-	-	-
		b	JFRLn4438.10x.38	0.556	0.00144	0.00621	0.00703	0.43636	0.444	0.81812	0.859287146	-	-
	13	-	JFRLn4438.10x.39	0.62588	0.00114	0.00082	-	0.37216	0.37412	-	-	-	-
	14	-	JFRLn4438.10x.283	0.53349	0.00107	0.00867	0.00999	0.45677	0.46651	0.8659	1.1537129	1.471559692	1.195128418
		-	JFRLn4438.10x.284	0.60061	0.00116	0.00132	-	0.39691	0.39939	-	-	-	-
	15	-	JFRLn4438.10x.28	0.49964	0.00137	0.00622	0.00812	0.49277	0.50036	1.17419	0.691540551	-	-
		-	JFRLn4438.10x.29	0.32617	0.00138	0.0019	-	0.67055	0.67383	-	-	-	-
	16	-	JFRLn4438.10x.286	0.51512	0.00129	0.00122	0.00239	0.48237	0.48488	1.21405	0.196861744	-	-
		-	JFRLn4438.10x.287	0.27083	0.00148	0.00117	-	0.72652	0.72917	-	-	-	-
	17	-	JFRLn4438.10x.53	0.49177	0.00087	0.01410	0.02947	0.49326	0.50823	1.2341	2.387975043	-	-
		-	JFRLn4438.10x.54	0.27413	0.00127	0.01537	-	0.70923	0.72587	-	-	-	-
	18	-	JFRLn4438.10x.48	0.51614	0.00129	0.00315	0.01767	0.47943	0.48386	1.24681	1.417216737	-	-
		-	JFRLn4438.10x.49	0.23704	0.00120	0.01452	-	0.74723	0.76295	-	-	-	-
	19	-	JFRLn4438.10x.288	0.50499	0.00126	0.00314	0.00425	0.49061	0.49501	1.28068	0.331854952	-	-
		-	JFRLn4438.10x.289	0.21433	0.00152	0.00111	-	0.78305	0.78567	-	-	-	-

Table 11: Values for area fractions of outside, vessels, plaques, and tissue that were quantified by the program from the cropped pictures of the HCs of the animal JFRLn4439. Fraction of total HC area, fraction of total HC area per HC, % of plaque area per HC, anterior and posterior means of HC plaque %, and the standard deviation of these means calculated for this animal.

Animal	Tissue section	Side	Picture HC	Outside Area	Vessels Area	Plaques Area	Total Area of Plaques per HC	Tissue Area	Total Area	Area of each HC	% Area of Plaques	Plaques Mean (Anterior/Posterior	Standard deviation
JFRLn4439	1	a	-	-	-	-	-	-	-	-	-	4.228965099	0.984872528
		b	-	-	-	-	-	-	-	-	-		
	2	a	-	-	-	-	-	-	-	-	-		
		b	-	-	-	-	-	-	-	-	-		
	3	a	-	-	-	-	-	-	-	-	-		
		b	-	-	-	-	-	-	-	-	-		
	4	a	-	-	-	-	-	-	-	-	-		
		b	JFRLn4439.10x.107	0.47424	0.00147	0.02566	0.02566	0.49863	0.52576	0.52576	4.880553865		
	5	a	-	-	-	-	-	-	-	-	-		
		b	JFRLn4439.10x.108	0.68317	0.00081	0.01554	0.01554	0.30048	0.31683	0.31683	4.904838557		
		a	-	-	-	-	-	-	-	-	-		
		a	JFRLn4439.10x.109	0.81765	0.00047	0.00503	0.00503	0.17685	0.18235	0.18235	2.758431588		
	6	-	-	-	-	-	-	-	-	-	-		
		b	JFRLn4439.10x.110	0.57807	0.00086	0.02299	0.02299	0.39808	0.42193	0.42193	5.448771123		
		b	-	-	-	-	-	-	-	-	-		
	7	a	-	-	-	-	-	-	-	-	-		
		b	-	-	-	-	-	-	-	-	-		
	8	a	-	-	-	-	-	-	-	-	-		
		b	-	-	-	-	-	-	-	-	-		
	9	a	JFRLn4439.10x.111	0.51242	0.00149	0.02257	0.02257	0.46352	0.48758	0.48758	4.628983962		
		a	-	-	-	-	-	-	-	-	-		
		b	JFRLn4439.10x.112	0.49908	0.00162	0.02154	0.02907	0.47776	0.50092	0.80131	3.627809462		
		b	JFRLn4439.10x.113	0.69961	0.00073	0.00753	-	0.29213	0.30039	-	-		
	10	a	JFRLn4439.10x.114	0.50903	0.00149	0.01982	0.0207	0.46966	0.49097	0.61729	3.353367137		
		a	JFRLn4439.10x.115	0.87368	0.00050	0.00088	-	0.12494	0.12632	-	-		
		b	JFRLn4439.10x.116	0.57814	0.00128	0.02565	0.03732	0.39493	0.42186	0.8593	4.343069941		
		b	JFRLn4439.10x.117	0.56256	0.00109	0.01167	-	0.42468	0.43744	-	-		
	11	-	JFRLn4439.10x.118	0.57739	0.00393	0.00265	0.00478	0.41603	0.42261	0.61937	0.771751941		
		-	JFRLn4439.10x.119	0.80324	0.00066	0.00213	-	0.19397	0.19676	-	-		
	12	-	JFRLn4439.10x.120	0.52047	0.00108	0.01644	0.01943	0.46201	0.47953	0.97462	1.993597505		
		-	JFRLn4439.10x.121	0.50491	0.00098	0.00299	-	0.49112	0.49509	-	-		
	13	-	JFRLn4439.10x.122	0.53970	0.00100	0.01849	0.02109	0.44080	0.46029	0.97096	2.17207712		
		-	JFRLn4439.10x.123	0.48934	0.00099	0.00260	-	0.50708	0.51067	-	-		
	14	-	JFRLn4439.10x.124	0.57958	0.00236	0.00421	0.00789	0.41385	0.42042	0.72294	1.091376878		
		-	JFRLn4439.10x.125	0.69748	0.00075	0.00368	-	0.29809	0.30252	-	-		
	15	-	JFRLn4439.10x.126	-	-	-	0.01236	-	-	0.80308	1.539074563	2.024577924	1.166996469
		-	JFRLn4439.10x.127	0.19693	0.00190	0.01236	-	0.78882	0.80308	-	-		
	16	-	JFRLn4439.10x.128	0.49979	0.00114	0.01328	0.04324	0.48578	0.5002	1.24608	3.470082178		
		-	JFRLn4439.10x.129	0.25412	0.00189	0.02996	-	0.71403	0.74588	-	-		
	17	-	JFRLn4439.10x.130	0.43452	0.00139	0.01163	0.01948	0.55245	0.56547	1.3571	1.43541375		
		-	JFRLn4439.10x.131	0.20836	0.00206	0.00785	-	0.78172	0.79163	-	-		
	18	-	JFRLn4439.10x.132	0.35814	0.00121	0.01603	0.018	0.62463	0.64187	1.28136	1.404757445		
		-	JFRLn4439.10x.133	0.36052	0.00125	0.00197	-	0.63627	0.63949	-	-		

Table 12: Values for area fractions of outside, vessels, plaques, and tissue that were quantified by the program from the cropped pictures of the HCs of the animal JFRLn4440. Fraction of total HC area, fraction of total HC area per HC, % of plaque area per HC, anterior and posterior means of HC plaque %, and the standard deviation of these means calculated for this animal.

Animal	Tissue section	Side	Picture HC	Outside Area	Vessels Area	Plaques Area	Total Area of Plaques per HC	Tissue Area	Total Area	Area of each HC	% Area of Plaques	Plaques Mean (Anterior/Posterior	Standard deviation
	1	a	-	-	-	-	-	-	-	-	-		
		b	-	-	-	-	-	-	-	-	-		
	2	a	-	-	-	-	-	-	-	-	-		
		b	-	-	-	-	-	-	-	-	-		
	3	a	-	-	-	-	-	-	-	-	-		
		b	-	-	-	-	-	-	-	-	-		
	4	a	-	-	-	-	-	-	-	-	-		
		b	-	-	-	-	-	-	-	-	-		
			JFRLn4440.10x.136	0.55232	0.00344	0.00261	0.00261	0.44163	0.47237	0.47237	0.552532972		
	5	a	JFRLn4440.10x.137	0.67941	0.00081	0.00284	-	0.31694	0.32059	-	-		
			JFRLn4440.10x.138	0.50187	0.00114	0.01997	0.01997	0.47702	0.49813	0.49813	4.008993636		
		b	JFRLn4440.10x.139	0.73419	0.00076	0.00748	-	0.25757	0.26581	-	-		
			JFRLn4440.10x.140	0.48541	0.00088	0.04348	0.04348	0.47023	0.51459	0.51459	8.449445189	5.278066242	2.810080925
	6	a	-	-	-	-	-	-	-	-	-		
		b	JFRLn4440.10x.141	0.46111	0.00101	0.02624	0.02624	0.51163	0.53888	0.53888	4.869359867		
			-	-	-	-	-	-	-	-	-		
	7	a	JFRLn4440.10x.142				-			-	-		
		b	JFRLn4440.10x.143				-			-	-		
	8	a	-	-	-	-	-	-	-	-	-		
		b	-	-	-	-	-	-	-	-	-		
			JFRLn4440.10x.144	0.43215	0.00104	0.04038	0.04038	0.52643	0.56785	0.56785	7.111032843		
	9	a	JFRLn4440.10x.145	0.84513	0.00063	0.00078	-	0.15346	0.15487	-	-		
			JFRLn4440.10x.146	0.45657	0.00100	0.04295	0.0468	0.49948	0.54343	0.70091	6.677034141		
		b	JFRLn4440.10x.147	0.84251	0.00052	0.00385	-	0.15311	0.15748	-	-		
			JFRLn4440.10x.148				0.00945			0.29933	3.157050747		
	10	a	JFRLn4440.10x.149	0.70068	0.00074	0.00945	-	0.28914	0.29933	-	-		
			JFRLn4440.10x.150	0.5113	0.00325	0.00935	0.01814	0.4761	0.4887	0.92747	1.955858411		
		b	JFRLn4440.10x.151	0.56123	0.00231	0.00879	-	0.42766	0.43877	-	-		
	11	-	JFRLn4440.10x.152	0.45578	0.00639	0.00761	0.01359	0.53022	0.54422	1.0007	1.358049365		
		-	JFRLn4440.10x.153	0.54352	0.00131	0.00598	-	0.44919	0.45648	-	-		
		-	JFRLn4440.10x.154	0.56147	0.00069	0.00535	0.01612	0.43249	0.43853	0.88046	1.830861141		
	12	-	JFRLn4440.10x.155	0.55807	0.00086	0.01077	-	0.43030	0.44193	-	-		
		-	JFRLn4440.10x.156	0.49956	0.00083	0.00433	0.0146	0.49528	0.50044	0.96079	1.519582843		
	13	-	JFRLn4440.10x.157	0.53965	0.00093	0.01027	-	0.44915	0.46035	-	-		
		-	JFRLn4440.10x.158	0.58518	0.00136	0.00438	0.00836	0.40908	0.41482	1.01482	0.823791411	1.894218367	1.110880904
	14	-	JFRLn4440.10x.159	0.40000	0.00132	0.00398	-	0.59470	0.6	-	-		
		-	JFRLn4440.10x.160	0.41779	0.00110	0.01280	0.02439	0.56830	0.5822	1.28967	1.891181465		
	15	-	JFRLn4440.10x.161	0.29253	0.00177	0.01159	-	0.69411	0.70747	-	-		
		-	JFRLn4440.10x.162	0.27540	0.00112	0.01322	0.01383	0.71026	0.7246	1.24576	1.110165682		
	16	-	JFRLn4440.10x.163	0.47884	0.00105	0.00061	-	0.51950	0.52116	-	-		
		-	JFRLn4440.10x.164	0.49739	0.00100	0.01725	0.02269	0.48436	0.50261	0.91531	2.478941561		
	17	-	JFRLn4440.10x.165	0.58730	0.00083	0.00544	-	0.40643	0.4127	-	-		
		-	JFRLn4440.10x.166	0.39211	0.00125	0.03987	0.05262	0.56677	0.60789	1.21579	4.328050074		
	18	-	JFRLn4440.10x.167	0.39209	0.00132	0.01275	-	0.59383	0.6079	-	-		
	19	-	JFRLn4440.10x.168	0.26867	0.00072	0.00280	0.00280	0.72780	0.73132	0.73132	0.382869332		
		-	-	-	-	-	-	-	-	-	-		

Table 13: Values for area fractions of outside, vessels, plaques, and tissue that were quantified by the program from the cropped pictures of the HCs of the animal JFRLn4441. Fraction of total HC area, fraction of total HC area per HC, % of plaque area per HC, anterior and posterior means of HC plaque %, and the standard deviation of these means calculated for this animal.

Animal	Tissue section	Side	Picture HC	Outside Area	Vessels Area	Plaques Area	Total Area of Plaques per HC	Tissue Area	Total Area	Area of each HC	% Area of Plaques	Plaques Mean (Anterior/Posterior	Standard deviation
JFRLn4441	1	a	-	-	-	-	-	-	-	-	-	3.418355886	2.039533856
		b	-	-	-	-	-	-	-	-	-		
	2	a	-	-	-	-	-	-	-	-	-		
		b	-	-	-	-	-	-	-	-	-		
	3	a	-	-	-	-	-	-	-	-	-		
		b	-	-	-	-	-	-	-	-	-		
	4	a	-	-	-	-	-	-	-	-	-		
		b	-	-	-	-	-	-	-	-	-		
	5	a	JFRLn4441.10x.169	0.50278	0.00159	0.02326	0.02326	0.47237	0.49722	0.49722	4.678009734		
			-	-	-	-	-	-	-	-	-		
		b	JFRLn4441.10x.170	0.58049	0.00104	0.01789	0.01789	0.40057	0.4195	0.4195	4.264600715		
			-	-	-	-	-	-	-	-	-		
	6	a	JFRLn4441.10x.171	0.77638	0.00054	0.01787	0.01787	0.20522	0.22363	0.22363	7.990877789		
			-	-	-	-	-	-	-	-	-		
		b	JFRLn4441.10x.172	0.70763	0.00131	0.00797	0.00797	0.28310	0.29238	0.29238	2.725904645		
			-	-	-	-	-	-	-	-	-		
	7	a	JFRLn4441.10x.173	0.85134	0.00052	0.00345	0.00345	0.14469	0.14866	-	-		
		b	JFRLn4441.10x.174	0.92240	0.00036	0.00050	-	0.07674	0.0776	-	-		
	8	a	-	-	-	-	-	-	-	-	-		
		b	-	-	-	-	-	-	-	-	-		
	9	a	JFRLn4441.10x.175	0.52979	0.00097	0.01205	0.01205	0.45720	0.47022	0.47022	2.562630258		
			JFRLn4441.10x.176	0.76395	0.00064	0.00285	-	0.23256	0.23605	-	-		
		b	JFRLn4441.10x.177	0.49278	0.00108	0.01918	0.01965	0.48696	0.50722	0.61667	3.186469262		
			JFRLn4441.10x.178	0.89055	0.00051	0.00047	-	0.10847	0.10945	-	-		
	10	a	JFRLn4441.10x.179	0.49708	0.00245	0.02209	0.02253	0.47838	0.50292	0.64205	3.509072502		
			JFRLn4441.10x.180	0.86086	0.00053	0.00044	-	0.13816	0.13913	-	-		
		b	JFRLn4441.10x.181	0.46097	0.00287	0.00404	0.00404	0.53211	0.53903	0.53903	0.749494462		
			-	-	-	-	-	-	-	-	-		
	11	-	JFRLn4441.10x.182	0.46082	0.00129	0.01893	0.01893	0.51896	0.53918	0.53918	3.510886902		
			-	-	-	-	-	-	-	-	-		
	12	-	JFRLn4441.10x.183	0.52196	0.00361	0.00662	0.00697	0.46780	0.47803	0.69311	1.005612385		
		-	JFRLn4441.10x.184	0.78493	0.00058	0.00035	-	0.21415	0.21508	-	-		
	13	-	JFRLn4441.10x.185	0.57771	0.00344	0.00822	0.00913	0.41063	0.42229	0.77524	1.177699809		
		-	JFRLn4441.10x.186	0.64705	0.00167	0.00091	-	0.35037	0.35295	-	-		
	14	-	JFRLn4441.10x.187	0.43709	0.00398	0.00595	0.01096	0.55299	0.56292	1.05366	1.040118374		
		-	JFRLn4441.10x.188	0.50927	0.00128	0.00501	-	0.48445	0.49074	-	-		
	15	-	JFRLn4441.10x.189	0.55380	0.00408	0.00618	0.01207	0.43594	0.4462	1.14566	1.053544119		
		-	JFRLn4441.10x.190	0.30054	0.00259	0.00589	-	0.69098	0.69946	-	-		
	16	-	JFRLn4441.10x.191	0.44255	0.00405	0.00920	0.00989	0.54421	0.55746	0.84424	1.171467829		
		-	JFRLn4441.10x.192	0.71322	0.00081	0.00069	-	0.28528	0.28678	-	-		
	17	-	JFRLn4441.10x.193	0.44121	0.00533	0.00509	0.01397	0.54837	0.55879	1.39553	1.001053363		
		-	JFRLn4441.10x.194	0.16326	0.00742	0.00888	-	0.82044	0.83674	-	-		
	18	-	JFRLn4441.10x.195	0.47287	0.00475	0.00902	0.01255	0.51336	0.52713	1.30138	0.964360909		
		-	JFRLn4441.10x.196	0.22574	0.00619	0.00353	-	0.76453	0.77425	-	-		
	19	-	JFRLn4441.10x.197	0.23334	0.00578	0.00429	0.00429	0.75660	0.76667	0.76667	0.559556278		
		-	-	-	-	-	-	-	-	-	-		
	20	-	JFRLn4441.10x.198	0.53614	0.00269	0.00964	0.01691	0.45153	0.46386	0.89342	1.892726825		
		-	JFRLn4441.10x.199	0.57044	0.00164	0.00727	-	0.42065	0.42956	-	-		
	21	-	JFRLn4441.10x.200	0.25094	0.00680	0.00663	0.00723	0.73564	0.74907	1.2641	0.571948422		
		-	JFRLn4441.10x.201	0.48497	0.00555	0.00060	-	0.50888	0.51503	-	-		
	22	-	JFRLn4441.10x.202	0.38001	0.00313	0.00427	0.00427	0.61258	0.61998	0.61998	0.688731895		
		-	JFRLn4441.10x.203	-	-	-	-	-	-	-	-		
		-	JFRLn4441.10x.204	0.14010	0.00268	0.00295	-	0.85427	0.8599	-	-		

Appendix 2- Cortex Pictures

Pictures of each side of the cortex were also taken, for each section of every J20+ animal, although they weren't used for the quantification of plaque load. Examples of those are presented below.

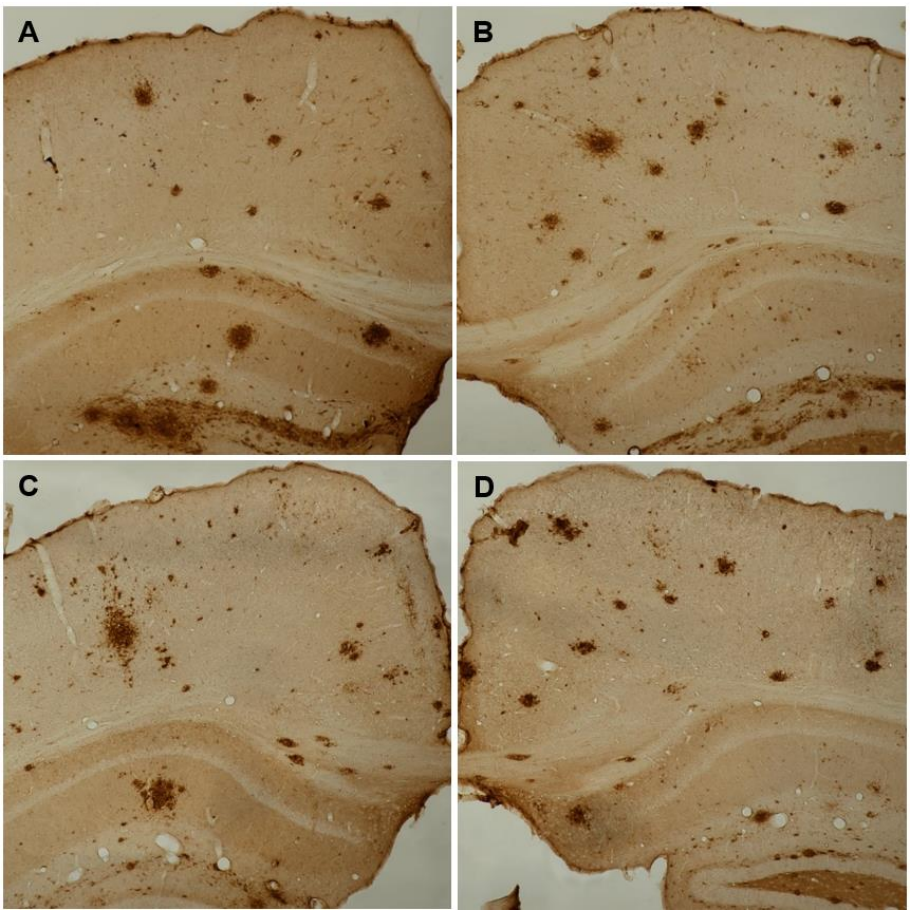

Figure 1: Superior cortex sections (10x magnification) of two J20+ mouse models. Pictures A and B correspond to one cortex section and pictures C and D correspond to another section. An IHC against Aβ was performed in both sections, being the Aβ plaques the darker stains.

Appendix 3- Cropped pictures of the hippocampus

More examples of the HC cropping done for the hippocampal Aβ plaque % quantification.

Figure 1: Cropping from a picture of a HC section of a J20+ mouse model (10x magnification). An IHC against Aβ was performed in this section, being the Aβ plaques the darker stains.

Figure 2: Cropping from 2 pictures of the same HC section of a J20+ mouse model (10x magnification). An IHC against Aβ was performed in this section.

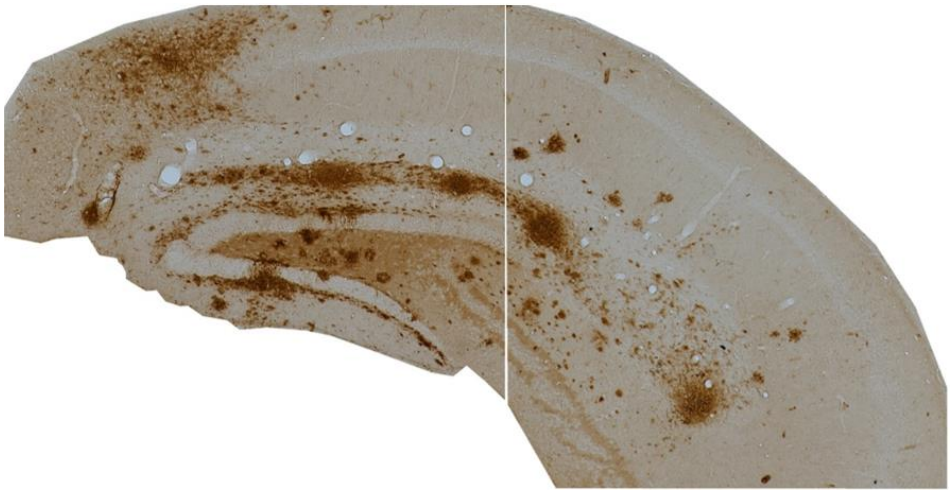

Figure 3: Cropping from 2 pictures of the same HC section of a J20+ mouse model (10x magnification). An IHC against Aβ was performed in this section. This HC section is from a more posterior brain region.

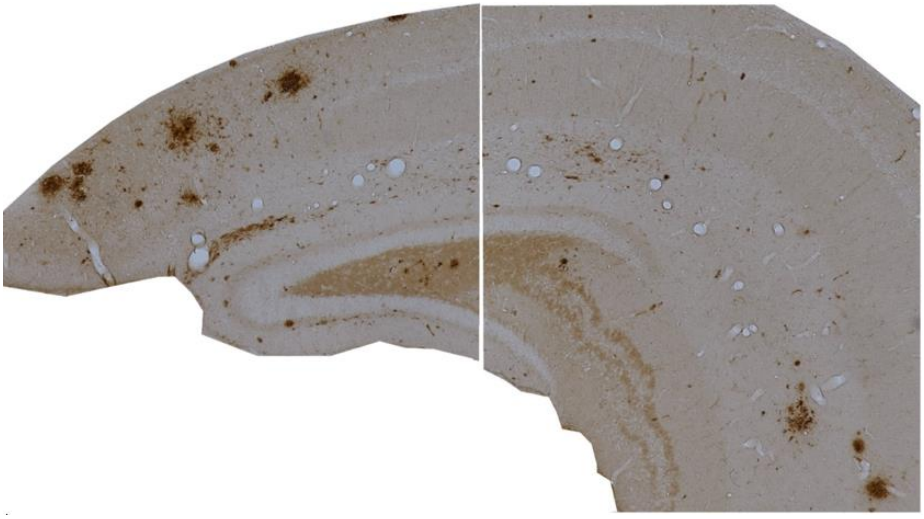

Figure 4: Cropping from 2 pictures of the same HC section of a J20+ mouse model (10x magnification). An IHC against Aβ was performed in this section. This HC section is from a more posterior brain region.